A SHIFTING MOSAIC: CLIMATE CHANGE AND BIOTIC CONTROLS DRIVE CHANGES IN COASTAL FORESTS ALONG FLORIDA'S BIG BEND COAST

By

AMY KATHLEEN LANGSTON

A DISSERTATION PRESENTED TO THE GRADUATE SCHOOL
OF THE UNIVERSITY OF FLORIDA IN PARTIAL FULFILLMENT
OF THE REQUIREMENTS FOR THE DEGREE OF
DOCTOR OF PHILOSOPHY

UNIVERSITY OF FLORIDA

2017

To my parents

ACKNOWLEDGMENTS

NEED TO WRITE.

TABLE OF CONTENTS

page

LIST OF TABLES

LIST OF FIGURES

LIST OF OBJECTS

LIST OF ABBREVIATIONS

ANOVA	Analysis of Variance
CE	Creek Edge
cm	centimeter
COT	Mangrove seedling with cotyledons
DI	Deionized water
FCC	Florida Climate Center
FDEM	Florida Division of Emergency Management
FF	Frequently Flooded
FNAI	Florida Natural Areas Inventory
HSD	Honest Significant Difference
IBM	Individual-based Model
IE	Island Edge
II	Island Interior
km	kilometer
LiDAR	Light Detection and Ranging
m	meter
MF	Moderately Flooded
MHHW	Mean Higher High Water
MP	Marsh Plain
mS	millisiemens
MT	Mature mangrove tree
NAVD	North American Vertical Datum
NCEI	National Centers for Environmental Information
NMS	Nonmetric Multidimensional Scaling

NOAA	National Oceanic and Atmospheric Administration
OAT	One-At-A-Time
OT	Old mangrove tree
PROP	Propagule
PSH	Predator Satiation Hypothesis
RF	Rarely Flooded
SAP	Mangrove sapling
SD	Mangrove seedling
YT	Young mangrove tree

Abstract of Dissertation Presented to the Graduate School
of the University of Florida in Partial Fulfillment of the
Requirements for the Degree of Doctor of Philosophy

A SHIFTING MOSAIC: CLIMATE CHANGE AND BIOTIC CONTROLS DRIVE CHANGES IN COASTAL FORESTS ALONG FLORIDA'S BIG BEND COAST

By

Amy Kathleen Langston

December 2017

Chair: David Kaplan
Major: Environmental Engineering Sciences

Climate change elicits short- and long- term changes in coastal plant communities by altering the physical conditions that affect ecosystem processes and species distributions. Along the Big Bend coast of Florida, sea level rise is driving the retreat of freshwater forest while fewer freeze events are allowing favorable growing conditions for northward range expansion of mangrove forest. By extending a dataset initiated in 1992, I evaluated tree survival, regeneration, and understory composition on islands of freshwater forest. Between 1992 and 2014, tidal flooding increased by 22-117%, corresponding with tree mortality and replacement of forest vegetation by salt marsh herbs and shrubs.

To test whether encroachment of black mangroves (*Avicennia germinans*) could modify the freshwater forest-to-salt marsh reassembly trajectory, I investigated abiotic and biotic controls on *A. germinans* establishment by comparing fates of caged and non-caged propagules across landscape positions. Within 12 days, grapsid crab, *Sesarma reticulatum*, consumed 99% of non-caged propagules. Establishment of caged propagules increased with increasing flooding frequency; however cages did not entirely prevent predation, which remained a primary cause of mortality. These findings reveal

that while relict forest islands and surrounding salt marsh can support *A. germinans*, propagule predation strongly suppress colonization, suggesting that mangrove expansion models should incorporate top-down biotic controls.

To identify the relationship between propagule density and propagule predation by *S. reticulatum,* I conducted a field experiment comparing rates of predation across three propagule densities (1, 25, and 100 propagules m^{-2}). I found that the proportion of propagules eaten decreased with increasing propagule density, consistent with a Holling type II functional response.

I incorporated my field results into a stage-based population growth model to simulate population growth under scenarios of varying propagule dispersal density, propagule predation intensity, and freeze event frequency. Results demonstrated that when fewer severe freezes occurred, forests were able to establish, except when influx density was low and predation intensity was high. Repeated influxes of propagules generally allowed the population to recover from freezes and overcome predation. If enough propagules survived to produce a single fecund tree, a regenerating population could persist under a wide range of freeze and predation intensities.

CHAPTER 1
INTRODUCTION

Since 1880, global mean surface temperature has increased by approximately 0.85 °C, and the past three decades are estimated to be the warmest of the last 800 years (IPCC, 2013). The degree and rate at which temperature is rising is largely the result of human activities, most prominently the burning of fossil fuels, land use changes, and agricultural activities, which are increasing the concentrations of greenhouse gases in the atmosphere (Keeling et al., 1989; Vitousek, 1994; Cox et al., 2000). Observed consequences of a warming planet include rising sea levels, ocean warming and acidification, extreme weather events, glacier retreat, and melting ice sheets. These phenomena affect organisms and ecosystems on global and regional scales (Vitousek, 1994; Walther et al., 2002; Parmesan & Yohe, 2003). Responses of organisms and ecosystems include phenological shifts, latitudinal and elevational range shifts of species or even entire ecosystems, loss of sensitive species and habitats, and replacement of sensitive species by those better adapted to altered conditions (e.g., Fitter et al., 1995, Grabherr et al., 1994, Pounds et al., 2006, Brown et al., 1997).

Coastal ecosystems are especially vulnerable the effects of climate change. Sea level rise, storm surges, and changing precipitation and temperature regimes exacerbate the naturally-stressed environmental conditions to which they have adapted. Coastal ecosystems are vulnerable to direct effects (e.g., mortality from flooding events, droughts, or storms) and indirect effects (e.g., altered hydrological, biophysical, and biogeochemical processes that facilitate habitat loss, disease, or salt stress) of climate change, which can have short- and long-term consequences for the survival, distribution, and health of coastal organisms (Michener et al., 1997).

In this dissertation, I investigated effects of climate change on coastal forests along the Big Bend coast of Florida. My overarching hypothesis was that climate change is shifting the composition of the Big Bend landscape from a mosaic of freshwater forest and salt marsh to a landscape composed exclusively of salt-tolerant communities (namely salt marsh and mangrove forest), in regions lacking major freshwater inputs (i.e., far from major rivers).

Islands of freshwater forest are unique to the Big Bend, and like many endemic ecosystems vulnerable to the effects of climate change, are disappearing (Williams et al., 1999a). In Chapter 2, I compared contemporary declines of forested islands to long-term trends of decline. I also explored the trajectory or vegetation reassembly occurring in forest islands using the perspective of community assemblage trajectories and turnover. I collected field measurements of vegetation and soil, and reviewed tidal and elevation datasets and climatological records to identify patterns of species turnover across a gradient of increasing tidal flooding frequency.

Building on Chapter 2, I sought to further explore modes of climate change-induced ecosystem transition. As freshwater forest retreats along the Big Bend, mangrove forest is expanding northward (Osland et al., 2013; Giri & Long, 2016). Mangrove range expansion is a striking example of a large-scale range shift occurring as a result of climate change and extensive research is being conducted on the abiotic (bottom-up) drivers of poleward expansion. However, top-down (biotic) pressure on mangroves encroaching into temperate salt marsh has been largely overlooked despite the importance of herbivory and seed predation in regulating plant populations (He & Silliman, 2016). To fill this knowledge gap, I conducted field experiments investigating

the bottom-up and top-down controls on *Avicennia germinans* (black mangrove) encroachment into salt marsh and transitioning forest islands. My goal was to determine whether encroaching A*. germinans* could modify the freshwater forest-to-salt marsh trajectory identified in Chapter 2. In Chapter 3, I present the findings of my field experiments and discuss the role of propagule predation in restricting mangrove colonization when abiotic conditions are favorable for seedling establishment.

In Chapter 4, I expanded upon my findings from Chapter 3 and examined three factors affecting mangrove population encroachment into salt marsh along the Big Bend: propagule density, propagule predation intensity, and mangrove mortality from freeze events. I conducted a field experiment testing the hypothesis that propagule predation by *Sesarma reticulatum* (purple marsh crab) would depend on propagule density. I then developed a stage-based population growth model that simulated mangrove forest establishment under scenarios of varying propagule density, propagule predation intensity, and freeze frequency and intensity. The model quantifies how propagule delivery frequency and density interact with top-down and bottom-up controls to predict spatial and temporal scales of mangrove expansion.

The research presented in this dissertation highlights ecological responses of coastal ecosystems to a changing climate, and provides insight into current trends of freshwater forest retreat, species reassembly, trophic interactions, and mangrove forest range expansion that are dynamically reshaping the landscape of the Big Bend coast.

CHAPTER 2
A CASUALTY OF CLIMATE CHANGE? LOSS OF FRESHWATER FOREST ISLANDS ON FLORIDA'S GULF COAST

Background

As chronicled in an ever-growing body of research, climate change is driving spatial and compositions shifts in vegetation at local, regional, and global scales (e.g., Walther et al., 2002, Kelly & Goulden, 2008, Svenning & Sandel, 2013, Leffler et al., 2016). In coastal areas, sea level rise, warming air temperatures, and changing rainfall regimes elicit short- and long-term changes in vegetation by altering physical conditions that affect the survival, distribution, and reproductive success of coastal plants (Scavia et al., 2002; Kirwan et al., 2009; Osland et al., 2016; Gabler et al., 2017; Liu et al., 2017). The maintenance of salt marsh, for example, largely depends on feedbacks among sediment availability, plant productivity, and the local rate of sea level rise (e.g., Craft et al., 2009; Fagherazzi et al., 2012; Kirwan & Megonigal, 2013; Reed, 1995). Increases in hurricane intensity resulting from increases in sea surface temperature are expected to produce larger storm surges with concomitant increases in the frequency of damage from scour, erosion, vegetation burial, and saltwater intrusion (Michener et al., 1997; Lin et al., 2012; Mendelsohn et al., 2012). Droughts, particularly in concert with sea level rise, also affect coastal vegetation by increasing salt concentrations in drying soil beyond specific tolerance levels (Williams et al., 2003; Angelini & Silliman, 2012; Cormier et al., 2013; White & Kaplan, 2017).

Reprinted with permission from Langston, A. K, D. A. Kaplan, & F. E. Putz, 2017. A casualty of climate change? Loss of freshwater forest islands on Florida's Gulf Coast. Global Change Biology 23: 5383-5397.

Coastal plants have adapted to survive periodic disturbances, but it is unclear how they will fare in a future with more frequent or severe pulse events coupled with chronic changes in sea level and temperature (Michener et al., 1997; Leonardi et al., 2016). To improve our understanding, we can investigate responses of coastal plants along coastlines largely undisturbed by land-use changes that exacerbate the effects of climate change. Of particular value are long-term field data that capture transitions in coastal vegetation communities.

The Big Bend coast of Florida is a relatively undisturbed, sparsely developed area that is ideal for studying long-term trends in coastal ecosystems. This 250-km stretch of coastline extends along the Gulf of Mexico from Apalachee Bay south to Anclote Key (Mattson et al., 2007). Hydrology along the Big Bend is driven by a combination of saltwater and freshwater sources. The Gulf of Mexico and an extensive network of tidal creeks deliver saltwater while freshwater is supplied by precipitation [127-152 cm annually (FCC, 2014)], springs from the Floridan aquifer, and several major rivers. The region is subjected to little subsidence due to the presence of a stable carbonate platform and experiences low wave energy (tidal range of approximately 1 m), but its low elevation and shallow topographic relief mean that small increases in sea level affect large areas (Williams et al., 1999b; Raabe et al., 2004; DeSantis et al., 2007; Williams et al., 2007b; Raabe & Stumpf, 2016). Based on the tide station in Cedar Key, Florida, mean sea level increased along the Big Bend coast by an average of 1.93 mm/year between 1914 and 2014 (NOAA, 2013). While local mean sea level is rising at a lower rate than in other coastal regions of Florida, changes in air temperature, barometric pressure, and ocean circulation have created variability in the rate of local

sea level change within this time period, including short-term, rapid increases much greater than 1.93 mm/year. These short-term increases may have greater effects on coastal plants than long-term mean sea level rise, as they occur on timescales similar to the turnover times of plant communities.

Storms and droughts have played important roles in shaping the Big Bend and altering vegetation communities. Recent major events include an extratropical storm in 1993, dubbed the “Storm of the Century,” which caused high tree mortality in stands of coastal forest and deposited sediment equivalent to 10 years of averaged accretion in Gulf Coast marshes (Goodbred & Hine, 1995). Following the 1993 storm, a 5-year drought (1998-2002), one of the worst in Florida’s history, resulted in record low freshwater flows along the Big Bend and also contributed to tree mortality (Williams et al., 2003; Verdi et al., 2006).

Historically, the Big Bend has been subject to high rates of vegetation community reassembly, making it a useful region for examining the effects of climate change on coastal vegetation. Historical changes in shoreline and intertidal habitats reported by a U.S. Geologic Survey show major transitions from upland forest to marsh and marsh to open water from 1852 to 1995 (Raabe et al., 2004). The Big Bend supports a diversity of coastal communities, including extensive salt marsh, coastal forest (bottomland hardwood swamp, slash pine flatwood woodlands, cypress-tupelo swamp forest, coastal hydric hammock, and tidal freshwater forest), scattered stands of mangrove, and seagrass beds. Characteristic of the region are islands of freshwater forest (hereafter, forest islands), which are isolated remnants of a formerly continuous forest that is retreating landward (Kurz & Wagner, 1957; Williams et al., 1999a; Williams et al.,

1999b; DeSantis et al., 2007; Williams et al., 2007b; Geselbracht et al., 2011). These islands are the focus of our study.

Forest islands, which are dominated by *Sabal palmetto* (cabbage palm) and *Juniperus virginiana* (southern red cedar) occur on elevated limestone substrate surrounded by salt marsh. Limestone rock is often exposed or near the surface and regional karst topography creates a dimpled surface with variable soil depths, affecting water storage potential across islands. Unlike continuous coastal forests that obtain freshwater from both direct precipitation and the Floridan aquifer, trees on forest islands are primarily dependent on precipitation (DeSantis et al., 2007; Williams et al., 2007b). Other trees common on healthy islands include *Quercus virginiana* (live oak), *Celtis laevigata* (sugarberry), and *Persea palustris* (swamp bay).Although considered a freshwater forest, tree species vary in their salt tolerances. More tolerant species are able to persist in more tidally inundated islands while others disappear (Williams et al., 1998). *Sabal palmetto*, one of the most salt-tolerant trees in the southeastern United States (Perry & Williams, 1996), is the sole tree species on the most saline islands.

Presented here are the most recent findings of a long-term field study of freshwater forest response to climate change drivers along a tidal creek, with new insight on community reassembly trajectories occurring in forest islands. Our findings are representative of vegetation change observed across the Big Bend, where the landscape is shifting from a mosaic of freshwater and saltwater communities to one composed exclusively of halophytic vegetation, particularly in regions lacking major freshwater inputs (i.e., far from major rivers). We hypothesized that contemporary declines of forest islands follow long-term trends and that the trajectory of community

reassembly in remnant forest islands varies with elevation and tidal flooding frequency. To address these hypotheses, we compare changes in tidal flooding and weather to long-term trends in tree mortality, regeneration, and understory vegetation in remnant forest islands.

Materials and Methods

Study Site

The study site is located along Turtle Creek, a tidal creek in Florida's Waccasassa Bay Preserve State Park (29° 7' N, 82° 47' W; Figure 2-1) approximately 5 km from the Waccasassa River, which is the nearest major surface freshwater source (mean annual discharge = 6.97 m^3/s; USGS, 2012). Plant communities at the study site include salt marsh dominated by *Juncus roemerianus* (black needle rush) and forest islands that transition to continuous coastal freshwater forest and pine flatwoods inland. Turtle Creek is the setting of several previous studies on forest retreat (Perry & Williams, 1996; Williams et al., 1998; Williams et al., 1999a; Williams et al., 2003; Castaneda & Putz, 2007; DeSantis et al., 2007; Geselbracht et al., 2011), all of which used data from 13 permanent sample plots established in 1992 and 1993. Of the 13 plots, 10 occur on forest islands in various states of decline: four were initially identified as "healthy" (H0, H1, H2, H3), three as "intermediate" (I1, I2, I3), and three as "decadent" (D1, D2, D3) when the study commenced. The remaining three plots are in continuous forest (C1, C2, C3) and, along with H0, were established in 1993. Each plot is 400 m^2, and all but one are 20 x 20 m (D1 is 40 x 10 m due to the narrow shape of the island).

Tidal Flooding Frequency, Ground Elevation, and Soil Depth

To evaluate the influence of tidal flooding on vegetation, we analyzed tidal and elevation datasets for the study plots and compared them to historical and recent field data. Weekly tidal flooding measurements were collected in nine of the 13 plots from May 1992 to January 1993 (Williams et al., 1999a). Plots C1-C3 and H0 were established after the tidal flooding study; these plots were assumed to flood no more frequently than plot H1. Using field data, Williams et al. (1999a) developed a tidal flooding model to calculate tidal flooding frequencies in other years. Tidal flooding frequency was defined as the number of weeks during which flooding occurred at least once and was predicted using median plot elevation, mean higher high water (MHHW) for a specified time period as recorded in Cedar Key, FL [National Oceanic and Atmospheric Administration (NOAA) Station 8727520], and plot distance from the mouth of Turtle Creek. We used this same model to estimate weeks of tidal flooding in 2014 (i.e., during the time of our most recent tree census) and 1994 (during which understory vegetation data were previously collected). The model was not applied to the three continuous forest plots or the two higher elevation healthy island plots (H0 and H1) because Williams et al. (1999a) found the model described tidal flooding well only in the eight lower elevation island plots.

We compared 1992-1993 elevation data reported in Williams et al. (1999a) to 2007 Light Detection and Ranging (LiDAR) data from the Florida Division of Emergency Management (FDEM) for Levy County, downloaded from the NOAA Digital Coast website (https://coast.noaa.gov/digitalcoast/). Raster data and shapefiles of plot boundaries were viewed in ArcGIS (v. 10.1; ESRI, Redlands, CA, USA). All data layers were in horizontal coordinate system WGS84 and the vertical spatial reference for the

raster file was NAVD88 (altitude resolution of 0.0328 ft.). We sampled 25 pixels within each plot in a 5 x 5m grid pattern, mimicking laser-level survey sampling reported by Williams et al. (1999a). The sampling pattern was repeated three times for a total of 75 sampled pixels per plot (with the exception of H2, C1, and C2, for which fewer pixels were sampled because the raster data were incomplete). Vertical pixel values were converted to meters and compared to elevation data reported in Table 1 of Williams et al. (1999a).

Soil depth to limestone was measured at ten random locations within the original nine island plots between fall 2015 and spring 2016 by inserting a pin flag into the soil until it hit rock, then measuring the inserted length with a metric ruler. We used the Kruskal-Wallis test to compare soil depths between plot types, and multiple regression to evaluate whether soil depth depended on elevation and flooding frequency. All statistical analysis, unless otherwise stated, was performed in R (R Core Team, 2017).

Precipitation, Climate, and Storms

We reviewed meteorological (precipitation and temperature) and storm data from 1955 to 2014 for the Big Bend coast to identify extreme weather events that occurred since the last tree census (2005) that may correlate with vegetation trends as well as to identify long-term climate patterns. Annual climatological summary data were obtained from NOAA: National Centers for Environmental Information (NCEI) for the Tampa International Airport weather station (#12842), which is approximately 140 km southeast of the study site and the nearest station with continuous historical temperature and precipitation records. Storm data for Levy County from 1955 to 2014 were obtained from NOAA NCEI Storm Events Database and were compared to NOAA National Hurricane Center historical summaries and NOAA Storm Predictor Center maps. La Niña events

recorded by NOAA National Weather Service Climate Prediction Center were reviewed to identify droughts that occurred since 2005. Waccasassa River discharge data from 1963 to 2014 (USGS gauge #02313700) were also reviewed as an integrated measure of regional-scale precipitation and temperature variability. Annual discharge data were summarized by calculating cumulative deviation from mean annual discharge. Years with above-average flow were given a value of +1 and years with below-average flow were assigned a value of -1. Long-term trends were assessed by summing cumulative wet and dry trends across the period of record.

Tree Demography Data

To test the hypothesis that contemporary declines of forest islands follow long-term trends, we censused trees in all 13 plots in summer 2014. Censuses (complete and partial) were previously conducted annually from 1992 to 1998, and in 2000 and 2005. During the 2014 census and previous censuses, tree species and status (live/dead) were recorded for each tree >2 m tall, with the exception of *S. palmetto*, for which census data were recorded for trees with above-ground trunks of any height. In summer 2015, we measured tree regeneration by counting all *S. palmetto* without visible trunks (“trunkless”) and all other trees <2 m tall, including small seedlings, in each plot.

We used a nonlinear least squares logistic model to evaluate relationships between 2014 vegetation data and tidal flooding frequency for all 13 plots. Correlation between tree death and salt marsh vegetation in 2014 was examined using simple linear regression. We compared tree regeneration of all species previously reported for 2005 in Table 1 of DeSantis et al. (2007) and compared 2014/15 census results [tree species richness, *S. palmetto* regeneration, and *S. palmetto* density (of trees with

trunks)] to 1992/93 census results (1992 data were used for all island plots except H0, and 1993 data were used for continuous forest plots and H0). 2014 *S. palmetto* regeneration data were compared to 1992/1993 regeneration by compiling trunkless *S. palmetto* counts reported in Table 1 of Williams et al. (1999a) and seedling counts estimated from Figure 5a in the same paper. Comparisons of tree species richness and *S. palmetto* regeneration were made using Wilcoxon signed rank tests. Densities of *S. palmetto* with trunks were compared using paired *t* tests. To evaluate trends in tree survival during the census period (1992-2014), we calculated annual mortality rates for *S. palmetto* and *J. virginiana* by plot type (continuous, healthy, intermediate, and decadent) using the mortality equation developed by Sheil et al. (1995). We fitted tree mortality in continuous and healthy plots with a simple linear model and intermediate and decadent plots with a nonlinear least squares logistic model to describe mortality trends.

Understory Composition

We conducted an understory survey in the fall and winter of 2014/2015 to test our hypothesis that community reassembly in forest islands varies with tidal flooding frequency. Plots were surveyed during three field visits, and understory species were surveyed using the same sampling grid of 25 1 m^2 random subplots per 400 m^2 study plot used in 1994, the only other time when understory vegetation was previously assessed. Subplots were located along five transects across each plot, and the same subplot grid was used for all 20 x 20 m plots. A separate sampling grid was created for D1 (40 x 10 m). Within each subplot, absolute percent cover of each non-tree species was recorded. A sample of each species was collected and pressed for reference, an those species that could not be identified in the field were later identified using floras,

keys, the Waccasassa floristic survey (Abbott & Judd, 2000), and the species list in the Appendix of Williams et al. (1999a). We compared overall species richness in 2014 to the 1994 understory composition (raw data provided by K. Williams) using a paired *t* test. We evaluated community reassembly patterns across tidal flooding frequencies between 1994 and 2014, and connected data points using a loess smooth function.

We compared understory composition in 1994 and 2014 with nonmetric multidimensional scaling (NMS) in PC-ORD (MJM Software Design, Gleneden Beach, OR, USA). Understory data in 1994 were recorded as number of subplots per plot in which each plant species occurred, which we assumed to be comparable to percent cover. We ran the NMS procedure for each dataset five times, each time with a new random seed, to verify consistency of our interpretation among the solutions, as recommended by Peck (2010). Convex hulls were used to outline ordination spaces of plots according to categorized tidal flooding frequencies (0-1 week, 2-9 weeks, 10-19 weeks, 20-29 weeks, and >30 weeks).

Results

Tidal Flooding Frequency, Ground Elevation, and Soil Depth

Tidal flooding frequency increased dramatically between 1992 and 2014 in the eight lowest elevation island plots (Table 2-1). The number of weeks in which tidal flooding of island plots occurred ranged from 0-27 in 1992 and 0-33 in 2014, but increased by approximately 6 weeks in each of the eight lowest elevation island plots. For healthy island plots H2 and H3, this corresponded to 117% and 86% increases in flooding frequency, respectively, within 22 years. Flooding frequencies of intermediate island plots (I1-I3) increased to 18-20 weeks (an average increase of 45%), and flooding in decadent plots increased to 24-33 weeks (an average increase of 26%) in

2014. In the two most frequently flooded plots (D2 and D3), tidal flooding events occurred during approximately 50% of weeks in 2014. Continuous forest plots and H0 were previously assumed to flood no more than H1, which flooded during 1 week in 1992. Continuous forest plots are inland enough that correlation between tidal flooding and elevation is weak, and we found no evidence of flooding in those plots or in H0 and H1 during repeated field visits in 2014, but we know that H1 is flooded during major storms. As such, we assumed flooding frequency in the continuous forest plots and H0 and H1 had not changed since 1992.

Median elevation derived from LiDAR data were mostly within 0.02 to 0.08 m of those from the original field data (Table 2-1). The largest difference was in plot H2 (median LiDAR elevation was 0.15 m higher than median field elevation), likely due to approximately 25% of pixels in the LiDAR raster file missing within the plot boundary, resulting in fewer sampled pixels. Elevation ranges from LiDAR data for all island plots were slightly higher than but completely overlapped with the original elevation ranges. Because field measurements were so precisely measured by Williams et al. (1999a), and little difference was found between the original measurements and median LiDAR data, we accepted the field measurements as the most accurate elevations for the study plots and used those values in the tidal flooding model and soil depth analysis.

Mean soil sample depths varied widely across the original nine island plots (2.54-30.23 cm; Figure 2-2). We found no differences in soil depths between islands in different states of decline (Kruskal-Wallis $\chi^2 = 1.00$, *p*-value = 0.61; based on median soil depth), although soil depth differed between intermediate plots (K-W = 17.82, *p*-value = 0.0001) and between decadent plots (K-W = 18.96, *p*-value < 0.0001). Within

plot variation was similar among decadent plots, relatively high in I2 and I3, and increased with elevation among healthy plots. Neither median elevation nor tidal flooding frequency explained soil depth across island plots ($F_{2,6}$ = 0.86, *p*-value = 0.47), due to high variation within plots and outlier soil depths in I2.

Precipitation, Climate, and Storms

Precipitation during 2005-2014 was within the 1955-2005 range (Figure 2-3a), a period of record previously evaluated by DeSantis et al. (2007). The 59-year annual mean (1955-2014) was 118 cm, compared to the 50-year annual mean (1955-2005) of 117 cm. For the period 2005-2014, we identified no unusual rain years, nor did we identify any anomalies in air temperature extremes. Very slight increases in mean annual, maximum, and minimum temperatures are evident since 1955 but rates did not approach the current rate of global annual temperature increase of 0.07 °C (NOAA, 2016). Three La Niña events, defined by NOAA as ocean temperatures deviating by at least -0.5 °C from the mean sea surface temperature of a 30-year base period (NOAA, 2015), occurred since 2005 (July 2007-July 2008, June 2010-May 2011, and July 2011-April 2012). Two La Niña events (2007-2008 and 2010-2011) corresponded to years that experienced negative deviations from the 59-year mean annual rainfall, but were far smaller than the negative deviations that occurred during the major 1998-2002 drought. Cumulative deviations from mean annual discharge from the Waccasassa River show that while annual discharge varied, flow declined overall since at least 1999 (and possibly since 1989, though data for 1993-1998 are incomplete; Figure 2-3b), which is the longest period of reduced flow in the 1963-2014 record.

The 1993 “Storm of the Century” and a 5-year drought (1998-2002) were previously identified as contributing to periods with increased rates of tree mortality in

the original nine island plots (Williams et al., 2003; DeSantis et al., 2007). We identified one year in our review of meteorological and storm data in which more recent extreme weather events occurred that could have affected the study site. In 2012, Hurricane Beryl produced a small (EF-0) tornado in Yankeetown, FL, approximately 11 km south of the study site, and a 1.4-m storm surge was documented one month later in Cedar Key from Hurricane Debby (Kimberlain, 2012).

Tree Census and 2014 Vegetation Trends

We found a strong relationship between 2014 *S. palmetto* mortality and tidal flooding frequency (Figure 2-4). In continuous forest plots and H0 and H1, which never or rarely flood, live *S. palmetto* (with trunks) relative to total *S. palmetto* (live and dead) per plot ranged from 89% to 100%. In the other two healthy island plots, where tidal flooding occurred during approximately 13 weeks of 2014, only 50%-54% of the trees were alive. Among the remaining six island stands in which flooding frequency ranged from 18 to 33 weeks, only two intermediate plots had any live *S. palmetto* in 2014. Both plots had one live tree each. The trend in *S. palmetto* survival across tidal flooding frequency was best described by a nonlinear least squares logistic model, which explained 98% of the variance between *S. palmetto* survival and tidal flooding frequency. We found a similarly strong but opposite trend between 2014 salt marsh species cover and tidal flooding frequency (R^2 = 0.99; Figure 2-4). Tree death was positively correlated with increased salt marsh cover across the 13 island plots (r^2 = 0.96; $F_{1,11}$ = 256.8, *p*-value < 0.0001). No salt marsh vegetation was present in the continuous forest plots or H0 and only 1% was found in H1. The proportion of salt marsh vegetation in the other two healthy island stands ranged from 61% to 69%, and

the understories of intermediate and decadent plots were composed of 96%-100% salt marsh species.

Fewer regenerating tree species were found in 2014 compared to 2005 in both continuous forest and island plots (Table 2-2). In continuous forest stands, regeneration of *Quercus laurifolia* (laurel oak), *C. laevigata*, *Pinus taeda* (loblolly pine), and *Diospyros virginiana* (persimmon) ceased by 2014 and regenerating *Q. virginiana* persisted only in C2. Small *Persea borbonia* (red bad; <2 m tall), which were absent in 2005, were found in C1 in 2014. *Sabal palmetto* and *J. virginiana* were still regenerating in continuous forest plots and in H0 and H1 in 2014. H1 was the only island plot with regenerating *Q. virginiana* in 2014. Tree regeneration ceased in all other island plots; *S. palmetto* in H2 and H3 converted to relict (non-regenerating) stands between 2005 and 2014.

The 2014 tree census revealed continued forest decline with increased tidal flooding on island plots as measured by species richness, *S. palmetto* regeneration, and *S. palmetto* density (Figure 2-5). Declines were pronounced with respect to species richness (V = 78, *p*-value = 0.002; Figure 2-5a) and *S. palmetto* regeneration (V = 55, *p*-value = 0.006; Figure 2-5b) between 1992/93 and 2014. Trunkless *S. palmetto* density was reduced by 85%-93% by 2014 in continuous forest plots, and by 79%-87% in H0 and H1. Smaller differences were found in intermediate and decadent stands, where lower elevations and greater susceptibility to tidal flooding and storm surges had already limited regeneration in 1992/93. Density of *S. palmetto* with trunks was also much reduced between 1992/93 and 2014 (t = 4.45, *p*-value = 0.0001; Figure 2-5c). *Sabal palmetto* density was much higher in healthy and intermediate islands subject to

more than 1 week of tidal flooding in 1992, whereas density remained similar in continuous forest and H0 and H1 between 1993 and 2014.

Looking across the >20-year period of record for plots along Turtle Creek, rates of tree mortality of the dominant tree species remained near zero in continuous forest and healthy island plots (Figure 2-6a, b), but increased very rapidly in intermediate and decadent island plots (Figure 2-6c, d). Mortality of *J. virginiana* increased rapidly and nonlinearly in intermediate and decadent plots over time, as demonstrated with well-fitted logistic curves (R^2 = 0.97 for intermediate plots; R^2 = 0.84 for decadent plots). Nonlinear trends of *S. palmetto* mortality in intermediate and decadent plots were also very well described by logistic curves (R^2 = 0.88, R^2 = 0.98, respectively). In intermediate plots, the rate of *J. virginiana* mortality increased faster than *S. palmetto* after 2000, reaching 100% by 2014. *Sabal palmetto* mortality was 24% by 2014. The rate of mortality of *S. palmetto* in decadent plots was also lower than *J. virginiana*, though, like *J. virginiana*, *S. palmetto* mortality reached 100% by 2014.

Understory Composition

In 1994, as tidal flooding increased, so did shrubby and herbaceous salt marsh cover, while forest vegetation decreased (Figure 2-7a). Plots with flooding frequencies of up to 6 weeks in 1994 (including all C and H plots) supported understory compositions dominated by forest species. Understories of continuous forest plots were dominated by the shrub, *Ilex vomitoria* (yaupon), climbing plants *Smilax bona-nox* (greenbrier) and *Toxicodendron radicans* (poison ivy), and by *Rayjacksonia phyllocephala* (camphor daisy), an annual forb. In healthy island plots, <10% of understory vegetation was composed of salt marsh plants, which included the halophytic shrub, *Lycium carolinianum* (Carolina wolfberry), climbing plant *Ipomoea*

sagittata (salt marsh morning glory), and perennial salt marsh grasses *Distichlis spicata* (salt grass) and *Spartina* spp. (cordgrass). Intermediate island plots supported mixed understories of forest forbs (mainly *R. phyllocephala* and *Solidago* sp. (goldenrod)), halophytic shrubs *L. carolinianum* and *Iva frutescens* (marsh elder), and *D. spicata* and *Spartina* spp. All but two forest species, *R. phyllocephala* and *Solidago* sp., disappeared from decadent plots, which flooded during 17-27 weeks in 1994 and supported *L. carolinianum*, *I. frutescens*, the perennial forb *Borichia frutescens* (seaside oxeye), and salt marsh grasses.

Between 1994 and 2014, distinct transitions from forest understory to salt marsh shrubs to herbaceous salt marsh had occurred along an increased tidal flooding gradient (Figure 2-7b). Relative cover of forest species decreased as salt marsh shrubs became dominant in moderately flooded plots and by 2014, herbaceous marsh plants almost exclusively dominated the most frequently flooded plots. As in 1994, plots with flooding frequencies of 0-1 week (continuous forest plots, H0, H1) maintained understories composed of forest species. In 2014, dominant plants in these plots included *I. vomitoria*, *S. bona-nox*, and two native grasses: *Oplismenus hirtellus* (woodsgrass) and *Dichanthelium dichotomum* (cypress witchgrass). Healthy plots H2 and H3, in which flooding frequency increased from 7 to 13 weeks, supported a combination of forest and salt marsh vegetation. Most common in these plots were perennial upland forbs *Dicliptera sexangularis* (sixangle foldwing) and *Iresine diffusa* (Juba's bush), salt marsh shrubs *L. carolinianum* and *I. frutescens*, and annual salt marsh forb *Suaeda linearis* (sea blite). Intermediate plots flooded during approximately 18-20 weeks and were dominated by *L. carolinianum* and *I. frutescens*, perennial salt

marsh forbs, including *B. maritime* and *Batis maritime* (saltwort), and the salt tolerant grass *D. spicata*. Forest vegetation was absent in decadent plots, which flooded during 24-33 weeks in 2014; these plots were dominated by *B. maritima*, *B. frutescens*, and *D. spicata*. Although species composition changed, no difference was found in overall species richness in the 13 plots between 1994 and 2014 (t = -0.22, p-value = 0.41).

We interpreted three-dimensional NMS solutions of plot ordination scores for 1994 and 2014 understory data that were significant according to randomization tests (1994; final minimum stress score = 0.730, p-value = 0.004; 2014: final minimum stress score = 0.553, p-value = 0.004). The NMS solution for 1994 compositional data show plots closer together in ordination space than in 2014 (Figure 2-8). Plots in the 2-9 weeks tidal flooding category (H2 and H3) in 1994 stretched between plots that received 0-1 week of tidal flooding and plots that received 10 or more weeks of flooding, whereas plots that flooded during 10 or more weeks were clustered tightly together. In 2014, plots occupied a wider ordination space and were clustered by tidal flooding group. Plots in the 0-1 week tidal flooding group were farther from the rest of the plots and H1 was shifted closer to the more frequently flooded stands. Increases in tidal flooding resulted in shifts in tidal flooding groups. Plots H2, H3, and I3 (10-19 weeks flooding group) overlapped slightly with ordination space occupied by plots in the 20-29 weeks flooding group. Compared to the 1994 ordinations, these plots occupied a more distinct space between the 10-19 weeks flooding group and >30 weeks flooding group.

Discussion

Physical Environment Dynamics

Spatial variation in tidal flooding frequency represents increased tidal flooding over time as a result of sea level rise. The rate of local mean sea level rise increased

from 1.5 mm/year from 1939-1993 to 1.93 mm/year from 1939-2014 (Williams et al., 1999a; NOAA, 2013), increasing the frequency of flooding on forest islands (Table 2-1). Tidal flooding in H2 and H3 doubled between 1993 and 2014, and came to match the frequencies in intermediate plots in 1992. Similarly, 2014 flooding frequencies in intermediate plots overlapped the D1 flooding frequency in 1992. While field observations indicate tidal flooding remained infrequent in continuous forest plots and H0 and H1 between 1992 and 2014, we found evidence of flooding in H1 from Hurricane Hermine, a category 1 storm that made landfall north of Turtle Creek in September 2016. Approximately 2-5 cm of wrack (composed mostly *J. roemerianus*) was deposited on the island containing plot H1.

Frequency of tidal flooding on islands is largely dependent on elevation, which ranged from 0.52 to 0.96 m NAVD (Table 2-1). Overlap between original field data and 2007 LiDAR data were sufficient to conclude forest island elevation remained stable over time, which is consistent with regional geology (Raabe et al., 2004; Castaneda & Putz, 2007; Williams et al., 2007b; Raabe & Stumpf, 2016) No relationship between elevation and tidal flooding frequency has been explicitly measured for continuous forest plots (C1, C2, C3), which ranged from 0.69 to 1.10 m NAVD. Continuous forest stands are located farther upstream from the Gulf of Mexico, buffered by surrounding forest, and located farther away from Turtle Creek than the island plots, which all reduce the incidence of tidal flooding.

Lack of correlation between soil depth and elevation or tidal flooding across forest island plots, and large soil depth variations within plots (Figure 2-2) indicate that a number of interactive physical processes are influencing rates of soil accretion,

deposition, organic matter decomposition, and erosion including elevation, tidal flooding frequency, storm events, micro-topography, and vegetation composition. The relatively deep soil in I2 may mean this island receives more sediment from coastal storms than other islands. However, (Williams et al., 2003) found forest islands received much less sediment from the 1993 “Storm of the Century” compared to the surrounding marsh. Alternatively, I2 may have more limestone dissolution holes that fill with sediment than the other islands, increasing overall soil depth and micro-topographic variation across the island.

While long-term temperature and precipitation data for our study area suggest that local climate conditions are relatively stable (Figure 2-3a), freshwater from the Waccasassa River is increasingly unavailable (Figure 2-3b). Declined flow may be related to the 1998-2002 drought, but the continued negative trend is not explained by reduced precipitation or increased temperatures causing higher regional evapotranspiration. Instead, declining river flow may be indicative of human impacts such as increased water withdrawal upstream and groundwater withdrawal from the regional aquifer (Marella, 2014).

Tree Survival Trends

In the 1980s, causes of *S. palmetto* die off and forest decline were attributed to land-use changes due to agriculture, residential and commercial development, and pine plantations (Vince et al., 1989). Not until the previously published studies on Turtle Creek was sea level rise identified as the primary driver of freshwater forest decline in Waccasassa. Simultaneous loss of *S. palmetto* and expansion of salt marsh vegetation in 2014 in forest islands affirms the loss of forest island with increased tidal flooding due to sea level rise (Figure 2-4). Dramatic decreases in species richness in trees, *S.*

palmetto regeneration, and *S. palmetto* survival have occurred over a relatively short time period (Figure 2-5). Forest islands that have flooded more than one week no longer support any tree regeneration (Table 2-2) and those that flooded more than 13 weeks no longer support any trees, and have converted to salt marsh. In 2014 two previously healthy island stands (H2 and H3) were more similar to intermediate stands in 1992, and intermediate stands in 2014 were generally more degraded than even the decadent stands in 1992. These shifts in forest health are consistent with previously noted impacts of salinity on freshwater forest trees along the Big Bend (Perry & Williams, 1996; Williams et al., 1998; Williams et al., 1999a; Doyle et al., 2010; Ross et al., 2014; Zhai et al., 2016; Liu et al., 2017).

Forest decline was apparent in continuous forest plots even though we observed no evidence of tidal flooding. While *S. palmetto* survival remained high, tree species richness and *S. palmetto* regeneration declined substantially between 1992/1993-2014 (Figure 2-5). One potential explanation is saltwater intrusion. Without a consistent buffering source of freshwater discharge from surface drainage of diffuse groundwater flow, an increase in sea level and tidal flooding along the coastal fringe may increase saltwater intrusion into the shallow aquifer (Kaplan et al., 2010b), which could decrease survival of young trees and seedlings in continuous forest stands (Kaplan et al., 2010a). Plot C3, which is adjacent to a brackish pond and has a much lower elevation than the other two continuous forest plots, may be most susceptible to potential saltwater intrusion. In addition to having few tree seedlings, its understory lacks the forest shrubs and grasses dominant in C1 and C2 that are typical of coastal freshwater forest. Instead, in 2014 the understory of C3 was dominated by *Cladium jamaicense*

(sawgrass), a sedge common in fresh and brackish marshes that can withstand salinities of up to five parts per thousand (Wolfe et al., 1990), and may signal fresh and saltwater mixing. In 1994, *C. jamaicense* was absent in C3, but was present in high density in plot I1, which indicated potential groundwater flow through the limestone dissolution holes to that forest island (Williams et al., 1999a). By 2014, more salt-tolerant species replaced *C. jamaicense* in I1. If, as identified by Williams et al. (1999a), declines in tree regeneration is the first major sign of forest die off in otherwise healthy-looking forest stands, we may be witnessing in continuous forest what was witnessed decades earlier on forest islands surrounded by salt marsh.

Long-term trends in tree mortality showed *S. palmetto* and *J. virginiana* mortality rates increased with time as forest health continued to decline in intermediate and decadent plots (Figure 2-6c, d). In contrast, mortality remained low and stable over time in continuous forest and infrequently flooded island stands (Figure 2-6a, b). Lower salt tolerance partially explains higher mortality of *J. virginiana* than *S. palmetto* in intermediate and decadent stands. Greater susceptibility to uprooting from the 1993 “Storm of the Century” and water stress (combined with tidal flooding) during the 1998-2002 La Niña drought also spurred *J. virginiana* mortality (Williams et al., 2003; DeSantis et al., 2007). Hurricanes Beryl and Debby and associated storm surges in 2012 may have punctuated tree loss in intermediate and decadent stands since 2005. Salt spray from storms may also have contributed to tree mortality by damaging young trees and new shoots (Wells & Shunk, 1938). In the absence of seedlings, *S. palmetto*, representing the last vestiges of relict freshwater forest, became the last to succumb to

the combined effects of tidal flooding, salinity, and severe weather events in decadent plots by 2014.

Community Reassembly

A historical high rate of change in coastal communities across the Big Bend region illustrates the dynamic and responsive nature of vegetation communities along this relatively undeveloped coastline. Not only is sea level rise driving long-term deterioration of coastal freshwater forest, but it is also driving community reassembly in relict stands. Loss of forest species creates available space in the landscape, providing opportunities for other communities (e.g., shrubby high marsh and herbaceous low marsh) to colonize islands that historically supported freshwater forest. We observed complete turnover in species composition on relict forest islands in response to changing environmental conditions over the course of 20 years (Figure 2-7). As trees died with increased tidal flooding, they were replaced by salt marsh shrubs, which in turn wre replaced by herbaceous salt marsh vegetation at higher tidal flooding frequencies. Replacement of freshwater forest by halophytic communities is just one of many examples of climate change-driven community reassembly (Schaefer et al., 2008; Novak et al., 2011; Scott & Morgan, 2012) observed in various systems around the world. For example, Beaugrand et al. (2008) found species turnover across trophic levels in marine ecosystems of the North Atlantic, a region particularly sensitive to changes in ocean temperature. Schaefer et al. (2008) found that the combined effects of increases in winter and spring temperatures and reduced spring precipitation led to the reassembly of migratory bird communities in Europe. Climate-driven community reassembly was also explored by Hamann & Wang (2006) using a climate model that predicted the replacement of coniferous forest by hardwoods in British Columbia as

dominant conifer species lost suitable habitat and hardwood species at their current climate limit expanded their distributions northward.

Species that composed forest, shrub, and herbaceous salt marsh communities remained similar between 1994 and 2014, hence compositions of more flooded stands serve as predictors for the future compositions of less frequently flooded stands in earlier stages of reassembly. However, coastal storms can also initiate shifts in understory composition in forests (Hook et al., 1991), complicating the turnover pattern driven by tidal flooding. This effect is most apparent in H2 and H3, which suffered severe damage during the 1993 storm (Williams et al., 2003; Williams et al., 2007b). Uprooting of trees in these plots opened up the canopy, which benefited salt marsh shrubs (*L. carolinianum* and *I. frutescens*). Dominance of these shrubs in 2014 accounts for the shifts in ordination space toward intermediate and decadent plots (Figure 2-8). Storm-induced disturbances also created opportunities for native species that thrive in disturbed sites but are not typical components of freshwater forest understory or salt marsh. By 2014, H2 and H3 supported dense herbaceous understories of the grass *Cenchrus myosuroides* (big sandbur) and perennial forb *I. diffusa*, two common followers of disturbance, which were present in 1994 but at lower densities. As noted by Williams et al. (2007b), both species may reduce tree regeneration via competition and thereby contribute to regeneration failures in these formerly healthy stands.

Informing Large-Scale Responses to Climate Change

Our study provides and in-depth account of the freshwater forest conversion into salt marsh phenomenon that is occurring all along the Big Bend coast. As sea level rise increases tidal flooding and intensifies coastal storms beyond salt tolerance levels of tree seedlings, regeneration ceases, trees die off, and forest vegetation is replaced by

halophytic shrubs, which are then replaced by herbaceous salt marsh (Figure 2-9). This trajectory was consistent among our study plots and reconnaissance observations of remnant forest islands along nearby tidal creeks confirmed this pattern is occurring on a larger scale. This pattern was also documented by Raabe & Stumpf (2016) in their review of historic topographic surveys and imagery of the Big Bend region. They found that 82 km^2 of coastal freshwater forest and 66 km^2 of halophytic shrubs and relict trees ("forest-to-marsh transitional habitat") along 295 km of coastline converted to salt marsh over 120 years (1875-1995). Although much of the freshwater forest along the Big Bend coast is in protected areas and the region is largely undeveloped, most of the property on the landward side is privately owned, which may restrict landward migration of forest island ecosystems (Doyle et al., 2010; Geselbracht et al., 2015; Enwright et al., 2016). Historically, extensive commercial harvesting of *S. palmetto, J. virginiana*, *P. taeda*, and hardwoods common in coastal freshwater forests has occurred on private lands along the Big Bend (Williams et al., 2007b). Due to low topographic relief of the region, large-scale acquisition may be required to accommodate future forest migration and prevent widespread loss of forest islands.

For forest islands with little to no regeneration, conversion into salt marsh is only as far away as the die off of the current generation of trees. While healthier regenerating islands may persist longer, if the rate of sea level rise continues increasing, even healthy stands will be replaced by salt-tolerant communities, potentially within a matter of decades. Forest islands, unique to a small portion of the coastal network of the United States, will completely disappear. Stands of continuous forest may persist for hundreds of years in the absence of direct human impacts or dramatic increases in sea

level or extreme weather events. However, as previously noted, low flow in the Waccasassa River and the potential for restricted landward migration threaten forest survival as climate change continues to alter natural coastal conditions.

Looking beyond the loss of forest islands, future research should evaluate other possible community reassembly trajectories in relict forest islands and changes in ecological functions provided by the Big Bend coast. For example, increasing temperatures and fewer freeze events are driving the expansion of mangrove populations northward along the east and west coasts of Florida (Cavanaugh et al., 2014; Osland et al., 2017a; Osland et al., 2017b). Replacement of coastal freshwater forest by *Avicennia germinans* (black mangrove) is already predicted along the southern Gulf Coast of Florida and in the Everglades (Doyle et al., 2010; Record et al., 2013)and the potential exists of *A. germinans* to become more prominent along the Big Bend. *Avicennia germinans* seedlings are present at the study site and we have found that relict forest islands and surrounding salt marsh can support *A. germinans* establishment, though top-down biotic controls limit colonization (Langston et al., 2017a). Another alternative that must be considered is the northward spread of *Schinus terebinthifolia* (Brazilian pepper) in coastal forests in Florida in response to sea level rise and warming temperatures. *Schinus terebinthifolia* has been reported on two of the 10 islands we studied and is actively treated by park staff. Due to many highly adaptable physical, reproductive, physiological, and genetic characteristics, its potential for widespread invasion along the Big Bend presents an alarming consequence of climate change (Spector & Putz, 2006; Williams et al., 2007a). The extent to which different communities replace forest islands largely depends on how these communities respond

to continued environmental changes resulting from climate change. We expect reassembly trajectories in relict forest islands will be dictated by local impacts from sea level rise, coastal storms, changing weather regimes, and temperature shifts that will continue to drive short- and long-term ecological changes in the region.

Table 2-1. Summary of elevations and tidal flooding frequencies in the study plots between 1992 and 2014.

	Median Elevation (m NAVD88)		Tidal Flooding Frequency (weeks)[c]		
Plot	Original[a]	LiDAR[b]	1992	1994	2014
C1	1.10	1.18	0	0	0
C2	1.09	1.06	0	0	0
C3	0.69	0.60	0	0	0
H0	0.96	1.01	0	0	0
H1	0.93	0.91	1	1	1
H2	0.78	0.93	6	6	13
H3	0.80	0.87	7	6	13
I1	0.60	0.68	14	13	20
I2	0.67	0.75	14	14	20
I3	0.66	0.78	12	11	18
D1	0.52	0.56	18	17	24
D2	0.58	0.62	26	25	32
D3	0.63	0.68	27	27	33

[a]From Table 1 in Williams et al. (1999a); elevations measured in the 1990s with a laser transit, 25 estimates per plot.
[b]Calculated from 2007 LiDAR data from FDEM for Levy County, FL.
[c]Flooding frequencies based on calendar year; flooding in H2, H3, I plots, and D plots calculated using model by Williams et al. (1999a); flooding in C plots, H0, and H1 assumed to be the same as in 1992. Values for 1992 differ from those reported in Williams et al. (1999a) because they were originally based on a 37-week study.

Table 2-2. Regeneration status of tree species in 2014 relative to 2005, arranged from lowest to highest flooding frequency.

Plot	C1	C2	C3	H0	H1	H2	H3	I3	I1	I2	D1	D2	D3
Flooding frequency (weeks)	0	0	0	0	1	13	13	18	20	20	24	32	33
Sabal palmetto (cabbage palm)[a]	R	R	R	R	R	[X]	[X]	L	X	X	L	L	-
Juniperus virginiana (southern red cedar)	R	R	R	R	R	X	L	L	L	-	-	-	-
Quercus virginiana (live oak)	X	R	[X]	X	R	L	L	-	-	-	-	-	-
Quercus laurifolia (laurel oak)	-	L	[X]	L	-	-	-	-	-	-	-	-	-
Celtis laevigata (sugarberry)	X	[X]	X	-	X	-	X	-	-	-	-	-	-
Morus rubra (red mulberry)	-	-	L	-	L	-	-	-	-	-	-	-	-
Pinus taeda (loblolly pine)	[X]	-	L	-	-	-	-	-	-	-	-	-	-
Diospyros virginiana (persimmon)	L	-	[X]	-	-	-	-	-	-	-	-	-	-
Ulmus alata (winged elm)	-	-	L	-	-	-	-	-	-	-	-	-	-
Ptelea trifoliata (hoptree)	-	L	-	-	-	-	-	-	-	-	-	-	-
Fraxinus caroliniana (Carolina ash)	-	L	-	-	-	-	-	-	-	-	-	-	-
Acer floridanum (Florida maple)	-	X	-	-	-	-	-	-	-	-	-	-	-
Gleditsia tricanthos (honey locust)	-	-	X	-	-	-	-	-	-	-	-	-	-
Persea borbonia (red bay)	**R**	-	-	-	-	-	-	-	-	-	-	-	-

[a]Following the same nomenclature as DeSantis et al. (2007), tree species are categorized as currently regenerating (R), relict stands (X), converted from regenerating to relict stands between 2005 and 2014 [X], observed in 2005 but absent in 2014 (L), and not present in 2005 but found to be regenerating in 2014 (**R**). Categories (L) and (**R**) were not used in DeSantis *et al*. (2007).

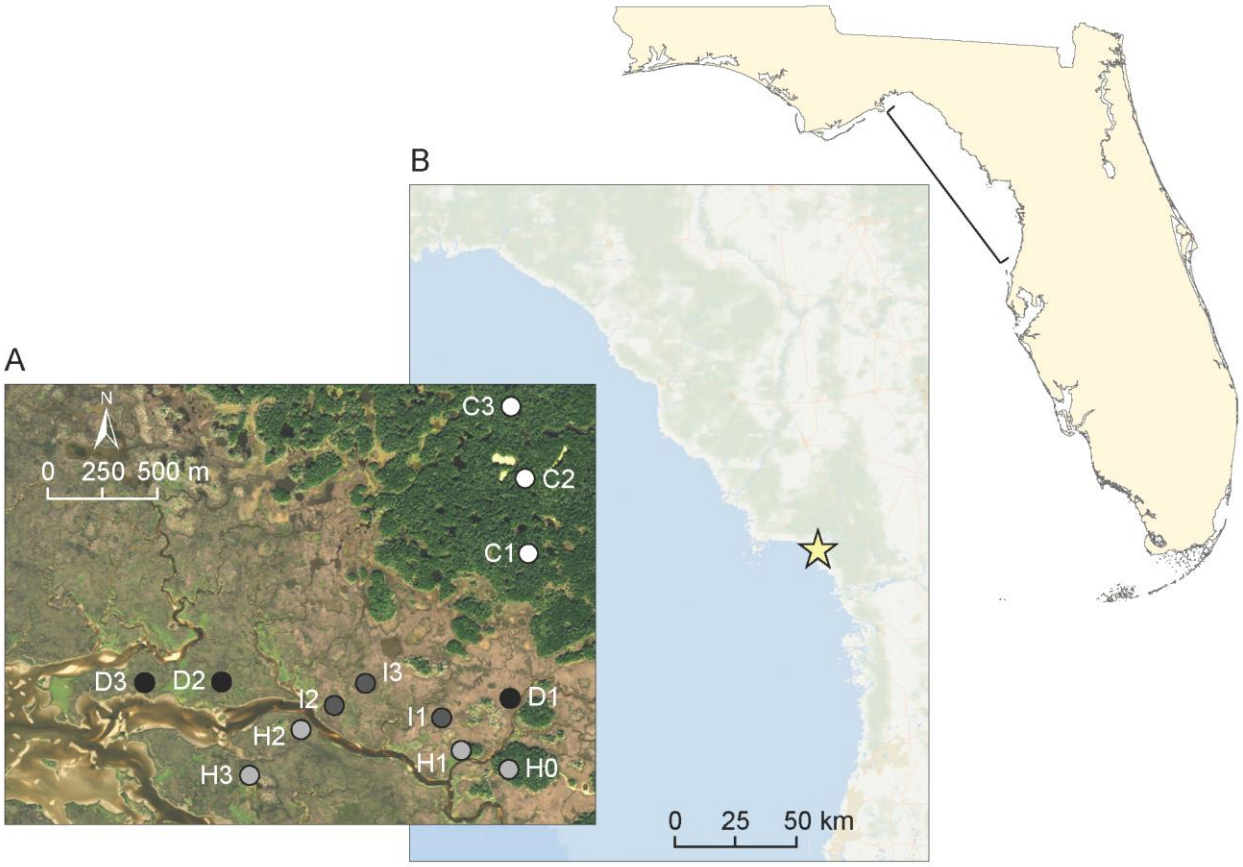

Figure 2-1. Study site at Turtle Creek on the Big Bend coast in Florida. A) Study plots along Turtle Creek are labeled by their condition in 1992 and 1993: H=healthy (light gray); I=intermediate (dark grey); D=decadent (black). C plots occur in continuous forest (white). B) Location of Turtle Creek along Big Bend coast is marked by a star.

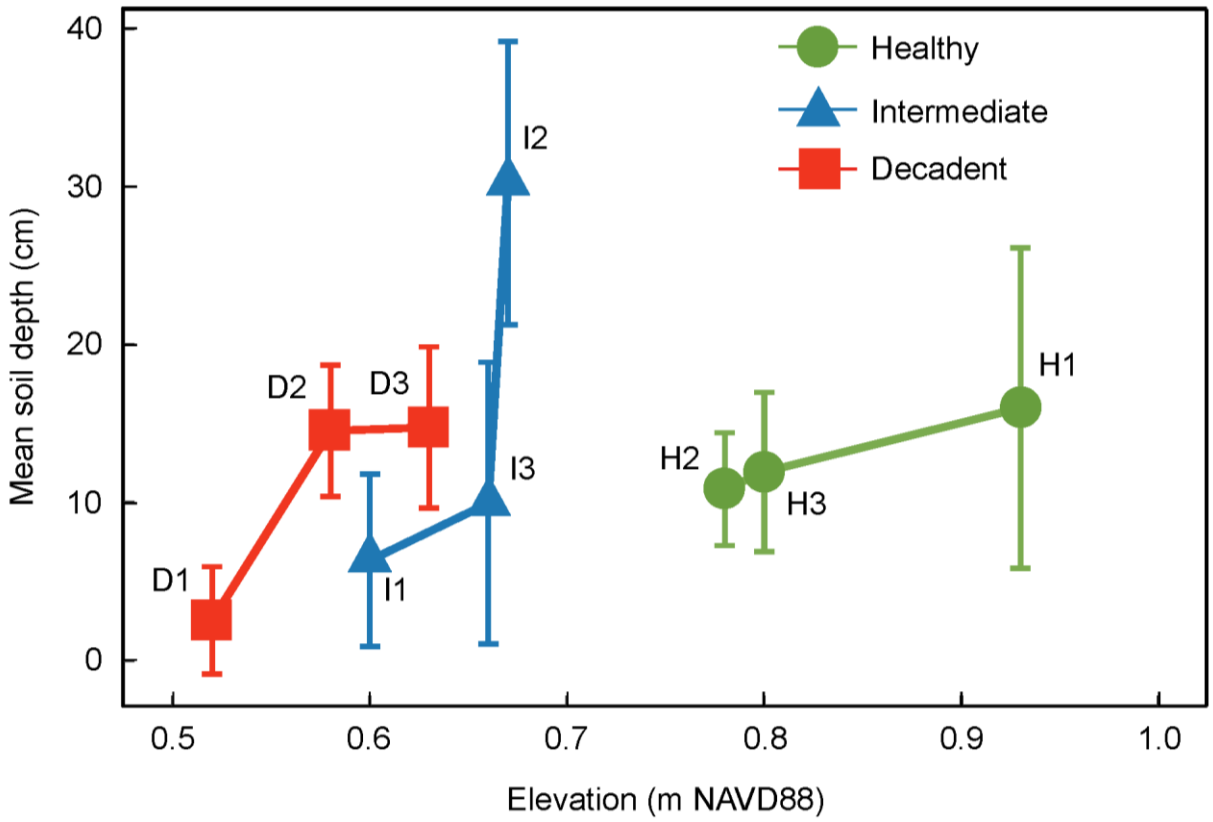

Figure 2-2. Mean soil depth (± standard deviation) across elevation for original nine plots. Soil depths are grouped by island condition as defined in 1992. Elevation data are from Williams et al. (1999a).

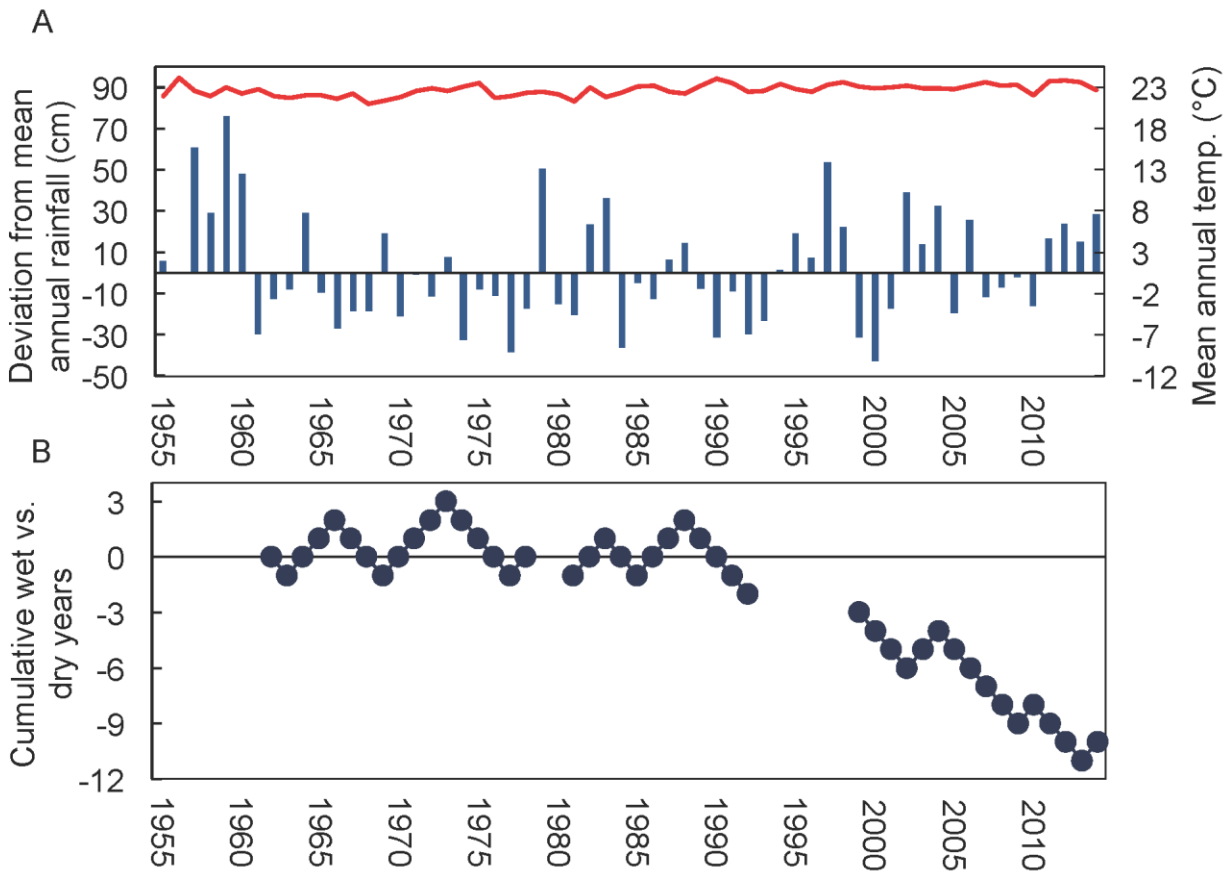

Figure 2-3. Trends in meteorological data and discharge from Waccasassa River. A) Mean annual temperature (line) and deviations from mean annual rainfall (bars) from 1955 to 2014. B) running total of cumulative years above and below long-term mean annual river discharge (horizontal line at 0) from 1963 to 2014, excluding data for which little or no data are available.

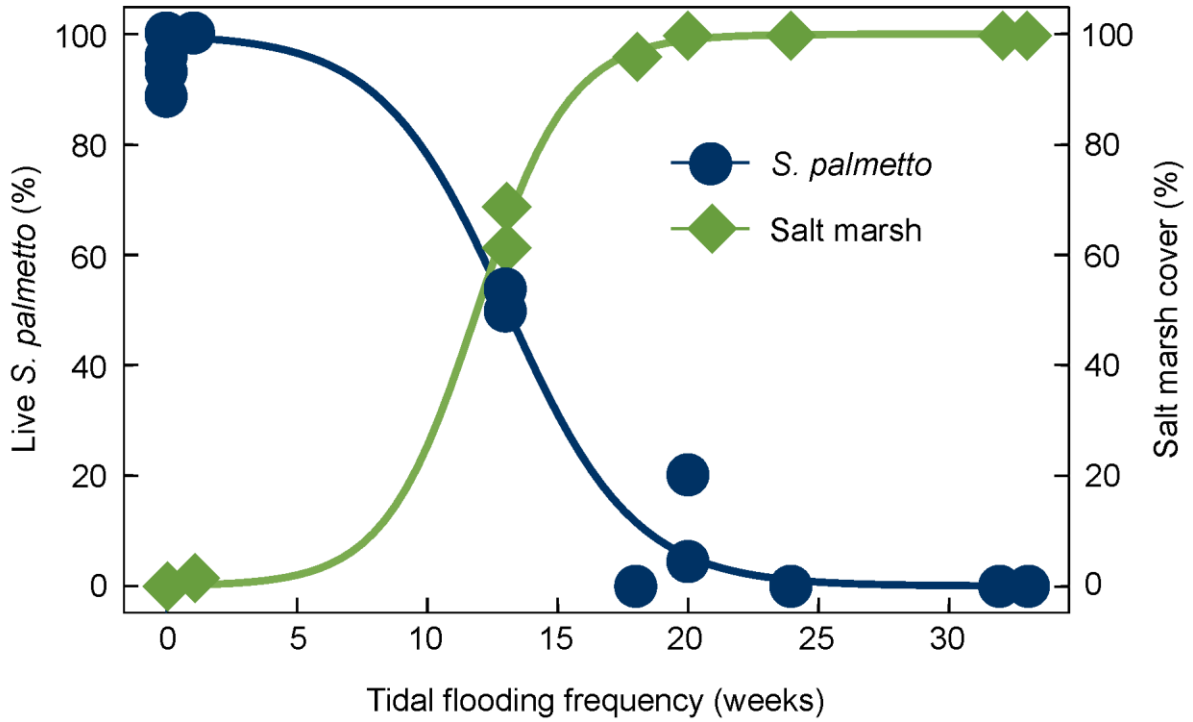

Figure 2-4. Percent of live *Sabal palmetto* of total *S. palmetto* present per plot in 2014 and percent salt marsh understory cover across a tidal flooding frequency gradient.

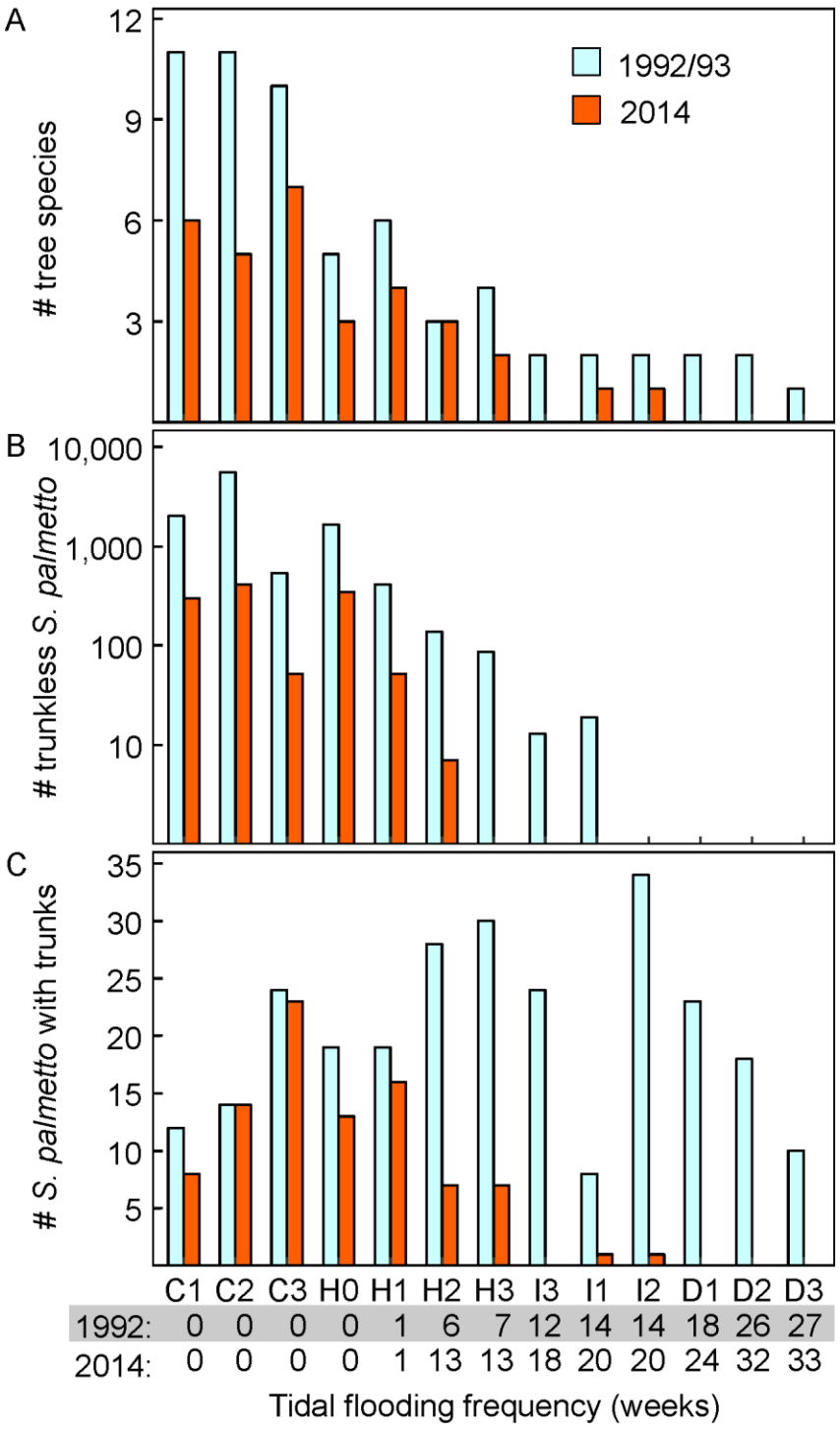

Figure 2-5. Comparison of 1992/1993 and 2014 tree census data. A) Declines in tree species richness. B) Declines in number of trunkless *Sabal palmetto* (counts shown on a log scale). C) Declines in number of live *S. palmetto* with trunks. Plots are arranged in order from low to high tidal flooding frequencies in 1992 and 2014.

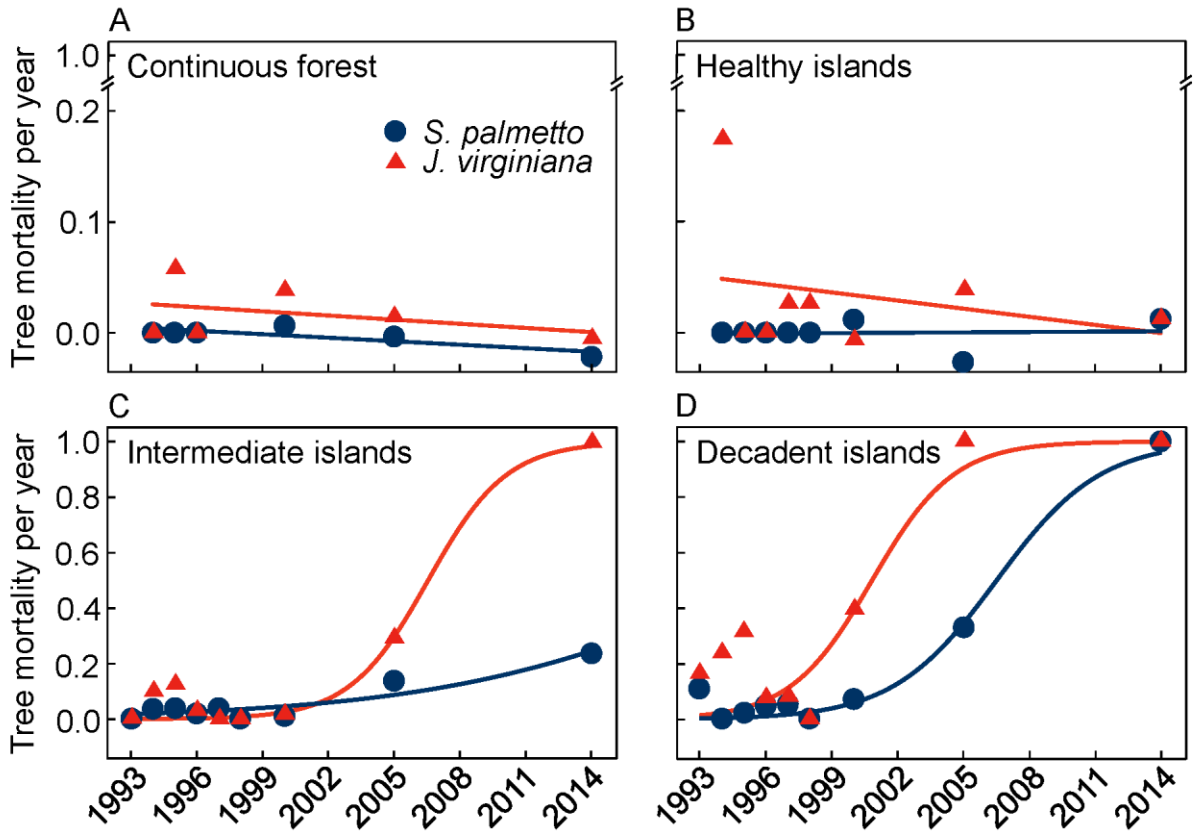

Figure 2-6. Annual mortality rates of *Sabal palmetto* and *Juniperus virginiana* trees. A) and B) show mortality in the continuous forest plots (n=3) and healthy forest islands (n=4), respectively, from 1993 to 2014 and are fitted with a simple linear model and the y-axes are scaled to make trends more visible. C) and D) show mortality in intermediate islands (n=3) and decadent islands (n=3), respectively, from 1992 to 2014 and are fitted with nonlinear logistic growth models.

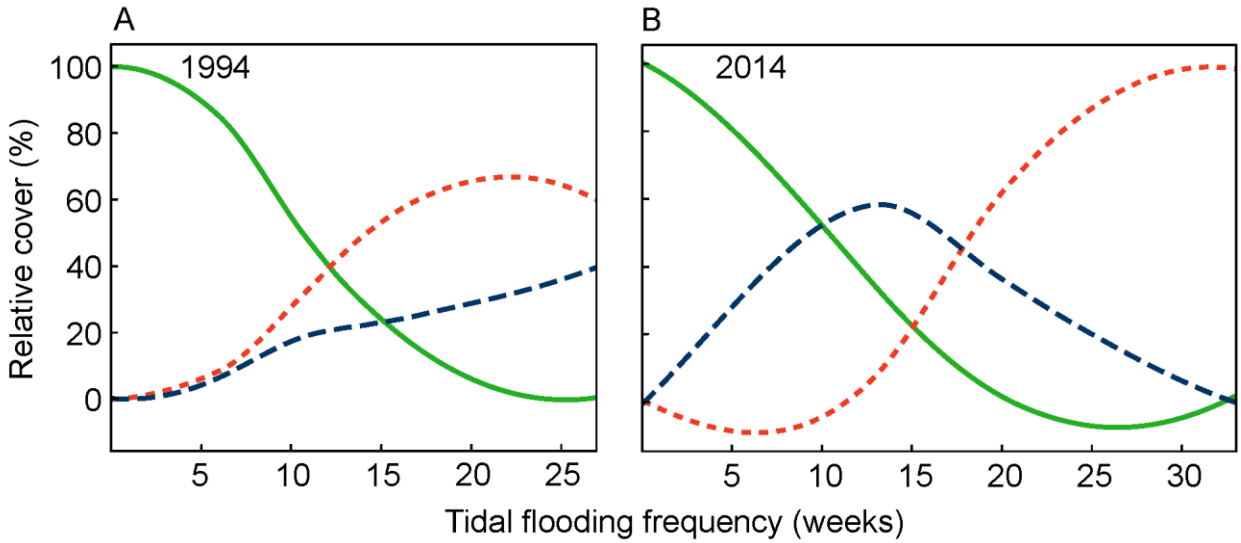

Figure 2-7. Comparison of understory vegetation type between 1994 and 2014. A) Understory vegetation across tidal flooding frequency in 1994. B) Understory vegetation across tidal flooding frequency in 2014. Increases in 2014 tidal flooding are indicated by an extended x-axis. For clarification, no forest species were present in the most flooded plots; upswinging tails are artifacts of loess smoothing.

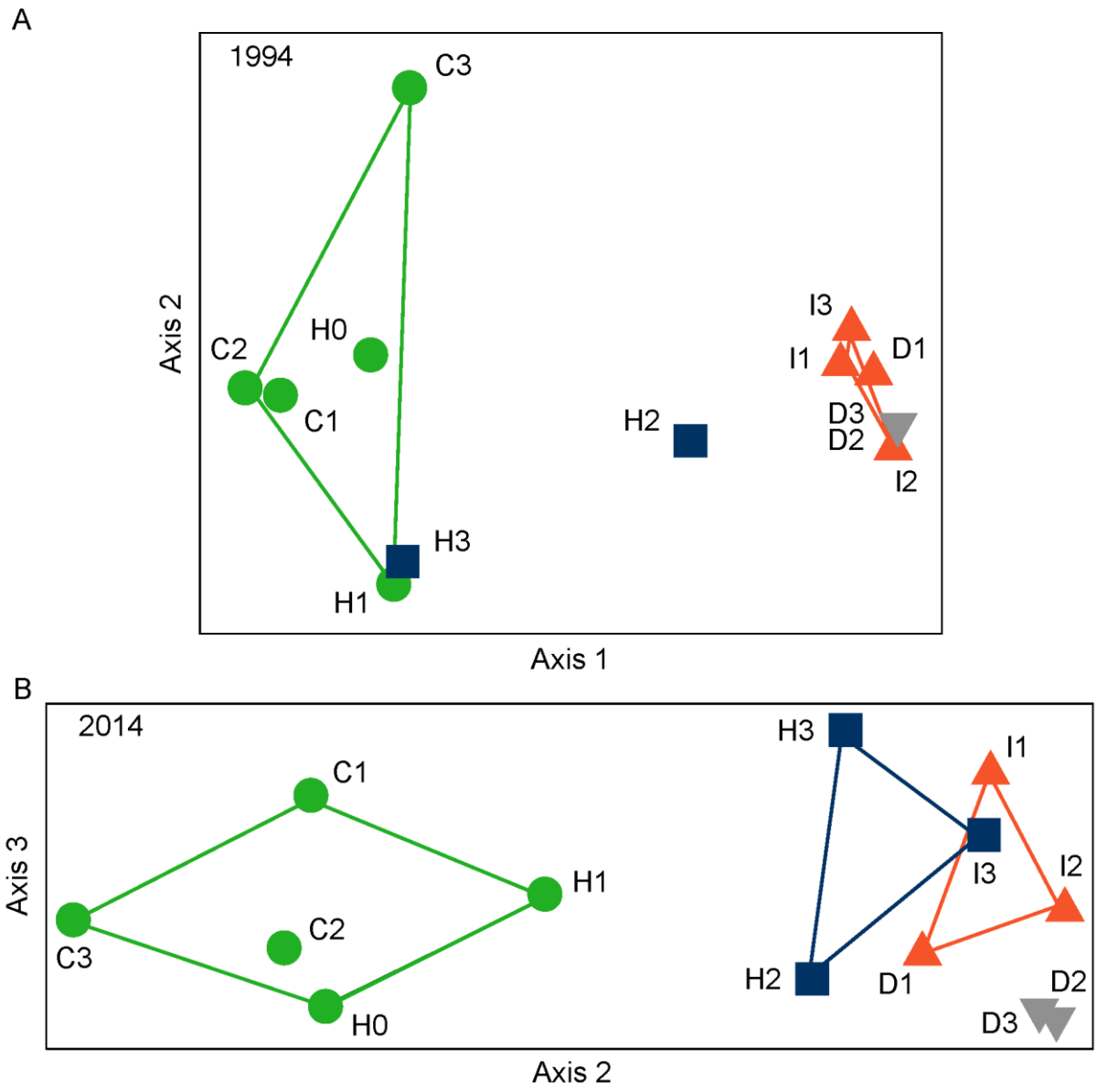

Figure 2-8. NMS solutions for 1994 and 2014 understory vegetation. Plots are grouped by flooding frequency categories. A) 1994 solution with three axes; 0-1 weeks of flooding: green circles, 2-9 weeks: blue squares, 10-19 weeks: red triangles, >20 weeks: gray inverted triangles. B) 2014 solution with 3 axes; 0-1 weeks of flooding: green circles, 2-9 weeks: blue squares, 20-29 weeks: red triangles, >30 weeks: gray inverted triangles.

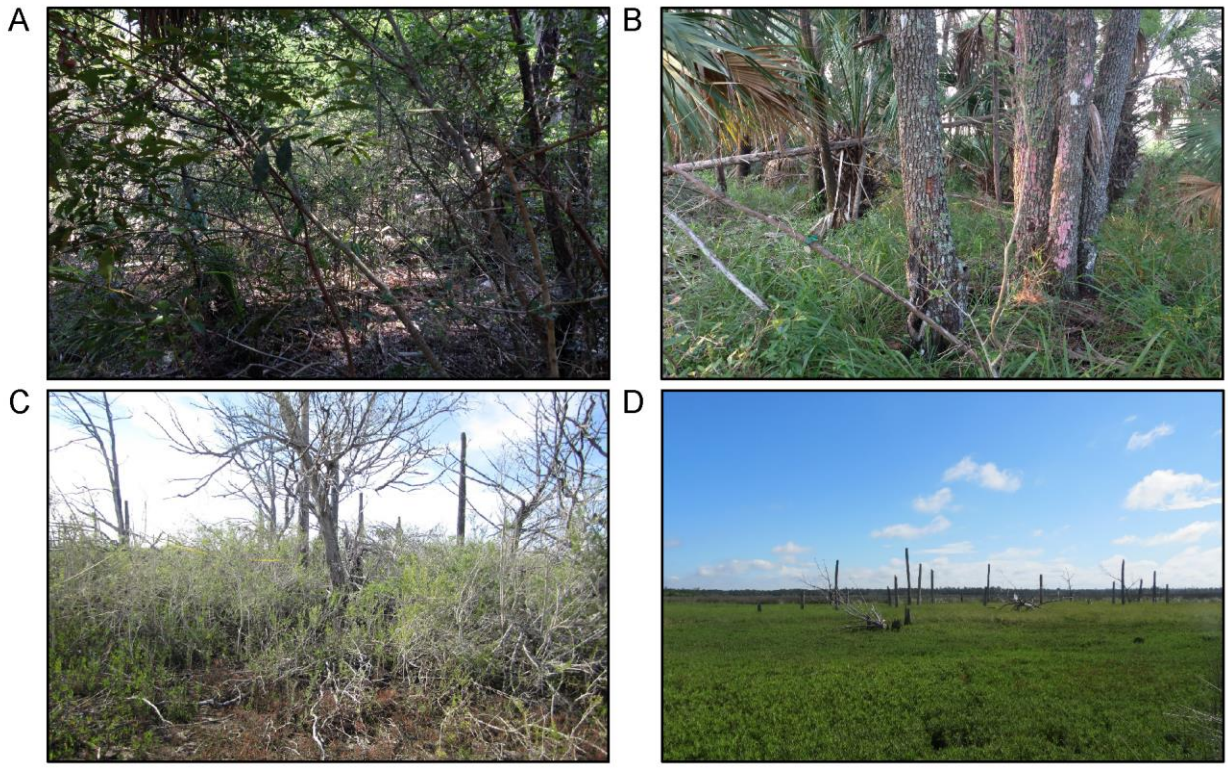

Figure 2-9. Pattern of community reassembly in coastal freshwater forest along a tidal flooding frequency gradient. A) Continuous forest supports many live trees, has reduced regeneration, understory of freshwater forest perennials and annuals. B) Infrequently flooding islands have reduced regeneration of dominant trees, understory freshwater forest, salt marsh encroaching on islands. C) Moderately flooded islands support relict forest with few live trees, understory of salt marsh shrubs. D) Frequently flooded islands have no live trees or forest regeneration, forest has converted to herbaceous salt marsh.

CHAPTER 3
PREDATION RESTRICTS BLACK MANGROVE (*AVICENNIA GERMINANS*) COLONIZATION AT ITS NORTHERN RANGE LIMIT ALONG FLORIDA'S GULF COAST

Background

Climate change is driving ecological shifts at population, community, and ecosystem scales globally, altering ecological functions via changes in habitat and species compositions (e.g., Walther et al., 2002; Parmesan & Yohe 2003; Parmesan 2006; Lancaster et al. 2016). Examples range from phenological shifts in flowering times (Fitter et al., 1995; Dunne et al., 2003; Inouye, 2008), bird migration (Møller et al., 2008; Travers et al., 2015), and butterfly migration (Sparks & Yates, 1997) to geographic shifts in floral and faunal ranges (Grabherr et al., 1994; Perry et al., 2005; Kelly & Goulden, 2008). In coastal regions, a notable geographic range shift occurring in response to climate change is the expanded coverage of mangroves into temperature latitudes.

Poleward expansion of mangroves is being observed as warming air temperatures and fewer freeze events promote suitable conditions of mangrove survival (Saintilan et al., 2014; Alongi, 2015; Kilkenny & Galloway, 2016; Ward et al., 2016; Osland et al., 2017b). Sea level rise also accommodates landward migration along undeveloped coastlines (Krauss et al., 2011; Nitto et al., 2014). Other effects of climate change, including increasing atmospheric CO_2 and changing precipitation regimes,

---

Reprinted with permission from Langston, A. K., D. A. Kaplan, & C. Angelini, 2017. Predation restricts black mangrove (*Avicennia germinans*) colonization at its northern range limit along Florida's Gulf Coast. Hydrobiologia 803: 317-331.

affect the ability of mangrove species to compete with salt marsh communities, further influencing future distributions of mangroves at temperate latitudes (McKee et al., 2012; Osland et al., 2016). With the effects of climate change becoming more pronounced at local, regional, and global scales, and mangrove ranges being historically sensitive to major abiotic shifts (Saintilan et al., 2014), considerable research is being conducted to better understand the effects of abiotic factors on future mangrove distributions. However, little work has focused on the coupled effects of bottom-up (abiotic) and top-down (biotic) controls on mangrove expansion at their temperate range limits.

In the southeastern United States, the frequency and severity of freeze events dictate periods of mangrove population expansion and contraction and, hence control mangrove coverage at the northern range limit (Lugo & Patterson-Zucca, 1977; Stevens et al., 2006; Osland et al., 2017a). Repeated extreme freezes during 1895-1905 and 1977-1989 seriously reduced mangrove coverage along the Atlantic and Gulf of Mexico Coasts (Stevens et al., 2006). Since the 1980s, recovery and expansion have yielded the greatest mangrove coverage in the northern Gulf of Mexico since at least 1893 (Osland et al., 2017a). In Florida (USA), northward mangrove migration is occurring on both Atlantic and Gulf Coasts. Along the Atlantic Coast, Cavanaugh et al. (2014) found that mangrove spatial extent has doubled since 1984, and along the Gulf Coast, Giri & Long (2016) found mangrove area had increased by 25-50% at the northern range limit since 1980.

The northern range of mangroves along the Gulf Coast of Florida occupies a stretch of coastline known as the Big Bend (Figure 3-1), a low elevation, low wave energy, and relatively undeveloped region. Three mangrove species grow along the Big

Bend: *Avicennia germinans* (black mangrove), *Rhizophora mangle* (red mangrove), and *Laguncularia recemosa* (white mangrove). However, *A. germinans* is the most common due to its higher tolerance to cool temperatures and freeze events (Osland et al., 2015). The transition zone between mangrove- and salt marsh-dominated landscapes along the Big Bend also supports coastal freshwater forests, including islands of remnant forest (hereafter, forest islands) that occur on elevation limestone substrate and are dominated by *Sabal palmetto* (cabbage palm) and *Juniperus virginiana* (southern red cedar). Many of these islands are converting to salt marsh as increased tidal flooding from sea level rise prevents tree regeneration (Williams et al., 1998; Williams et al., 1999a; Castaneda & Putz, 2007; DeSantis et al., 2007). Mangrove encroachment has the potential to modify this freshwater forest-to-salt marsh reassembly trajectory and transform temperate coastal landscapes into regions dominated by saline coastal forests characteristic of tropical and subtropical climates. Mangrove encroachment into salt marsh along the northern Gulf Coast in Texas was found to rapidly alter microclimate, sediment accretion, soil organic carbon, and other ecosystem characteristics (Guo et al., 2017). Similar changes to ecosystem functions are likely from mangrove expansion in salt marsh along the Big Bend, and may be compounded by mangroves replacing freshwater forest as the dominant forest type.

This study was prompted by out observations of *A. germinans* seedlings naturally establishing in salt marsh vegetation positioned along creek edges near transitioning forest islands. These observations motivated three initial hypotheses: 1) *A. germinans* could also establish in forest islands, potentially modifying the forest-to-salt marsh trajectory currently in progress; 2) abiotic factors, particularly tidal flooding frequency,

would dictate *A. germinans* colonization success in forest islands; 3) *A. germinans* establishment success would be similar in islands with sufficient flooding and in surrounding *Juncus roemerianus* (black needle rush) marsh, and would be higher at creek edges. Creek edges most closely resemble lower elevation, cordgrass-dominated (*Spartina alterniflora*) creek bank habitats where *A. germinans* colonization has been observed in northern Gulf Coast marshes (Patterson et al., 1997; McKee & Rooth, 2008). After discovering high rates of propagule predation by grapsid crab, *Sesarma reticulatum* (purple marsh crab) during our initial experimental deployment, we expanded the study to quantify top-down biotic controls on *A. germinans* colonization through measurements of propagule predation and seedling herbivory.

In tropical regions, propagule predation and herbivory have been investigated extensively to explain regeneration success within mangrove forests, zonation patterns of co-occurring mangal species, and establishment success of mangroves into adjacent habitat (Smith, 1987; Smith et al., 1989; Osborne & Smith, 1990; McKee, 1995; Farnsworth & Ellison, 1997; Dahdouh-Guebas et al., 1998; Sousa & Mitchell, 1999; Bosire et al., 2005; Cannicci et al., 2008). *Avicennia* are especially susceptible to top-down pressure in the form of propagule predation due to their soft, fleshy cotyledons that lack a protective coat, relatively high nutrition content, relatively low concentrations of herbivore-deterring compounds, and small size (Smith, 1987; McKee, 1995). These features make them palatable to a variety of fauna including crabs, snails, insects, mammals, and fish (Smith et al., 1989; Steele et al., 1999; Sousa et al., 2003). As seedlings and adults, *Avicennia* like other mangals, are susceptible to herbivory by insects and crabs that consume leaves, flowers, and woody tissue, which can lead to

defoliation, reduced growth rates, and limited propagule production (Cannicci et al., 2008). However, the roles of propagule predation and seedling herbivory in mediating range expansion of *A. germinans* in the northern Gulf of Mexico have not previously been addressed. Here we present our findings on the effects of both bottom-up and top-down controls on *A. germinans* expansion in a region where abiotic conditions are usually considered the primary drivers of mangrove colonization.

Materials and Methods

Experimental Setting

Manipulative field experiments were conducted along Turtle Creek, a tidal creek in Waccasassa Bay Preserve State Park, located along the Big Bend coast of Florida (Figure 3-1). The study area comprises a mosaic of salt marsh and forest islands in various stages of health, ranging from healthy, regenerating tree stands to relict stands now dominated by salt-tolerant shrubs, forbs, and grasses. Continuous freshwater forest dominated by *S. palmetto* and *J. virginiana* and upland pine flatwoods occur landward of the study area (Vince et al., 1989; Williams et al., 2007b), and an established population of *A. germinans* is located seaward along the coastal fringe, approximately 3 km to the southwest. Propagules from *A. germinans* float into Turtle Creek and wash up on creek banks, and small stands (<25 m^2) of short (<1 m tall) mangroves are also scattered throughout the marsh.

We established three sites along Turtle Creek, each including a forest island. The sties are approximately 0.7 km apart and are referred to by the relative frequency of tidal flooding each island receives: frequently flooded, moderately flooded, and rarely flooded, based on frequencies reported in Williams et al. (1999a). Flooding frequencies in the marshes surrounding each island are approximately the same between sites. The

frequently flooded island is a relict forest (non-regenerating) with no live trees and has converted to herbaceous salt marsh. The moderately flooded island supports few live trees and has a mixed understory of halophytic shrubs and herbaceous salt marsh plants. The rarely flooded island supports healthy, regenerating forest with an understory of typical coastal freshwater forest vegetation. Islands at all three sites are surrounded by salt marsh dominated by *J. roemerianus*. Along the creek edge, vegetation is dominated by *S. alterniflora* and also includes other plants common in high marsh: *Distichlis spicata* (salt grass), *Salicornia* sp. (glasswort), and *J. roemerianus*.

Experimental Design

At each site, we tested propagule survival and seedling establishment in four landscape positions: island interior, island edge, marsh plain, and creek edge. We selected island interior positions representative of the overall island habitat and island edge positions that were on the creek side of the islands. Marsh plain positions were located between island edge and creek edge positions. Creek edge positions were within 1 m of the creek bank slope. We calculated tidal flooding frequencies (number eof weeks during which flooding occurred over the course of the experiment) in forest island interiors and edges using a model developed by Williams et al. (1999a) specifically for these islands. The model requires elevation data, which we obtained for island interiors from Williams et al. (1999a) and estimated for island edges using 2007 Light Detection and Ranging (LiDAR) data for Levy County, downloaded from the NOAA Digital Coast website (http://coast.noaa.gov/digitalcoast/). For marsh plain and creek edge positions, tidal flooding was assumed to occur daily during high tide based on observations made during the monitoring visits and previous field work in the area.

In addition to tidal flooding frequency, we quantified soil salinity, soil depth, percent cover of plant species, and crab burrow density for all landscape positions at each site. Soil salinity was measured from five soil samples collected in June 2016 at each landscape position at each site. Samples were air dried for 12 days, then oven dried at 40 C for 3 days, sieved, and analyzed using the saturated paste method (Rhoades, 1996; Reddy et al., 2013) with a 1:5 soil weight per DI water volume ratio. Salinity of the soil slurry was measured using a conductivity meter (Thermo Scientific Orion Star A215). Soil depth was measured at 10 random locations by inserting a pin flag into the soil until it made contact with underlying limestone bedrock, then measuring the length that was inserted with a metric ruler. Percent cover of plant species was measured in four 1-m^2 quadrats. We counted *S. reticulatum* burrow density as a proxy for herbivorous crab density within eight randomly placed 0.25-m^2 quadrats. *Sesarma* burrows were identified by features described by Bertness et al. (2009).

The initial experimental deployment consisted of placing 10 non-caged *A. germinans* propagules approximately 25 cm apart in four 0.25-m^2 plots in each of the four landscape positions, for a total of 16 plots per site and 48 plots total. Propagules were set out in October 2015 and had hypocotyls extending 0-1 cm. Plots were marked at each corner with a flag and had no physical barriers separating them from the surrounding area. We planned to count the number of propagules present and record propagule fate approximately every 2 weeks in each landscape position at each site; however, during the first monitoring event on day 12, we observed 99% propagule predation. Based on this finding, the non-caged experiment terminated and the caged experiment was initiated.

To determine the relative importance of landscape position and flooding frequency on propagule and seedling fates, we attempted to control for *S. reticulatum* predation by placing propagules in cylindrical cages (20 cm height, 10 cm diameter) made of galvanized steel cloth (0.6-cm^2 mesh). Each cage was placed on top of a square of steel cloth buried in the soil and covered by another square of steel cloth secured to the top of the cage with zip ties. Cages were anchored in place with landscape stakes. Ten cages were placed in each landscape position. We placed one propagule each in five cages and fives propagules each in the remaining five cages to additionally test for density effects on propagule establishment, survival, and growth. Given observations of equivalent predation and propagule viability across density treatments, data for all caged propagules were later pooled, resulting in n=30 propagules per landscape position per site. Propagules were placed in the cages in December 2015 and typically had hypocotyls extending between 1 and 3 cm but had no budding roots. All propagules used in caged and non-caged experiments were collected from the established mangrove forest southwest of Turtle Creek (Figure 3-1) and had already dropped from parent trees. Only propagules with no signs of predation or decay were used.

Fates of caged propagules were recorded on days 2, 7, 15, 32, 54, 78, 100, 140, and 200 of the experiment, a period spanning from December 2015 to June 2016, as the propagules developed into seedlings. On each monitoring date, propagules were assigned one of the following fates (Figure 3-2a-d); viable [including viable propagules with predation damange (i.e., hypocotyl and cotyledons intact but with grazing scars or <50% of cotyledons consumed)], total predation (i.e., non-viable propagules, defined as

>50% cotyledons consumed and/or the hypocotyl missing or cut through), missing (counted as total predation), desiccated, or rotted. Desiccated and rotted propagules lacked apparent predation damage and were assumed to be non-viable due to unfavorable abiotic conditions. Viable propagules included all those that became established seedlings over the course of the caged experiment. A propagule was considered an established seedling when it rooted in the ground and supported upright cotyledons. As propagules developed into established seedlings, they remained caged through day 200, during which we continued to record their fates over time. Seedling fates were determined by visually inspecting leaves and stems for signs of damage and consisted of no herbivory, mild herbivory (damage to leaves), moderate herbivory (damage to leaves and stems), and fatal herbivory, defined by the entire aboveground portions of seedlings missing or seedlings uprooted with some portion of leaves and/or stems missing (Figure 3-2e-h). Cause of mortality was recorded as “undetermined” for propagules and seedlings with no apparent signs of damage or with damage from multiple sources. We also recorded the height of each seedling at each visit. Metrics for comparing colonization success between landscape positions included percent of live, established seedlings, rate of seedling establishment, and seedling growth. On day 200, all cages were removed, and seedlings in five-propagule cages were thinned so that only the single, healthiest seedling remained; live seedlings in one-propagule cages were left intact. All other seedlings and non-viable propagules were discarded. Remaining propagules were monitored in July 2016 (day 232) and in December 2016 (day 372), during which fate and seedling height were recorded.

Data Analysis

We analyzed the effects of flooding frequency and landscape position on soil salinity, soil depth, percent cover of salt marsh vegetation (i.e., all halophytes), and burrow density using analysis of variance and Tukey's HSD for post hoc multiple comparisons. Fates of caged propagules and seedlings were compared by landscape position at each site using Pearson's χ^2 tests. Because propagule survival was confounded by inconsistent caging effectiveness, we combined viable and predation fates in our statistical analysis of abiotic controls on propagule survival. Additionally, mild and moderate herbivory on seedlings were combined for analysis. We assessed the correlation between caged propagule predation and burrow density using univariate linear regression. To correct for an increased change of Type I error from multiple ANOVA and χ^2 tests, we compared *p*-values to α=0.0167, instead of a standard α=0.05.

Heights of caged seedlings between monitoring intervals were compared using a repeated measures, mixed model ANOVA, with site and landscape position set as fixed effects. Because differences in seedling establishment times and mortality created variation in sample sizes between time intervals and overdispersion in the data within landscape positions, the ANOVA model was a poor fit. Therefore, we analyzed the dataset using ANOVA and Tukey's HSD in separate analyses for each site and sampling interval. The effects of environmental variables and burrow density on the survival of pooled post-cage removal seedlings were evaluated using multiple regression. All statistical analyses were performed in R (R Core Team, 2017).

Results

Characteristics of Landscape Positions Across Sites

At the frequently flooded site, model estimates indicated that tidal flooding occurred during every week of the caged experiment (28 weeks) in the island interior and island edge. At the moderately flooded site, tidal flooding occurred during 21 weeks in the island interior and 23 weeks at the island edge. At the rarely flooded site, no flooding occurred in the island interior during the caged portion of the experiment (though a hurricane flooded the island interior in September 2016), and the island edge flooded during 23 weeks. Marsh plain and creek edge positions at all sites were assumed to have flooding events during every week at all three sites.

Between landscape positions, soil salinity varied least at the frequently flooded site and most at the rarely flooded site (Figure 3-3a). At the frequently flooded site, mean conductivity range from 6.8 to 11.5 mS/cm. At the moderately flooded site, mean conductivity ranged from 6.0 to 12.7 mS/cm and only differed with regard to the marsh plain, which was more saline than the island interior and edge ($F_{3,12} = 5.39$, *p*-value = 0.014). At the rarely flooded site, conductivity was lowest in the island interior (1.9 mS/cm) and highest along the island edge (9.4 mS/cm), which was similar to conductivity in the marsh plain and creek edge ($F_{3,12} = 14.77$, *p*-value = 0.0002). Soil depths followed a general pattern across sites, with deeper soils occurring at the creek edge and marsh plain and shallower soils occurring in the island interiors and edges (Figure 3-3b), as expected based on differences in sediment delivery driven by tidal flooding frequency and distance from creek. Creek edge and marsh plain soil depths ranged from an average of 28.5 to more than 45 cm and were two to three times deeper across all sites than island interior and edge positions, which ranged from an average of

12.4 to 30.4 cm (p-value < 0.0001); differences in soil depths between island interior and edge positions were only significant at the moderately flooded site ($F_{3,36}$ = 106.8, p-value < 0.0001). Both the frequently and moderately flooded sites were characterized by a predominance (>50%) of salt marsh vegetation across all landscape positions (Figure 3-3c). At the rarely flooded site, salt marsh cover dominated the creek edge, marsh plain, and island edge positions, but was significantly reduced in the island edge where total vegetation cover was only 10%, of which, 8% was salt marsh vegetation, and was absent in the island interior ($F_{3,12}$ = 578.7, p-value < 0.0001).

Sesarma reticulatum burrows were present everywhere except the interior of the rarely flooded island, demonstrating the wide distribution of *S. reticulatum* across sites (Figure 3-3d). At the frequently flooded site, mean burrow density ranged from 22.5 to 35.5 m^{-2} and was not significantly different between landscape positions ($F_{3,28}$ = 1.46, p-value = 0.25), likely due to similarities in tidal flooding and vegetation cover across the relatively homogeneous, low-elevation site. At the moderately flooded site, mean burrow densities in the marsh plain and creek edge were more than twice as high (32 m^{-2}) as in the island edge and interior (9-13.5 m^{-2}), given more frequent flooding and deeper soil depths more characteristic of salt marsh closer to the creek ($F_{3,28}$ = 19.3, p-value < 0.0001). Burrow densities were most variable at the rarely flooded site, where burrow density increased from 0 in the island interior to 41 m^{-2} in the creek edge ($F_{3,28}$ = 26.3, p-value < 0.0001).

Biotic Pressure on Non-Caged Propagules

Non-caged propagules experienced extremely low survival (<1%) regardless of site or landscape position after 12 days, providing a measure of ambient predation pressure. We identified predation by *S. reticulatum* as the primary cause of

disappearance based on the moderate to high crab burrow density present across sites and landscape positions (with the exception of the island interior of the rarely flooded site), and video footage of *S. reticulatum* taking a propagule and pulling it into a burrow that we recorded during a separate experiment at the site. Propagule disappearance in the island interior of the rarely flooded site was likely depredation by other fauna such as small mammals or wild boars, which are present on regenerating forest islands, though we were unable to confirm this assumption.

Caging Experiment: Propagule Establishment Success and Seedling Growth

Over the course of the experiment, we observed crab burrows appearing inside cages, indicating that caging did not completely exclude propagule predation by *S. reticulatum*. Soil disturbance from crab burrowing and tidal flooding likely shifted cages, creating gaps between cage sides and bases through which *S. reticulatum* could burrow. The single caged propagule that was depredated in the island interior of the rarely flooded site was assumed to be consumed by a small predator other than *S. reticulatum*. Despite the susceptibility of caged propagules to predation, more than 50% developed into established seedlings (i.e., were viable; Figure 3-4). In island interiors of the frequently and moderately flooded sites, confirming our initial hypothesis that *A. germinans* could successfully establish in forest islands and our second hypothesis that establishment requires sufficient tidal flooding.

When we disregarded predation due to the confounding results of inconsistent caging effectiveness, we found that the fate of caged propagules depended on landscape position at the frequently flooded site ($\chi^2 = 35.7$, p-value < 0.0001), where rot and undetermined causes of mortality reduced viability in the island interior by 20% and

creek edge by 37%. Landscape position was also important at the rarely flooded site (χ^2 = 112.5, *p*-value < 0.0001), where desiccation prevented propagule survival in the island interior, further demonstrating propagules' reliance on adequate tidal flooding. At the moderately flooded site, non-predation causes of mortality were low and consistent across landscape positions ((χ^2 = 5.44, *p*-value = 0.49). Across sites, seedling establishment at creek edge positions was not higher compared to other positions, contrary to our hypothesis. Overall seedling establishment on day 200 was correlated with more frequent tidal flooding and salt marsh vegetation cover and decreased with deeper soils and higher burrow density, but was not affected by soil salinity ($F_{5,90}$ = 28.3, *p*-value < 0.0001, r^2 = 0.59).

Rates of seedling establishment varied over time between landscape positions at all three sites (Figure 3-5). Of note, there was a consistently low rate of seedling establishment at the frequently flooded site creek edge (Figure 3-5a). At the moderately flooded site, establishment rates were similar among positions over time until days 140-200, when 37% of seedlings in the island interior suffered mortality (Figure 3-5b). At the rarely flooded site, a similar mortality event caused 90% of seedling mortality in the creek edge position between days 140-200 (Figure 3-5c), and establishment rates were generally lower than at other sites, with no seedling establishment in the island interior.

As propagules matured into seedlings, mild to moderate herbivory was common across sites and occurred in all landscape positions where seedlings established (Figure 3-6). Notwithstanding mild and moderate herbivory, >50% of caged seedlings were alive on day 200 in all landscape positions at all sites, except along the creek edge of the rarely flooded site where only one seedling established. Seedling fate depended

on landscape position at both the frequently flooded ((χ^2 = 40.2, *p*-value < 0.0001) and rarely flooded ((χ^2 = 28.8, *p*-value < 0.0001) sites, and varied strongly (nearly significantly) between positions at the moderately flooded site ((χ^2 = 15.4, *p*-value = 0.017 vs. α = 0.0167). At the frequently flooded site, seedlings with no signs of herbivory were most common in the marsh plain. Non-fatal herbivory exceeded 90% in the island interior and edge, and 22% of seedlings suffered mortality due to herbivory in the creek edge. At the moderately flooded site, herbivory was most intense in the island interior and fatal herbivory decreased from the island interior towards the creek edge. At the rarely flooded site, fatal herbivory was highest in the creek edge (71%) where only one seedling survived. Growth rates of caged seedlings increased in all landscape positions at all sites through March (Figure 3-7). When the seedlings began outgrowing their cages in April, moderate and fatal herbivory began to confound growth rates and affect seedling heights. In general, seedlings at the frequently flooded site were significantly taller in the creek edge than in other landscape positions by June ($F_{3,58}$ = 13.5, *p*-value < 0.0001; Figure 3-7a) and were taller in the marsh plain and creek edge than island interior or edge at the moderately flooded site ($F_{3,46}$ = 14.6, *p*-value < 0.0001; Figure 3-7b). At the rarely flooded site, in contrast, seedlings in the island edge consistently grew more than seedlings in other landscape positions ($F_{2,16}$ = 38.9, *p*-value < 0.0001; Figure 3-7c) and by June, had also outgrown seedlings at the other sites.

Seedling Survival and Growth After Cage Removal

Post-cage removal, seedling survival declined between June and December 2016 in all landscape positions of all three sites where seedlings had established

(Figure 3-8a, c, e). Fatal herbivory caused declines in seedling survival through July; causes of mortality were harder to determine in December because missing seedlings in the creek edge and marsh plain positions could have resulted from herbivory or Hurricane Hermine in September 2016. The number of surviving seedlings by December was not correlated with burrow density or any environmental variable ($F_{5,5}$ = 2.8, *p*-value = 0.15). Seedling heights were similar between landscape positions at the frequently flooded and moderately flooded sites, except in the island interior of the moderately flooded site where the short height of the single surviving seedling resulted from moderate herbivory (Figure 3-8b, d). At the rarely flooded site, only seedlings in the island edge survived to December, which continued to grow faster than all other seedlings at all other landscape positions and sites (Figure 3-8f). The large standard deviation was due to recent herbivory observed in December on one of the seedlings (the top portion of the plant was on the ground) that reduced its height from 100 to 37 cm.

Discussion

We found that top-down biotic pressure exerted significant control over *A. germinans* propagule and seedling survival, establishment, and growth from creek edges to forest island interiors across a range of tidal flooding regimes. In the absence of caging, propagules suffered nearly 100% predation. *Sesarma reticulatum* was the primary predator, but propagules in the island interior of the rarely flooded site, where *S. reticulatum* burrows were absent, also suffered intense predation, likely by small mammals or wild boars. Herbivory also decreased survival of established seedlings. Caging reduced but did not exclude predation on propagules or herbivory on seedlings as they grew to cage capacity. Soil disturbance from tidal flooding and burrowing activity

(by *S. reticulatum* and other crab species present in the area, including *Uca* spp., which do not consume propagules) likely shifted the sides of cages off their bases, creating subsurface gaps through which *S. reticulatum* could access propagules. Soil disturbance is likely most intense in creek edge positions due to stronger effects of tidal flooding and generally higher burrow densities (Figure 3-3), which may explain high predation rates on caged propagules in that landscape position.

Where caging successfully prevented predation, propagules were able to survive in forest islands and develop into seedlings, provided there was sufficient tidal flooding, as hypothesized. Only in the rarely flooded island interior, where propagules suffered desiccation in the absence of tidal flooding during the experiment, did abiotic conditions exert greater pressure on caged propagules than did top-down biotic controls (Figure 3-4). Rot and undetermined cause(s) of mortality reduced propagule survival in other landscape positions at each site, and resulted in significant differences in propagule viability between landscape positions at the frequently flooded site, but no clear pattern emerged across sites that could be explained by differences in landscape position characteristics.

Relatively fast rates of seedling establishment in the island interior and edge of the frequently flooded site suggest that conditions at these landscape positions might be more favorable than in the surrounding marsh, though slower establishment in the marsh plain did not result in lower total establishment compared to other positions at the three sites (Figure 3-5). Unfortunately, the inconsistent exclusion of *S. reticulatum* from cages undermines our ability to clarify the relationships between increased seedling establishment and increased flooding, salt marsh vegetation, and decreased soil depth

and burrow density across all positions and sites. Consequently, it is unclear from these results whether sufficiently flooded forest islands provide bottom-up conditions that support *A. germinans* colonization success at rates similar to the surrounding marsh or whether creek edges, in the absence of predation, provide more (or less) favorable abiotic conditions for seedling establishment compared to other landscape positions.

Ambient predation intensity observed at the frequently, moderately, and rarely flooded sites is comparable to *Avicennia* propagule predation reported in tropical and subtropical mangrove forests: 72% of *A. germinans* propagules were non-viable from predation within 4 days in south Florida (Smith et al., 1989); 60% of *A. germinans* propagules were depredated within 9 days in Belize (McKee, 1995); 100% of *A. marina* propagules in northern Australia were consumed within 20 days (McGuinness, 1997); and 98-100% of *A. schaueriana* propagules were consumed within 18 days in Brazil (Souza & Sampaio, 2011). Among the more extreme cases, 100% of 200 *A. marina* propagules were non-viable from predation within 60 minutes in Kenya (Van Nedervelde et al., 2015). Whether intense predation pressure and generally high burrow densities of *S. reticulatum* along Turtle Creek are representative of other potential mangrove colonization areas along the Big Bend requires further investigation. Critically, studies investigating *A. germinans* colonization in temperate regions focus largely on abiotic drivers (Stevens et al., 2006; McKee & Rooth, 2008; Comeaux et al., 2012; Osland et al., 2013; Cavanaugh et al., 2014; Saintilan et al., 2014). The nearest study conducted in a similar habitat that addressed predation took place in Louisiana, where Patterson et al. (1997) found only 11% mortality of *A. germinans* from propagule predation [by *S. cinereum* and *Littoraria irrorata* (snail)] in a *Spartina*-dominated marsh, suggesting there

may be significant spatial variability in predation pressure across the northern mangrove range limit.

Propagules that survived predation continued to face mild to intense herbivory as seedlings (Figure 3-6). Seedling mortality from herbivory was not as prevalent as crab predation of propagules, though most seedlings suffered some degree of herbivory. *Sesarma reticulatum* may have contributed to seedling herbivory by continuing to consume fleshy cotyledons of young seedlings. Then, as seedlings matured and produced true leaves, insects most likely replaced crabs as the main seedling consumers, limiting survival and growth (Figure 3-7). Insects are important herbivores in mangrove forests, affecting all stages of tree development (Robertson et al., 1990; Sousa et al., 2003; Minchinton, 2006; Cannicci et al., 2008). We suspect that grasshoppers were responsible for most seedling herbivory at our study site, as they are common grazers of *J. roemerianus* in marshes along the Gulf Coast (Parson & De La Cruz, 1980; Sparks & Cebrian, 2015) and were present in spring 2016 when seedlings were leafing out.

In addition to top-down biotic controls, competition with salt marsh may have also affected seedling growth. Seedlings grew best at the edge of the rarely flooded island, appearing healthier and developing faster than all seedlings at the frequently and moderately flooded sites. This was most apparent at the end of the caging experiment (April-June; Figure 3-7) and post-cage removal (Figure 3-8). The tallest seedling (115 cm) had developed visible pneumatophores by December 2016 (day 372). Salt marsh vegetation cover was much lower than at all other landscape positions where seedlings established (Figure 3-3c), suggesting these seedlings may have faced less pressure

from competition with salt marsh plants. Patterson et al. (1993) and McKee & Rooth (2008) found that growth rates of *A. germinans* decreased in the presence of *S. alterniflora*, and Guo et al. (2013) found that biomass of *A. germinans* seedlings was lower when grown adjacent to salt marsh plants, all of which were attributed to resource competition. However, other studies have found that salt marsh plants can benefit seedling establishment (Lewis & Dunstan, 1975; McKee et al., 2007). Further work is needed to better understand the role of competition as an additional biotic control on mangrove range expansion.

This study demonstrates that as remnant forest islands convert to salt marsh and become more suitable for mangrove colonization, they also become more suitable for fauna that commonly regulate mangrove populations. *Sesarma reticulatum* is common in salt marshes in the eastern and southeastern U.S. (Holdredge et al., 2009), and grapsid crabs are among the most pervasive and intensive propagule predators wordwide (Smith et al., 1989; McGuinness, 1997; Van Nedervelde et al., 2015). Though not observed depredating propagules at Turtle Creek, snails and salt marsh insect grazers may also become common fauna in relict islands, creating additional potential predation pressure on propagules and seedlings as islands convert to salt marsh. The flooding regime of the marsh and transitioning islands along Turtle Creek may also contribute to predation intensity. Time between daily tidal inundation is greater than the period of time in which the marsh, including creek edge, is flooded (personal observation) and transitioning forest islands are more often not flooded than flooded. Time between flooding events could allow plenty of opportunity for foraging, a

hypothesis posed by Osborne & Smith (1990) to explain higher predation in high versus low intertidal zones in Australia.

As the effects of climate change drive increased tidal flooding and fewer freeze events in the region, favorable habitat for mangrove colonization will increase in the northern Gulf of Mexico and U.S. Atlantic Coast. However, our findings suggest that natural colonization of persisting and encroaching mangrove populations will require high propagule density to overcome biotic pressure. Currently, natural propagule density along Turtle Creek is relatively low (which we mimicked in our study), and crab densities were sufficiently large to prevent propagule establishment in non-caged experiments. Delivery of high densities of propagules from coastal storms may be required to sustain encroaching mangrove populations, and we are currently working to identify propagule density thresholds (if present) required to overcome predation pressure. Critically, the long-term persistence and expansion of mangrove populations in any location will be driven by the interactive effects of environmental variables (sea level rise, stochastic freeze events, coastal storms) and biotic controls (propagule density, predation, competition). Thus, both bottom-up and top-down drivers need to be considered when projecting future mangrove range expansion.

As sea level rises and global warming accelerates, more coastal habitat will become suitable for mangrove colonization. Along the Big Bend coastline in the northern Gulf of Mexico, we showed that forest islands that are currently transitioning to salt marsh and adjacent marsh landscapes can also support *A. germinans* colonization. The current freshwater forest-to-marsh trajectory may be thus modified to include the eventual replacement of a freshwater forest community by a mangrove community,

shifting the temperate coastal landscape to one dominated by tropical saline forest. However, as forest islands convert to salt marsh, they also support fauna that regulate mangrove populations via herbivory. Without large influxes of propagules, mangroves may be unable to overcome the resulting strong, top-down predation control present in these transitioning habitats. While bottom-up controls like temperature and tidal flooding are known to dictate large-scale patterns and rates of mangrove expansion, our study supports the recommendation by He & Silliman (2016) that top-down controls need to be evaluated alongside abiotic controls when investigating and modeling mangrove expansion in coastal systems.

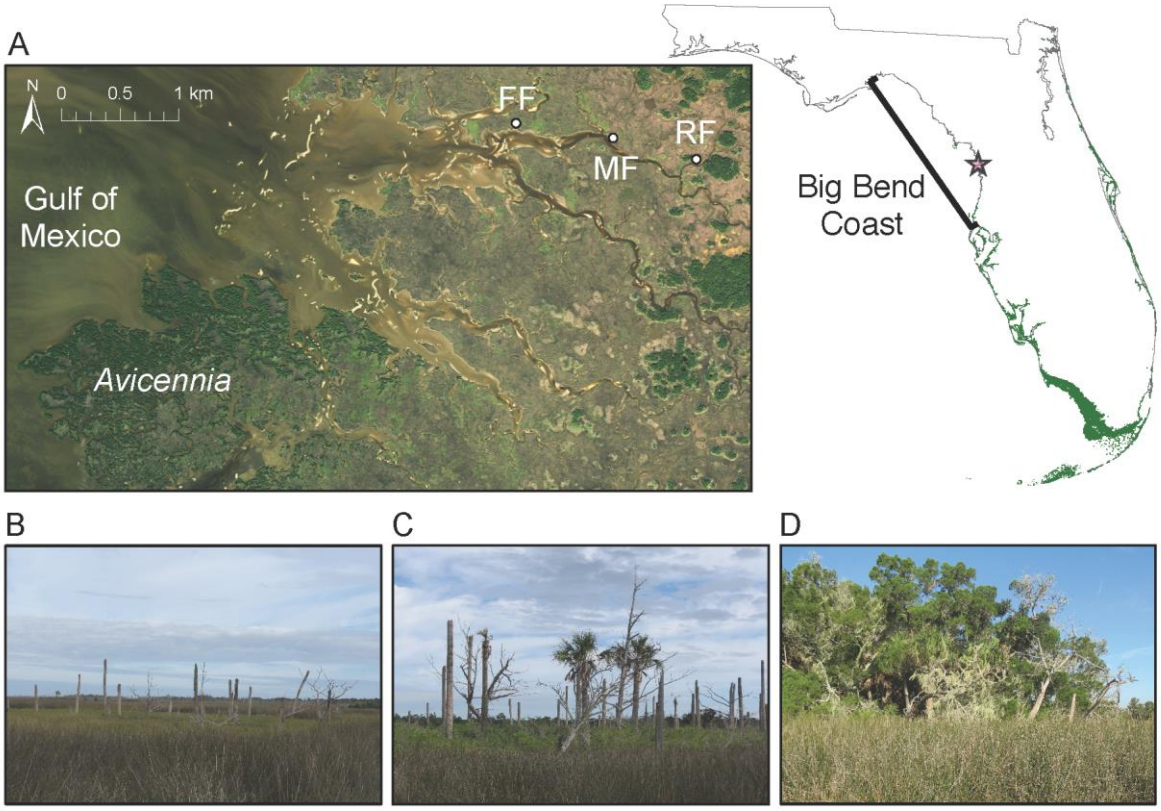

Figure 3-1. Location map of the experimental setting. A) Extent of mangrove forest in Florida (in green; FNAI 2015) and locations of the 3 study sites: FF (frequently flooded), MF (moderately flooded), RF (rarely flooded) and nearest mangrove population along Turtle Creek on the Big Bend coast. B) Frequently flooded site. C) Moderately flooded site. D) Rarely flooded site.

Figure 3-2. Categories of caged propagule and seedling fates. A) Caged propagule. B) Non-viable propagule from predation. C) Non-viable propagule from unfavorable environmental conditions that caused desiccation or rot. D) Viable propagule that developed into an established seedling. E) No signs of herbivory damage on mangrove seedling. F) Mild herbivory damage on leaves of seedling. G) Moderate herbivory damage on leaves and stem of seedling. H) Seedling mortality due to herbivory (total herbivory).

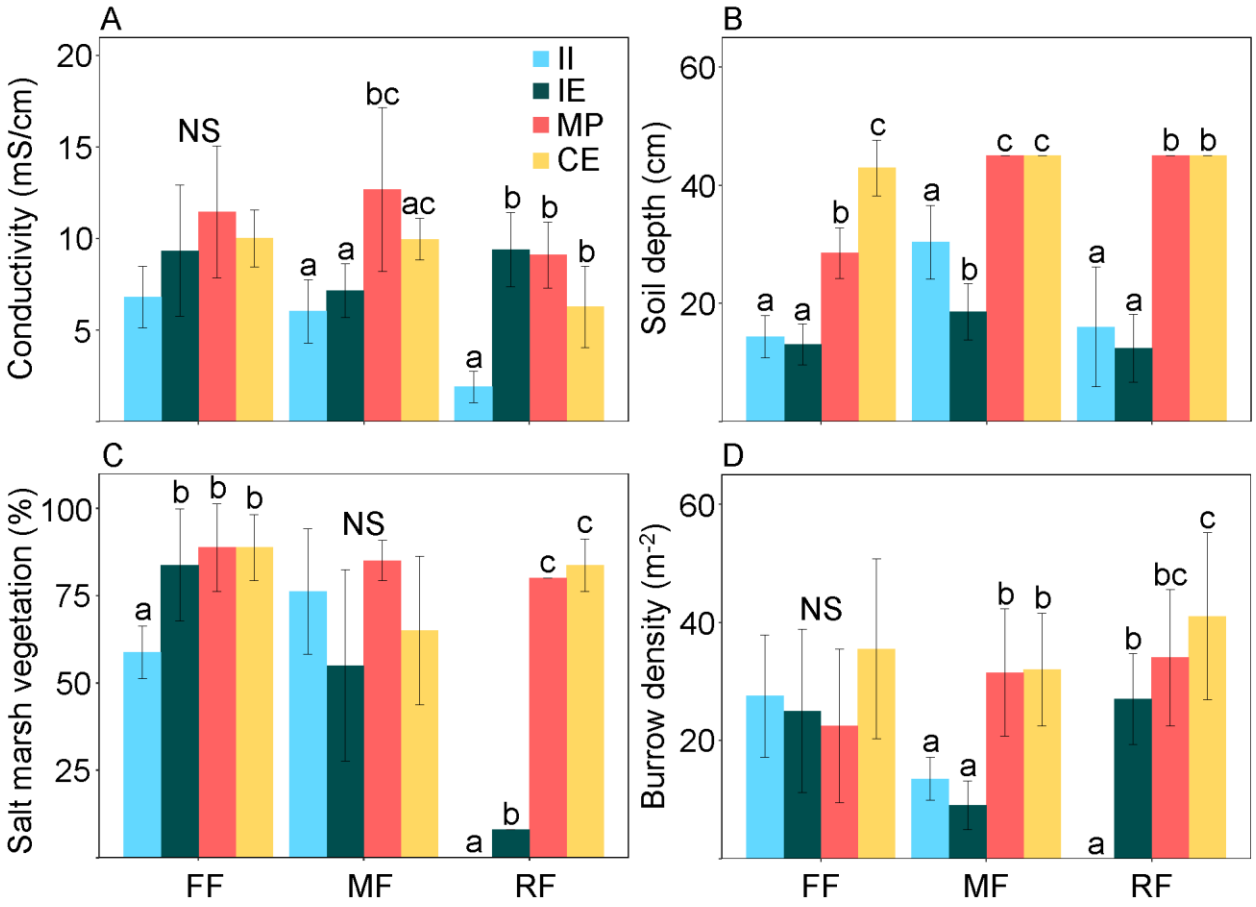

Figure 3-3. Comparisons (mean, sd) of bottom-up conditions between landscape position at each site. A) Soil salinity. B) Soil depth. C) Percent salt marsh vegetation cover. D) *Sesarma reticulatum* burrow density. Letters above bars denote statistically significant differences between landscape positions. II: island interior, IE: island edge, MP: marsh plain, CE: creek edge. FF: frequently flooded site, MF: moderately flooded site, RF: rarely flooded site.

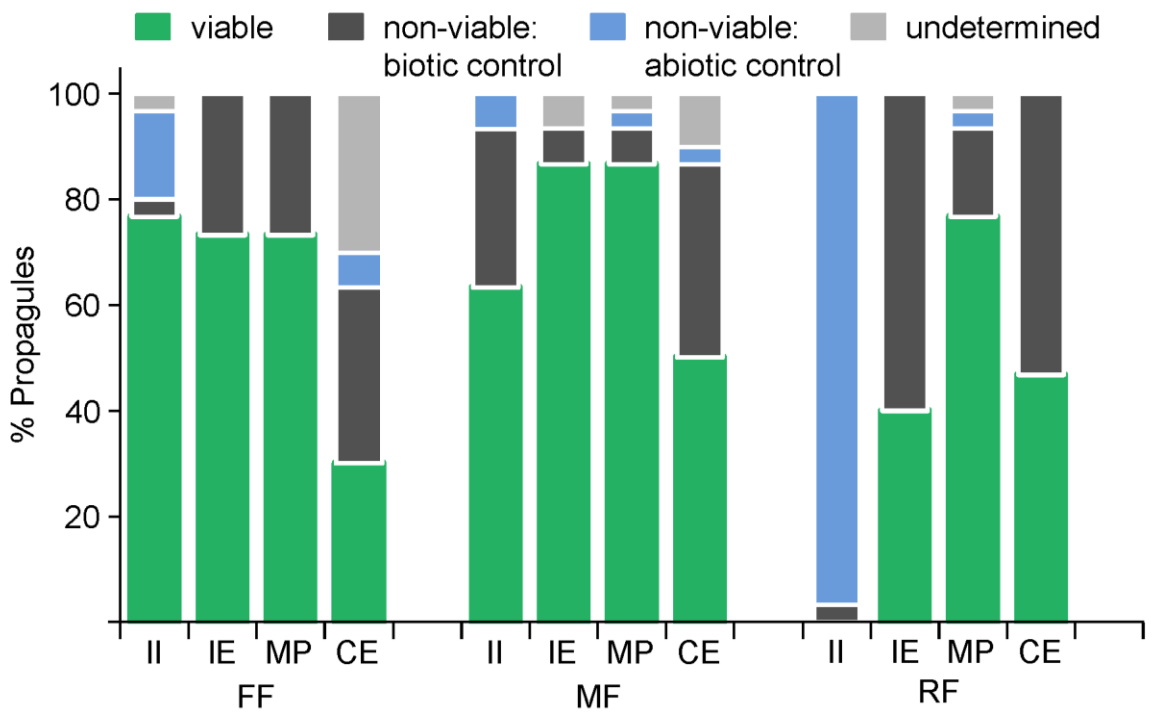

Figure 3-4. Percent of caged propagules that met each fate by day 200 in each landscape position at each site. II: island interior, IE: island edge, MP: marsh plain, CE: creek edge. FF: frequently flooded site, MF: moderately flooded site, RF: rarely flooded site.

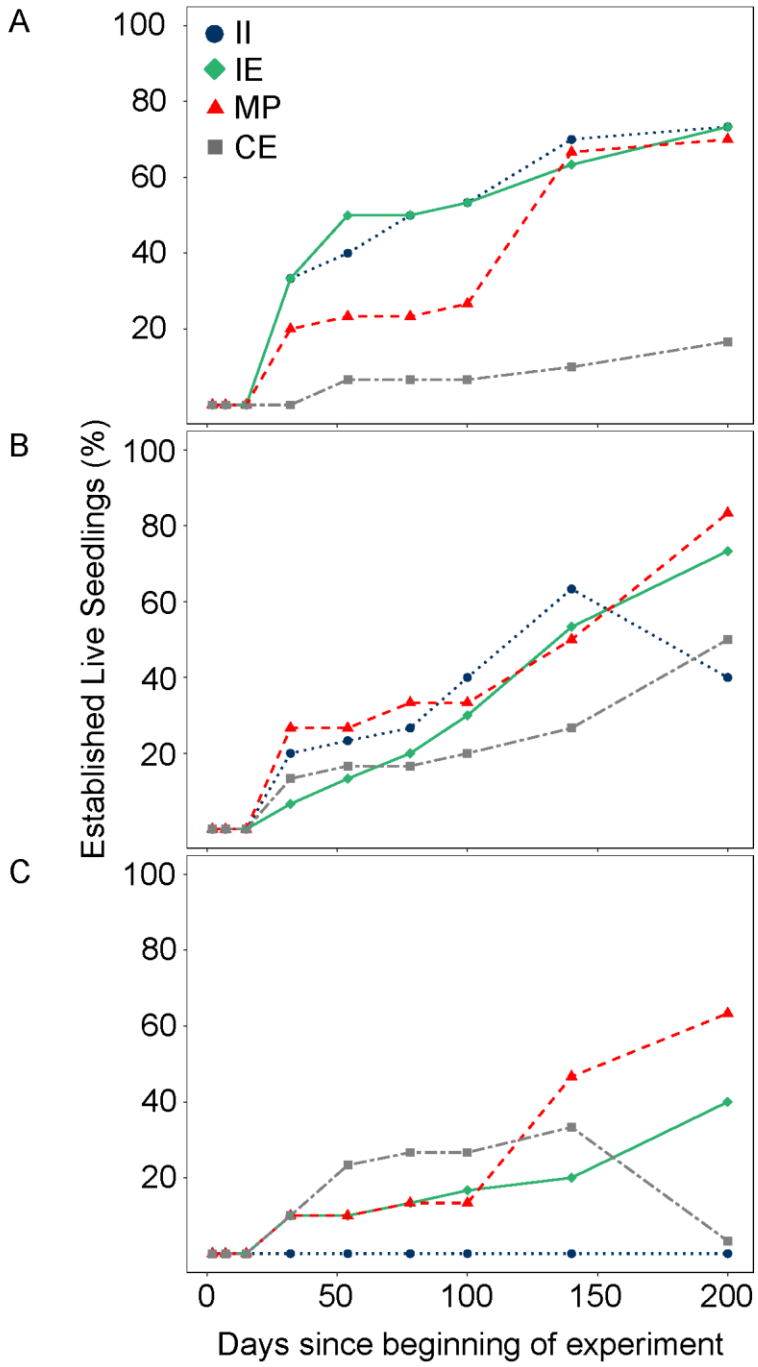

Figure 3-5. Percent of established live seedlings from caged propagules over time. A) Frequently flooded site. B) Moderately flooded site. C) Rarely flooded site.

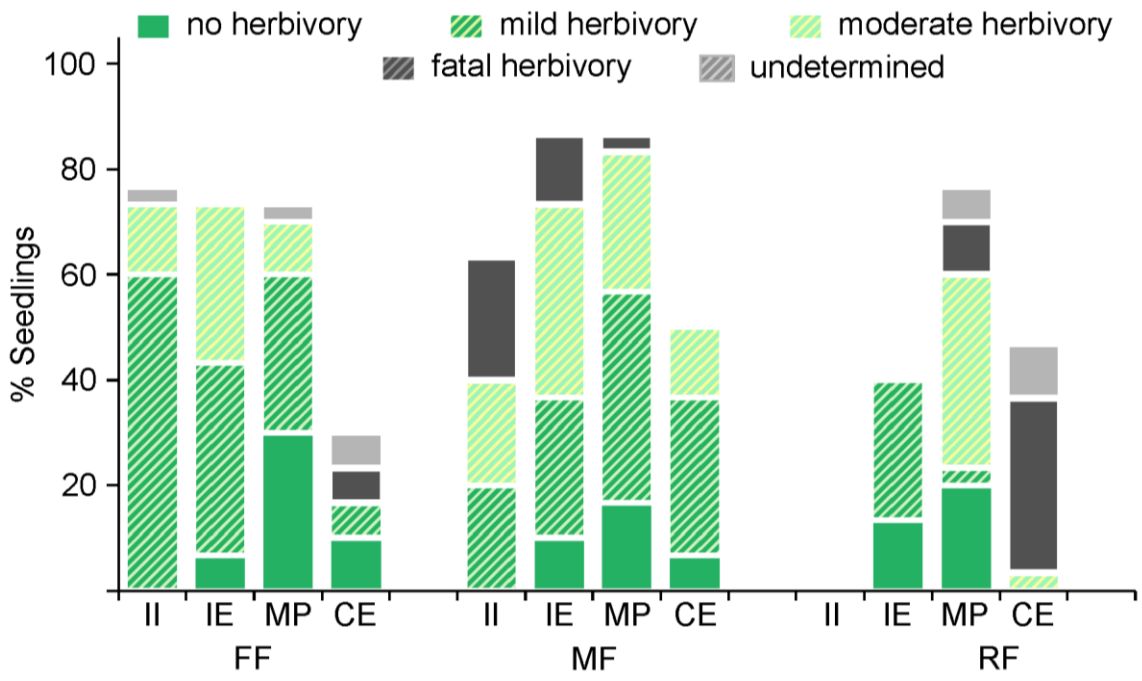

Figure 3-6. Percent of caged seedlings that met each fate by day 200 in each landscape position at each site. Seedlings include only the subset of propagules that were viable as shown in Figure 3-4. II: island interior, IE: island edge, MP: marsh plain, CE: creek edge. FF: frequently flooded site, MF: moderately flooded site, RF: rarely flooded site.

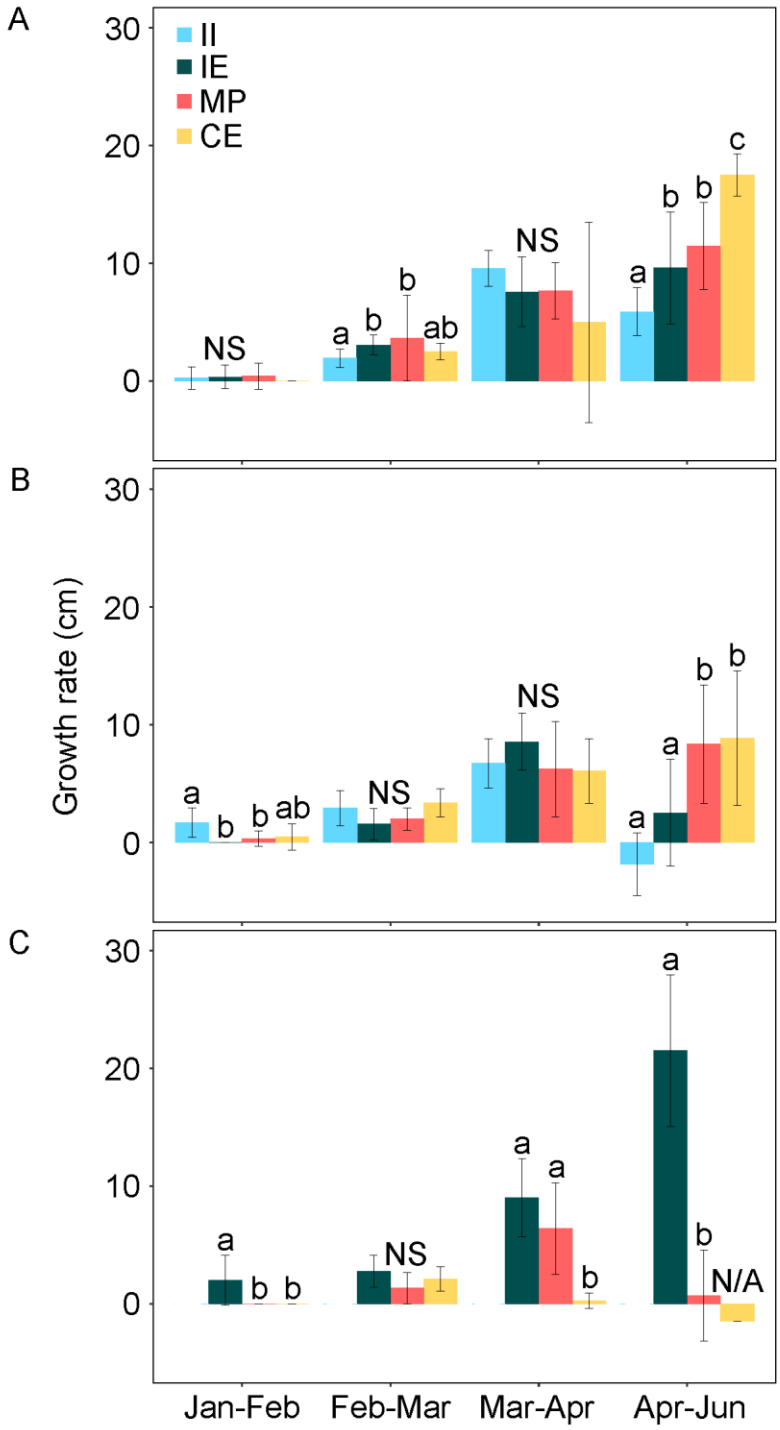

Figure 3-7. Mean seedlings growth rates (± sd) during caged experiment. A) Frequently flooded site. B) Moderately flooded site. C) Rarely flooded site.

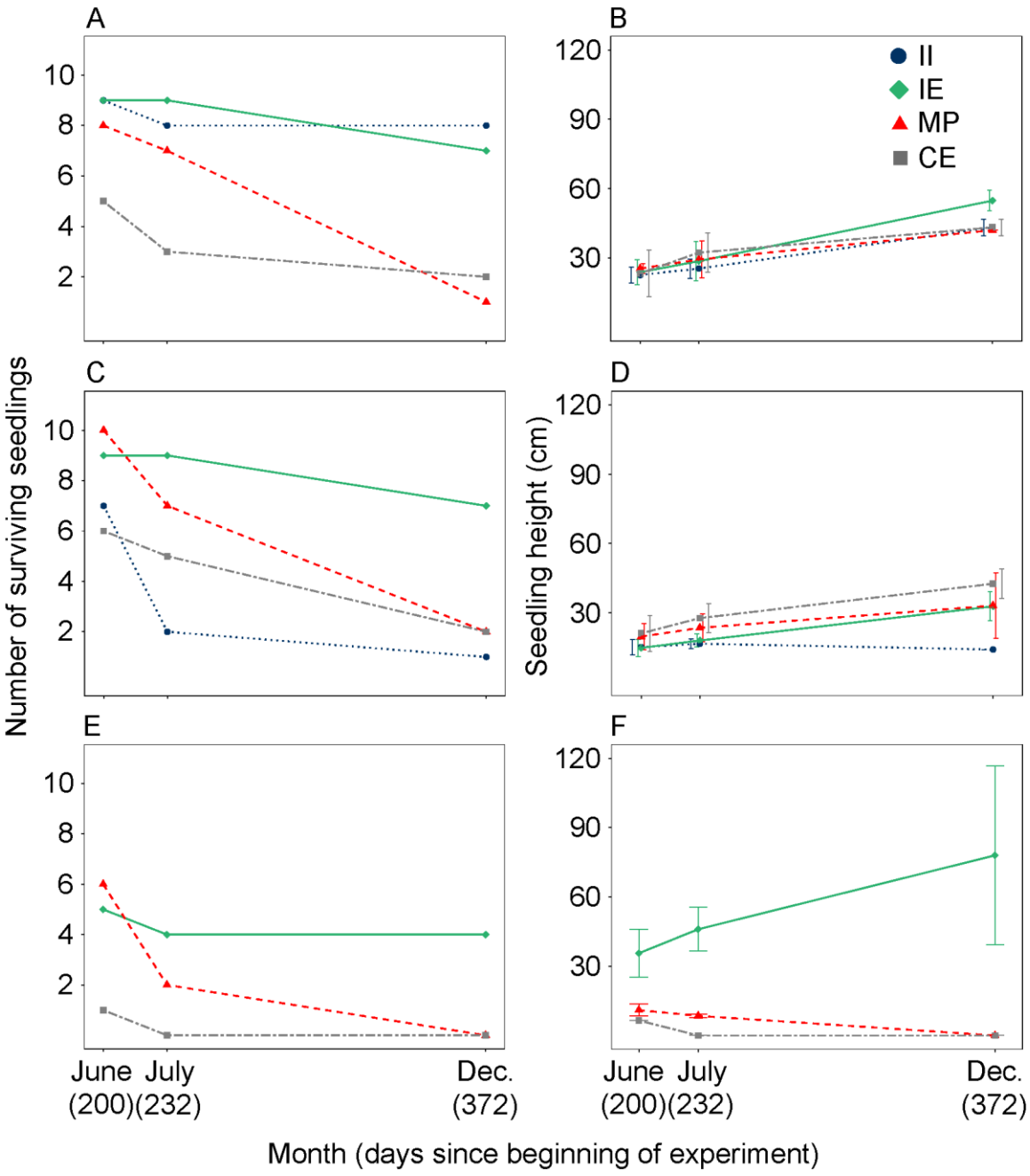

Figure 3-8. Number of surviving seedlings post-cage removal and mean heights (± sd) in June, July, and December 2016. A) Seedling survival at the frequently flooded site. B) Seedling heights at the frequently flooded site. C) Seedling survival at the moderately flooded site. D) Seedling heights at the moderately flooded site. E) Seedling survival at the rarely flooded site. F) Seedling heights at the rarely flooded site.

Object 3-1. Video footage of *Sesarma reticulatum* taking an *Avicennia germinans* propagule (.m4v file 18.2 MB)

CHAPTER 4
EVALUATING FREEZES, PREDATION PRESSURE, AND DISPERSAL DENSITY ON NORTHWARD EXPANSION OF BLACK MANGROVES (*AVICENNIA GERMINANS*) USING A STAGE-BASED POPULATION MODEL

Background

Historically, mangrove forests have been restricted to tropical latitudes where winter temperatures stay above freezing and sufficient precipitation prevents hypersaline growing conditions (Lugo & Snedaker, 1974; Tomlinson, 2016; Osland et al., 2017b). Altered temperature and precipitation regimes driven by climate change are affecting the distribution of mangroves, particularly at poleward range limits, where reduced frequencies of severe freeze events allow mangrove expansion into temperate climates (Osland et al., 2013; Cavanaugh et al., 2014; Saintilan et al., 2014; Ward et al., 2016). Much research is being conducted to understand how a changing climate alters the abiotic controls that affect mangrove coverage at poleward range limits and predict potential rates and patterns of encroachment into coastal regions currently dominated by salt marsh. However, as explained by He & Silliman (2016), top-down biotic controls (e.g., predators, herbivores) play critical roles in regulating coastal plant communities, yet are generally overlooked when evaluating coastal vegetation growth and survival.

Along the Big Bend coast of Florida, where mangroves on the west coast of Florida reach their northern range limit, population expansion over the past 30 years is attributed to fewer freeze events (Stevens et al., 2006; Giri & Long, 2016). Mangrove coverage generally expands and retreats in the region depending on the frequency and intensity of freezes. Since the last series of severe freeze events in the 1980s, mangrove coverage has expanded extensively along the entire southeastern US (Osland et al., 2013). Of the three mangrove species in Florida, *Avicennia germinans*

(black mangrove) is the most tolerant to cold temperatures and most common along the Big Bend. However, *A. germinans* propagules are also the most susceptible to predation (Smith et al., 1989; Souza & Sampaio, 2011; Van Nedervelde et al., 2015). As *A. germinans* expands into temperate salt marsh, it faces local predation pressure by *Sesarma reticulatum* (purple marsh crab), a grapsid species common in salt marshes along the eastern and southeastern coasts of the US (Subrahmanyam et al., 1976; Bertness et al., 2009). In a previous study, I found that propagule predation by *S. reticulatum* was the predominant control on *A. germinans* colonization in a Big Bend salt marsh (and in islands of freshwater forest converting to salt marsh) when abiotic conditions were favorable and propagule density was low (Langston et al., 2017a; Langston et al., 2017b). While we know abiotic factors (temperature, precipitation, tidal flooding) dictate patterns and rates of mangrove expansion, top-down biotic controls need to be evaluated alongside abiotic controls when evaluating mangrove encroachment into temperate salt marsh (Figure 4-1).

Sesarma species are common predators of *Avicennia* propagules within mangrove forests (Cannicci et al., 2008). *Sesarma reticulatum* is not among those species found in tropical mangrove forests, but can occur in high densities in salt marshes. A study by Subrahmanyam et al. (1976) ranked *S. reticulatum* fifth in density and biomass among species found in a north Florida salt marsh. Seiple (1979) reported a mean density of 25 m^{-2} of *S. reticulatum* in a North Carolina salt marsh, and I found densities ranging from 0-41 m^{-2} in a previous study in Waccasassa Bay Preserve State Park along the Big Bend (Langston et al., 2017a). *Sesarma reticulatum* is typically found in intertidal areas along creek banks and in salt marshes at mean tide level (Seiple,

1979; Zimmerman & Felder, 1991). They feed primarily on *Spartina alterniflora* (cordgrass) and are considered highly mobile (though specific travel distances are unknown; Seiple & Salmon 1982).

Despite being important regulators of propagule density in mangrove forests, studies on the feeding behaviors of *Sesarma* species are scarce. Considering the high rates of consumption recorded in propagule predation studies, it is surprising how little is known about the feeding habits of *Sesarma* species, in terms of how they handle propagules, how much time they spend searching for propagules, how many propagules an individual crab can eat, or how quickly they consume them. Such behaviors are typically evaluated to determine the functional response of a seed predator to seed density (Berryman, 1992; Fletcher et al., 2010; Moreira et al., 2017). According to the Predator Satiation Hypothesis (PSH; Holling 1959a; Holling 1959b), seed predators exhibit three potential types of functional responses to seed density: 1) no response, 2) decreased seed consumption with increasing seed density, and 3) peak consumption at an intermediate density (Figure 4-2). Determining the response that best describes the relationship between *S. reticulatum* and propagule density can provide insight into how likely a mangrove forest is to result from different densities and frequencies of propagule dispersal events into salt marsh-dominated areas. If the trend of declining freeze frequency continues, the Big Bend could soon support expansive mangrove forests; local biotic pressure may become the primary control regulating rates and patterns of mangrove establishment.

This study examined three factors affecting mangrove population expansion into salt marsh along the Big Bend: influx density of propagules into salt marsh, propagule

predation by marsh crabs (biotic control), and mangrove mortality from freeze events (abiotic control). I examined these factors using a controlled field experiment and a stage-based population growth model. The field experiment tested the hypothesis that propagule predation would depend on propagule density, consistent with a Holling type II functional response. I expected all propagules to be consumed when propagule density was low, and a decreasing portion of propagules to be consumed at increasing propagule densities. My hypothesis did not consider propagule dispersal distance from parent trees (see Janzen 1970 & Hubbell 1980) because along the Big Bend, propagule dispersal far from parent trees places propagules in new habitats in which they encounter different seed predators.

Quantifying the relative effects of propagule predation and freeze events would be most accurately addressed through field experiments and long-term field observations. However, these research endeavors would require experiments spanning large spatial and temporal scales (100s of km and decades to centuries) to capture changes in *A. germinans* coverage across abiotic and biotic variables. Where direct observation and experimentation is unfeasible, modeling approaches based on empirical and mechanistic understanding of system components can be used to gain insight about system dynamics (Jackson et al., 2000). Many approaches exist for modeling ecosystem change, each with its set of limitations. While no model can perfectly capture real-life dynamics, a well-formulated model can be a useful tool for testing hypotheses and predicting outcomes under different scenarios (Jørgensen, 1999).

I developed a stage-based population model to test the hypothesis that the combined effects of regional freeze events (intensity and frequency), propagule dispersal (density and frequency), and local predation pressure (based on relative densities of propagules and marsh crabs) determine population establishment success into new areas and affect growth rates of successfully established populations. By evaluating these controls in modeled scenarios informed by my field data and the literature, climate of the Big Bend, and the life history of *Avicennia*, we can more accurately predict mangrove colonization along the Big Bend.

Materials and Methods

Field Experiment

The field experiment was conducted in November 2016 at the Withlacoochee Gulf Preserve in Yankeetown, Florida (Figure 4-3). To test the hypothesis that propagule predation would depend on propagule density, I set out propagules of *A. germinans* in a cordgrass-dominated marsh in three density treatments: 1, 25, and 100 m^{-2}, and recorded propagule mortality from predation over the course of 22 days. Each density treatment plot consisted of nine 1-m^2 subplots (Figure 4-3). The center subplot was my experimental unit and contained tethered and non-tethered propagules. The surrounding subplots served as buffers between the experimental unit and the surrounding marsh matrix. All nine subplots contained the same density treatment, and the buffer plots bounded the center subplot, defining the density treatment area. I monitored propagules in the center subplot only. I set out six replicates of each density treatment and randomized treatments across the 18 plots. All propagules were collected from Cedar Key, Florida and had already dropped from parent trees.

Propagules were monitored daily at first and then with declining frequency. Typically, propagules either succumb to mortality or establish within 17-21 days once they are stranded on substrate (Osborne & Smith, 1990; McKee, 1995; Patterson et al., 1997), so I monitored propagules for 22 days. During monitoring events, I counted all propagules present in the center subplots; of the propagules present, I counted how may were still viable (i.e., showing no visible signs of damage or decay). I assumed missing propagules were eaten. To quantify the population of *S. reticulatum* in the experimental area, I counted *S. reticulatum* burrows within each center subplot. *Sesarma* burrows were identified using the description in Bertness et al. (2009); burrow density is an accepted proxy for *Sesarma* density (1 burrow=1 crab).

I compared the proportion of propagules eaten across density treatments using 1-way ANOVA. I used a logistic model to evaluate the relationship between propagules consumed and propagule density to determine whether it conformed with a Holling type II functional response. I also used a logistic model to evaluate the relationship between the proportion of propagules consumed and the ratio of crabs to propagules for use in the population model. All analyses were performed in R (R Core Team, 2017).

Stage-Based Population Growth Model

I developed a stage-based population growth model quantifying the effects of propagule dispersal density, predation, and freeze events on mangrove forest establishment in R using the deSolve (Soetaert et al., 2010) and simecol (Petzoldt & Rinke, 2007) packages. The model tracked forest development through mangrove life stages for 100 years on a 1-year time step (Figure 4-4). Freeze events and predation were explicitly modeled controls restricting population growth; influxes of propagules and propagule production within the population increased population growth. The model

required an initial influx of propagules for a forest to develop. As propagules matured to trees, probabilities of remaining in the same life stage, maturing to the next life stage, or dying from additional causes of mortality (rot, uprooting, local disturbance, crowding) determined rates of development, in addition to freeze events and predation. The spatial extent of the model was no geographically specific; rather the model domain represented a generic 100 m^2 area of habitable salt marsh (i.e., low elevation herbaceous marsh).

Because stage-based models for *A. germinans* are absent in the literature, I relied on stage-based models for two other *Avicennia* species: *A. marina* and *A. bicolor* developed by Clarke (1995) and Delgado et al. (1999), respectively. *Avicennia marina* (grey mangrove) is a relatively small mangrove species found in Australia and New Zealand and forms monospecific stands at its southern range limit where it intersperses with salt marsh (Burns & Ogden, 1985). In many respects (structure, size, range limit), *A. marina* in southeastern Australia is the southern hemisphere analog of *A. germinans* in the southeastern US. In the absence of life table statistics for *A. germinans*, I assumed that values and probabilities for *A. marina* are reasonable estimates for *A. germinans*.

State variables

State variables represented densities of seven life stages of a mangrove: propagule, seedling with cotyledons attached, seedling without cotyledons, sapling, young tree, mature tree, and old tree (Table A-1). They are defined by differences in annual probabilities of maturing from one stage to the next (maturing), remaining in the same stage (remaining), mortality from freez

es, predation, crowding, and from miscellaneous causes (described below), and by fecundity, rather than by size (i.e., height, biomass) or age. These are the same life stages used in the model by Clarke (1995).

Propagules included only those that had settled onto habitable salt marsh. They were assumed to be propagules that survived rot, desiccation, or other causes of mortality besides predation. Propagules either dispersed into the model domain (influx) or were produced by parent trees that matured within the population over time. Seedlings with cotyledons referred to newly established seedlings in which cotyledons were still attached. Base on field observations, viable propagules that settle onto substrate reach this stage within the same year. As seedlings mature, cotyledons fall off. These seedlings represented the later seedling stage included in the model and could remain seedlings for multiple time steps. Saplings were individuals that matured from seedlings but had not reached reproductive maturity (Clarke, 1995). Young trees, mature trees, and old trees were distinguished by differing annual rates of fecundity (i.e., propagules produced per year). Younger trees produce fewer propagules than mature trees, which produce fewer propagules than old trees (Clarke, 1992).

Parameters

Life stage probabilities. Probabilities of individuals maturing, remaining, or suffering mortality from miscellaneous causes at each life stage were based on those used by Clarke (1995) and Delgado et al. (1999) and on field data I collected in previous studies (Table A-1). The general equation used for calculating changes in the population density of each life stage (except propagules) at each time step was:

$$\frac{dx_i}{dt} = x_i r_i + x_{i-1} m_{i-1} \quad (4\text{-}1)$$

where x_i is the population density of a life stage, r_i is the probability of individuals remaining in that life stage, x_{i-1} is the population density of the previous life stage, and m_{i-1} is the probability of individuals from the previous life stage maturing to the next life stage. The probability of miscellaneous mortality is the difference of $1- r_i - m_{i-1}$. Causes of miscellaneous mortality are those not explicitly included in the model, such as rot, desiccation, herbivory on non-propagule life stages, uprooting, or local disturbances such as lightning. Mortality probabilities from crowding and freeze events (see subsequent sections) were applied to life stage densities after applying Eq. 4-1.

$$\frac{dp}{dt} = p_{influx} + p_{yt} + p_{mt} + p_{ot} \quad (4\text{-}2)$$

where p is propagule density, p_{influx} is the density of propagules dispersing into the model domain, and p_{yt}, p_{mt}, and p_{ot} are propagules produced by young trees, mature trees, and old trees within the model population that settle onto habitable substrate and do not succumb to miscellaneous causes of mortality. No propagules from the previous time step (t-1) remained in the next; they either matured into seedlings or died. (This was also true for seedlings with cotyledons.) Probabilities of mortality from predation and freezes were applied to the total propagule density.

Fecundity. Young, mature, and old trees were those individuals that were able to produce propagules. Fecundity of trees was based on modeled rates by Clarke (1995) and field measurements by Clarke (1992) for *A. marina*. I assigned annual fecundity ranges of 0-100 propagules/young tree, 0-3000 propagules/mature tree, and 0-5300 propagules/old tree (Table A-1). Fecundity varied between trees in each tree stage at each time step. Ranges were used to introduce a source of stochasticity into the model and account for individual trees producing widely variable numbers of propagules from

one year to the next. Ranges included zero because individual trees are not fecund every year (Clarke, 1995).

Density limitations on the model population. Life stage density maxima were used to account for density limitations on population growth. Density maxima were applied to seedlings with cotyledons, older seedlings, saplings, and all three tree stages (Table A-1). According to Jimenez et al. (1985), seedling density of *Avicennia* can reach 330 m^{-2}. I split this density between the two seedling life stages (200 m^{-2} for seedlings with cotyledons, 130 m^{-2} for older seedlings). Saplings and seedlings are especially sensitive to crowding and shading and suffer mortality at high densities. I used a maximum sapling density of 0.41 m^{-2}, which is about 20% higher than the mean sapling density of *A. bicolor* measured in a 6-year study by Delgado et al. (1999). Following the stage-based model by Clarke (1995), when sapling density exceeded the maximum density, probabilities of younger life stages remaining and maturing were reduced to zero. Canopy tree density in *Avicennia* forests stabilizes around 0.1 m^{-2} (Clarke, 1995). However, to allow old trees to develop on a realistic time frame (within 100 years), I assumed that young trees were lower in the canopy than mature and old trees, and set maximum density to 0.1 m^{-2} for each tree life stage. Though higher than reported by Clarke (1995), even under optimal scenarios (i.e., with no freezes or propagule predation), total tree density of all tree stages produced by the model stabilized at approximately 0.15 m^{-2}, meaning that life-stage probabilities also limited tree density.

Propagule mortality from predation. I used the ratio of crabs to propagules as a relative measure of crab density to test different propagule predation intensities (none, low, moderate, high; Table A-1). Use of a predator to prey ratio is recommended when

evaluating the functional response of a predator, which occurs on short time scales of minutes or hours, and the effect of predation on prey population dynamics, which occurs over years (Arditi & Ginzburg, 1989; Berryman, 1992). Ratios were calculated from field experiment results and previously collected field data. Non-linear regression of propagules consumed versus crab:propagule ratios from the field experiment (Figure 4-6) was used to calculate relative propagule mortality from predation.

$$y = 0.165 \ln x + 0.7184 \quad (4\text{-}3)$$

where y is the proportion of propagules depredated, and x is the ratio of crabs to propagules. Propagule consumption maxes out at 1.0.

External forces: influx and freeze events. Mangrove encroachment in the model is driven by an initial influx or propagules into the domain. To investigate the relationship between propagule density, predation, and freeze events, I ran the model with low (100), moderate (500), and high (1000) initial influxes of propagules (Table A-1). A high influx density reflects pulse events, such as storms, that can deliver high densities of propagules to a new area. Moderate and low influx densities reflect propagule delivery to by high tide. I also ran the model with varying frequencies of influxes: an initial influx only, low influx frequency (10 additional influxes randomly over timed over 100 years), and high influx frequency (yearly influxes for 100 years). To compare densities across the same influx frequencies, subsequent influx densities depended on the initial influx density: when the initial influx was 100 propagules, subsequent influxes ranged from 1-110, when the initial influx was 500, subsequent influxes ranged from 1-550, and when the initial influx was 1000, subsequent influxes

ranges from 1-1100. Variation in influxes density introduced another source of stochasticity into the model.

To test the effects of freeze event intensity and frequency, I applied moderate, severe, and series of severe freezes to the modeled population (Table A-1). Moderate freezes represented events that caused low rates of mortality at life stages more sensitive to freezing temperatures; seedlings, saplings, and young trees. Mortality rates were based on rates measured by Osland et al. (2015) during freezes in which temperatures ranged between 0 ˚C and -6.5 ˚C for less than 24 hours. Severe freezes represented severe freeze events during a single winter that caused low to moderate rates of mortality for seedlings (with and without cotyledons), saplings, and young, mature, and old trees, and prevented regeneration for a single year. Severe events represented freezes in which temperatures reached -6.5 ˚C for at least 24 hours, as occurred during the winter of 1995/1996 in Cedar Key, Florida (Stevens et al., 2006). Rates of mortality reflected those reported by Stevens et al. (2006) and Pickens & Hester (2011). Series of severe freezes spanning two or more winters are most damaging to mangroves and cause massive die-offs of forests. According to Montague & Odum (1997), the series of freezes that occurred in the 1980s along the Big Bend resulted in mortality of 98% of mangroves in Cedar Key. In the model, series of severe freezes caused 98% mortality at all life stages, except propagules, which were not produced in years in which any severe events occurred.

Three scenarios of freeze intensities (i.e., moderate, severe, series of severe freezes) were applied to the model: historical, reduced, and none. Historical freeze frequency included 15 moderate freeze events, 14 severe freeze events, and 1 series of

severe freezes during 100 years. Moderate freezes have occurred nearly every year of the last 100 years, but not all moderate freezes cause mortality, so I assumed a small fraction of potential moderate freezes caused mortality in the model. From the late 1890s to late 1990s, 17 severe freezes have occurred along the coast of the southeastern US (Stevens et al., 2006; Osland et al., 2017a), including a series of severe freezes. Historically, one series of severe freezes occurs every hundred years (Stevens et al., 2006). Reduced freeze frequency included 8 moderate freezes (that could cause mortality), 8 severe freezes, and no series of severe freezes during 100 years. Reduced frequency reflected potential reduced frequency from climate change. The timing of events were randomized across years during each model simulation to evaluate the effects of freezes on forest at different developmental stages and densities.

Model scenarios. Each scenario began with an initial influx of propagules; all other life stages were zero. Scenarios varied by propagule predation intensity (none, low, moderate, high) at each freeze frequency (historical, reduced, none). These combinations were carried out for three influx densities (1000, 500, 100 propagules) and for three influx frequencies (1/100 years, 10/100 years, every year for 100 years), for a total of 108 scenarios (Figure 4-4). Each scenario was simulated 10 times. Variations in output between each simulation for a given scenario was driven by the stochasticity in timing of freeze event and influx event occurrences, and by varying densities of propagules produced by fecund trees within the population. During each of the 10 simulations for a given scenario, I ran model 1000 times and calculated mean density (and standard deviations) of each life stage at year 100. The metric used for evaluating each scenario was whether there was an established, regenerating mangrove forest in

year 100. This meant the population had to have at least one fecund tree sustaining the forest, rather than requiring influxes of propagules from outside the population to persist.

Results and Discussion

Field Experiment

The percent of propagules eaten during the field experiment differed between density treatments ($F_{2,15}$= 156.5, *p*-value < 0.001). As expected, all propagules in the 1 m^{-2} treatment were consumed during the experiment and a lower percent of propagules in the 100 m^{-2} treatment were consumed compared to those in the 25 m^{-2}. The percent of viable propagules decreased over time more slowly with increased density (Figure 4-5). By day 22, an average of 55% of propagules in the 25 m^{-2} treatment and an average of 26% of propagules in the 100 m^{-2} treatment were gone. The relationship between the number of propagules eaten and propagule density followed a Holling Type II functional response (Figure 4-6a). The percent of propagules eaten increased nonlinearly with greater crab to propagule ratios and the logistic regression equation that best fit the data was used to quantify propagule predation by *S. reticulatum* in the population model (Figure 4-6b).

The relationship between predation and propagule density suggests that *S. reticulatum* can consume only a finite number of propagules from the time propagules first settle onto substrate to when they establish as seedlings with cotyledons (approximately 17 days). At low propagule densities (assuming high crab:propagule ratios), *S. reticulatum* are able to consume all available propagules. At higher densities (and lower crab:propagule ratios), marsh crabs may be either satiated before all propagules are consumed, or not have enough time to consume all propagules before

they establish. Without knowing more about the feeding behaviors and movement of *S. reticulatum*, it is unclear what exactly limits propagule consumption. However, the nonlinear trend observed during the experiment is still useful for estimating the degree to which *S. reticulatum* regulates *A. germinans* establishment, as a function of the relative densities of *S. reticulatum* and propagules.

Stage-Based Population Model

Results of all simulations are summarized in Figure 4-7. Representative output for each scenario is presented in Figure 4-8 through Figure 4-34, and in Table C-1, which lists mean density for each life stage for each scenario at year 100. The output provided shows examples of the most common result from each scenario (i.e., if an established forest persisted in year 100 in 8 out of 10 simulations of a given scenario, the corresponding figures and means show the output from one of those 8 simulations. The R script for the model is included in Appendix B.

Scenarios with one initial influx event (for all predation intensities)

Historical frequency of freeze events. At a historical frequency of freeze events, mangrove forest from an initial influx of propagules was least likely to establish and persist after 100 years, compared to scenarios with a reduced freeze frequency or no freezes. At a high influx density, forest only persisted 40-70% of the time when predation intensity was low or absent, and never at moderate or high predation intensities (Figure 4-8). At influx densities of 500 and 100 propagules/100 m^2, forest establishment only persisted 30-40% of the time, and only in the absence of predation (Figures 4-9, 4-10). Forest die-off and temporary cessation of propagule production from a series of severe freezes reduced propagule densities such that they could not overcome any predation pressure.

Reduced frequency of freeze events. Under a reduced freeze frequency and initial influx of 1000 propagules, mangrove establishment always occurred except when predation intensity was high (Figure 4-11). Without a series of severe freezes drastically reducing population density, propagule densities were generally high enough to overcome predation pressure. Predation intensity had an increasing negative effect on forest establishment at lower influx densities (Figures 4-12, 4-13), but only prevented establishment from an influx of 500 propagules when the ratio of crabs to propagules was high. On the other hand, propagule predation was the primary control at all intensities when influx density was low.

No freeze events. In the absence of any freeze events, propagule predation had less of an effect on forest establishment for influxes of 1000 and 500 propagules (Figures 4-14, 4-15). A forest was always able to persist by year 100 under all predation intensities from an influx of 1000 propagules. A forest was also always able to persist from an influx of 500 propagules, except when predation intensity was high (which always prevented establishment). Forest from an influx of 100 propagules always established when predation intensity was absent or low, but never under moderate or high intensities (Figure 4-16).

Propagule intensity, the proportion of propagules consumed during each time step, was a constant value for each scenario. Without stochasticity from freeze events affecting propagule production, propagule influx density was either high enough to overcome predation mortality or was below the density threshold required to withstand predation. An influx density of 1000 propagules was high enough to overcome all levels of predation intensity. When supplied with an influx density of 500 propagules, not

enough survived predation to support the establishment of later life stages under high predation intensity. The maximum predation intensity propagules could overcome corresponded with a crab:propagule ratio between 2 and 4 crabs per propagule. An influx of 100 propagules was too low for enough propagules to survive to the next life stages when the ratio of crabs to propagules was 2 or more.

Scenarios with low influx frequency (for all predation intensities)

Historical frequency of freeze events. The potential for forest establishment increased noticeably with additional influxes of propagules. Forest establishment was possible under all predation intensities with moderate and high propagule influxes (though only occurred 1 out of 10 times with moderate influxes and high predation intensity; Figures 4-17, 4-18). Forest establishment could also result from a repeated low density influx of propagules when predation intensity was low (Figure 4-19). However, the combination of freeze events and moderate or high predation intensity prevented forest establishment when influx densities were low.

Environmental and demographic stochasticity greatly influences population dynamics, especially when populations are small (Lande et al., 2003; Bonsall & Hastings, 2004). When a stochastic event, like a severe freeze, occurred while the forest population was small or composed of few fecund trees, the probability of the population recovering was low. However, if a freeze of the same intensity occurred when the forest population was larger or supported many fecund trees, the forest could likely recover within 20-30 years (Stevens et al., 2006). Likewise, the stochastic timing of an immigration event (in this case, an influx event) affected the probability of the local model population going extinct. An influx after a series of severe freezes often allowed a new forest stand to replace the forest that had been destroyed by freezes.

Reduced frequency of freeze events. Mangrove forest was nearly always possible in scenarios with a reduced frequency of freeze events (Figures 4-20, 4-21, 4-22). Without a series of severe freezes causing massive die-off and with recurring influxes of propagules, predation had no effect on populations supported by high and moderate propagule influxes. Forests were less likely to persist with low influxes of propagules and a moderate intensity of predation. Only when influx density was low and predation intensity was high was forest consistently unable to establish.

No freeze events. With moderate or high initial influxes of propagules, 10 additional influxes of propagules over 100 years, and no freeze events, mangrove forest was always able to persist, regardless of predation intensity (Figures 4-23, 4-24). Low influxes supplied enough propagules for mangrove forests to consistently establish at low and moderate predation intensities (Figure 4-25). However, repeated low influxes of propagules were never enough to overcome high predation intensity. As was found with a single influx event of low propagule density, infrequent, repeated low influxes still did not supply enough propagules to overcome the constant threshold of predation mortality. The maximum predation intensity propagules could overcome corresponded with a crab:propagule ratio between 2 and 4 crabs per propagule.

Scenarios with influx events every year (for all predation intensities)

Historical frequency of freeze events. With annual high, moderate, or low influxes of propagules, modeled populations were generally able to overcome a historical frequency of freeze events and predation pressure (Figures 4-26, 4-27, 4-28). Under high predation intensity, populations supported by moderate or high influxes of propagules failed to persist only 10-20% of the time. Populations supported by low influxes of propagules were always able to persist in the absence of predation or when

predation intensity was low, and nearly always under moderate predation intensity. However, historical freeze frequency and high predation pressure always prevented forest establishment when the population was supported by low annual influxes of propagules. Higher frequency of severe freezes (compared to reduced frequency scenarios) and a series of severe freezes consistently reduced propagule production below a propagule density threshold that could overcome constant, high intensity predation. At higher influx densities, the forest population was still occasionally vulnerable to propagule densities decreasing below a high predation intensity tolerance threshold. This demonstrated that predation pressure could exacerbate negative effects of freezes on a mangrove population to the point that local extinction could occur.

Reduced frequency of freeze events and no freeze events. With annual influxes of propagules and no series of severe freezes, populations were always able to establish and persist by year 100 under all predation intensities and influx densities, whether a reduced frequency of freezes occurred (Figures 4-29, 4-30, 4-31) or no freezes occurred (Figures 4-32, 4-33, 4-34). Annual influxes were able to provide enough propagules for forests to recover from moderate and severe freeze events under a reduced freeze frequency and overcome high predation intensity. While rates of population growth and densities of propagules and seedlings varied between scenarios of different influx intensities, population densities of saplings and young trees eventually reached maximum capacities (0.41 m^{-2} and 0.1 m^{-2}), and mature and old trees stabilized at similar densities (0.026-0.034 m^{-2} and 0.01-0.023 m^{-2}).

Model limitations and next steps

The stage-based population growth model is a useful tool for assessing potential mangrove encroachment under different abiotic and biotic scenarios; however, the

model has limitations that restrict its reflection of *A. germinans* forest development in any specific location. The model is based on life-stage probabilities, fecundity rates, and density maxima for *Avicennia* species not found in Florida, which may differ from those that best describe *A. germinans* population growth. Updating the model with measurements of propagule production and life-stage population densities within *A. germinans* stands along the Big Bend would improve the representativeness of the model.

The model also does not capture spatial variability in propagule or crab densities or salt marsh habitat in the model domain. In other words, all propagules were equally susceptible to predation for a given predation intensity. In the real world, propagules and crabs do not occur uniformly across the landscape, nor is a salt marsh a homogeneous landscape. Accounting for spatial variability in propagule and crab distributions (by incorporating tidal activity and elevation into the model) would allow for more complex scenarios that better simulate variable rates of propagule predation. Likewise, conducting feeding trials with *S. reticulatum* to measure feeding behaviors (searching rates, handling times, distances of movement) and incorporating results into the model would increase the accuracy of predation rates across propagule densities.

Despite the limitations and simplicity of the model, it is a reasonable reflection of real-world mangrove population dynamics. For example, though life stages were not based on age, fecund trees typically matured within the population after five or more years, depending on the conditions of a given scenario, which is consistent with tree fecundity reported by Clarke (1995). Even though several assumptions were made about the effects of freeze intensities on life-stage densities and the frequencies of

freeze events, the model also shows that forest recovery from severe freeze events takes 20-30 years, which is similar to mangrove forest recovery in Cedar Key (Stevens et al., 2006).

A one-at-a-time (OAT) sensitivity analysis will be conducted to test the relative importance of each parameter on model output. During repeated runs of the model, the value of a single parameter value will be varied by 20% above and below its original value while the other parameters remain fixed (Hamby, 1994). Changes in output will be compared to identify the parameters to which the model is most sensitive. I expect that the model will be most sensitive to parameters related to life-stage mortality from freezes, because forest establishment depended so often on mortality from freeze events in model simulations, and to life table probabilities for younger life stages, because they often need to be high for the population to overcome abiotic and biotic controls. I expect the model will be less sensitive to density maxima or life table probabilities for older life stages.

Implications for Mangrove Encroachment Along the Big Bend

The stage-based population density model demonstrates that as long as enough propagules survive for a single fecund tree to develop, a mangrove population can develop and persist under a wide range of freeze and predation intensities and influx densities. The model also shows that rates of forest growth may very between influx densities, but if fecund trees develop, the populations eventually reach similar densities. In the absence of a series of severe freeze events and reduced frequencies of single severe freeze events, mangrove encroachment can generally occur (Figure 4-7). Reduced frequency and severity of freeze events are predicted to promote mangrove expansion along the southeastern coast of the US (Cavanaugh et al., 2014; Osland et

al., 2017a) and the model shows that establishment of a new, regenerating mangrove stand can require only a single influx of propagules into suitable salt marsh habitat.

Crab predation was less likely to prevent forest establishment than expected. The model demonstrates that propagule predation pressure is greatest at high ratios of crabs to propagules when propagule density is low, even if subsequent, but infrequent, influx events occur. In such cases, forest establishment may never occur. This suggests that predation has a bigger effect in salt marsh where small densities of propagules occasionally settle. Rates at which salt marshes along the Big Bend convert to mangroves could vary depending on *S. reticulatum* density, but given enough time, predation is not likely to restrict regional mangrove encroachment along the Big Bend.

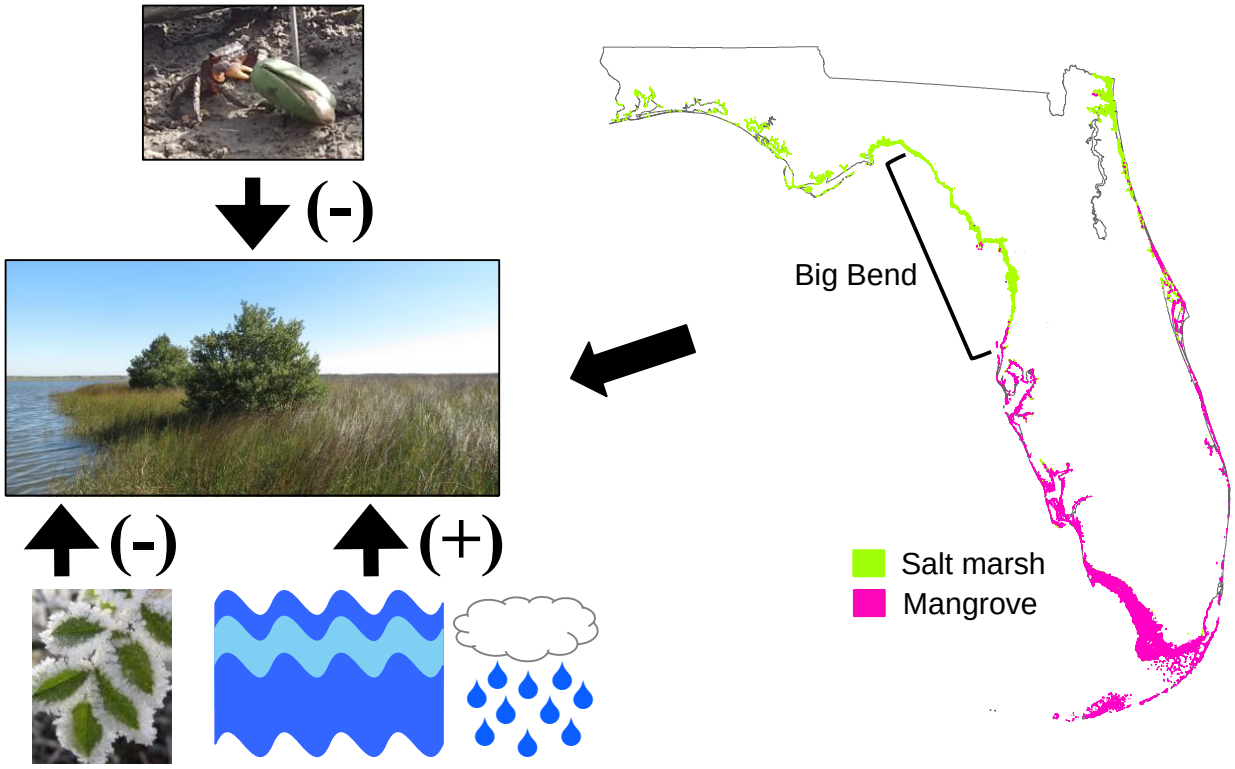

Figure 4-1. Bottom-up and top-down controls on *Avicennia germinans* encroachment into salt marsh at its northern range limit on the Big Bend coast of Florida. Salt marsh and mangrove extent from FNAI (2017).

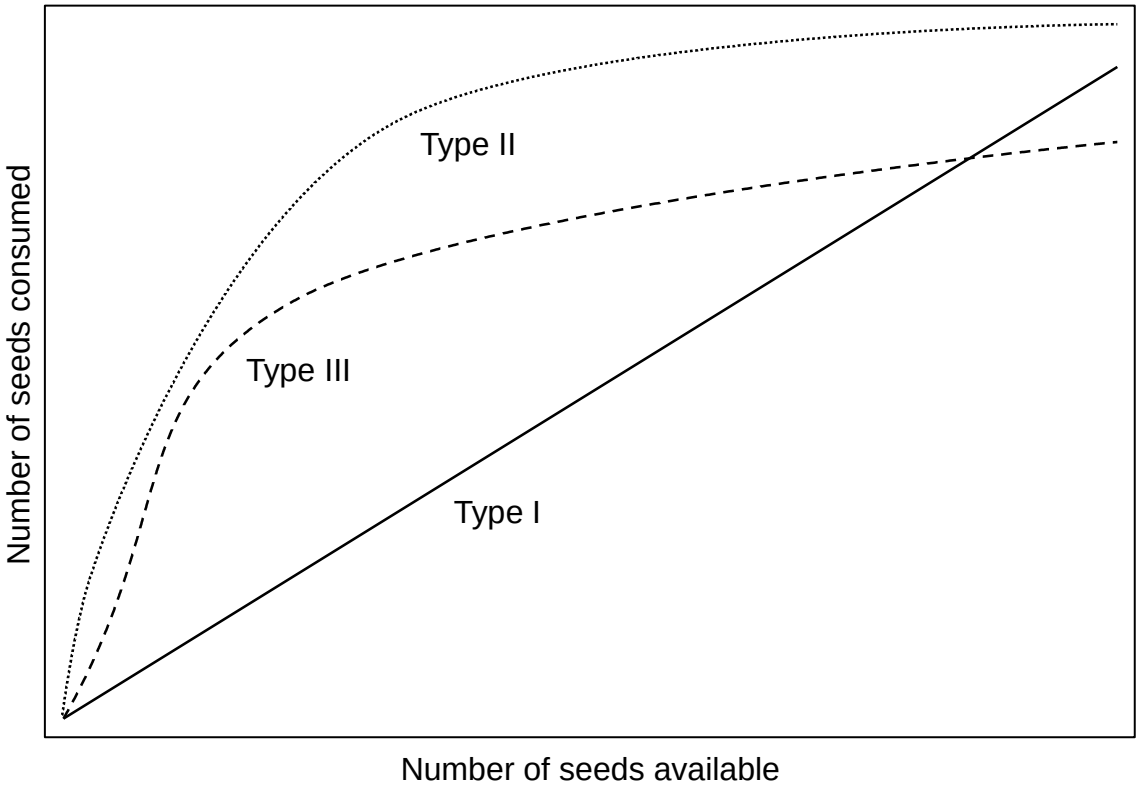

Figure 4-2. Functional responses of a seed predator according to the Predator Satiation Hypothesis. Type I: no response to seed density, Type II: predator satiation occurs with increasing seed density, Type III: peak rate of seed consumption at an intermediate seed density. Figure based on Figure 1 in Fletcher et al. (2010).

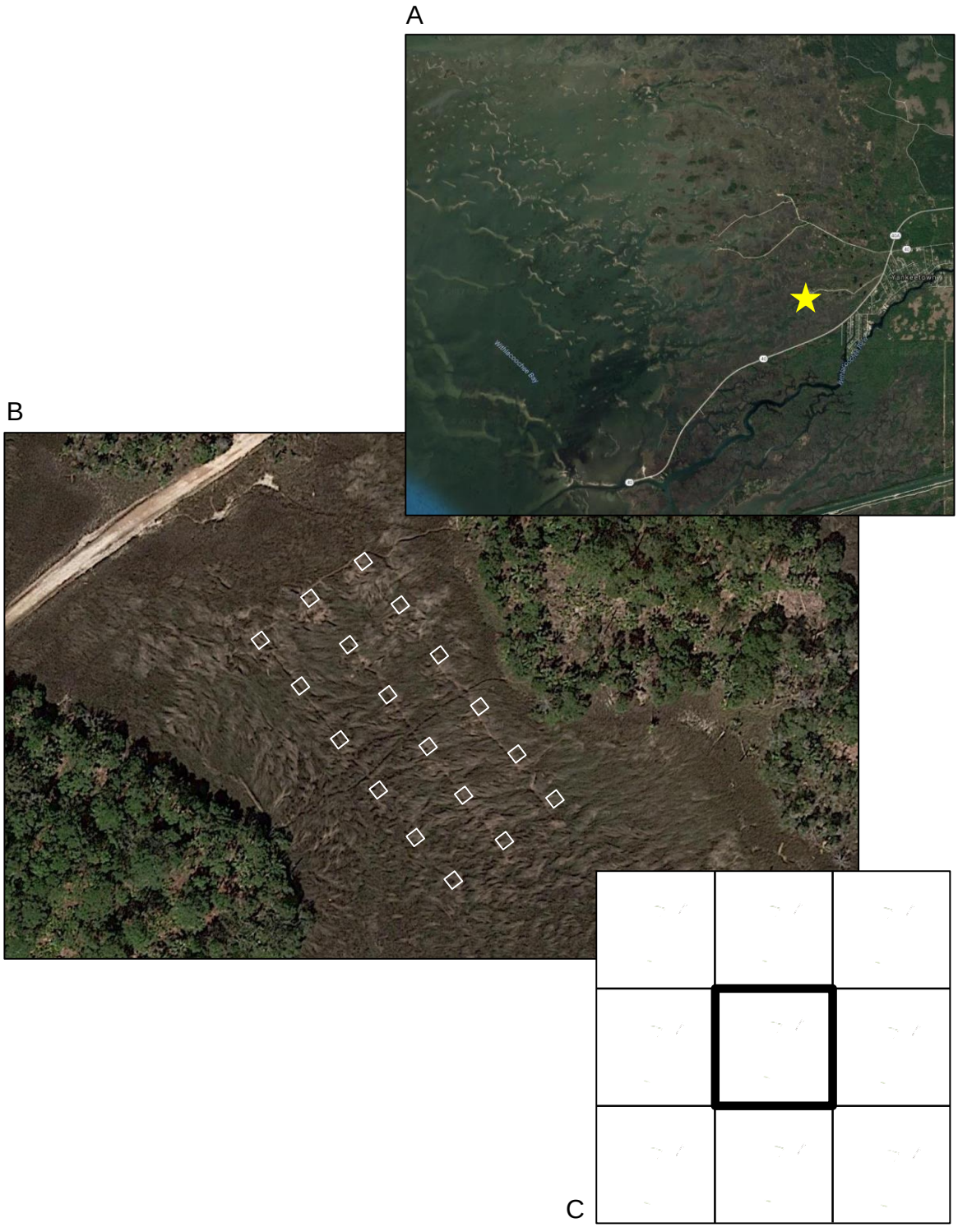

Figure 4-3. Design of propagule density experiment at Withlacoochee Gulf Preserve, Yankeetown, Florida. A) Location of experiment. B) Arrangement of the 18 density plots. C) Design of each plot, comprising 1 center experimental subplot and 8 surrounding buffer subplots; each subplot was 1 m^2.

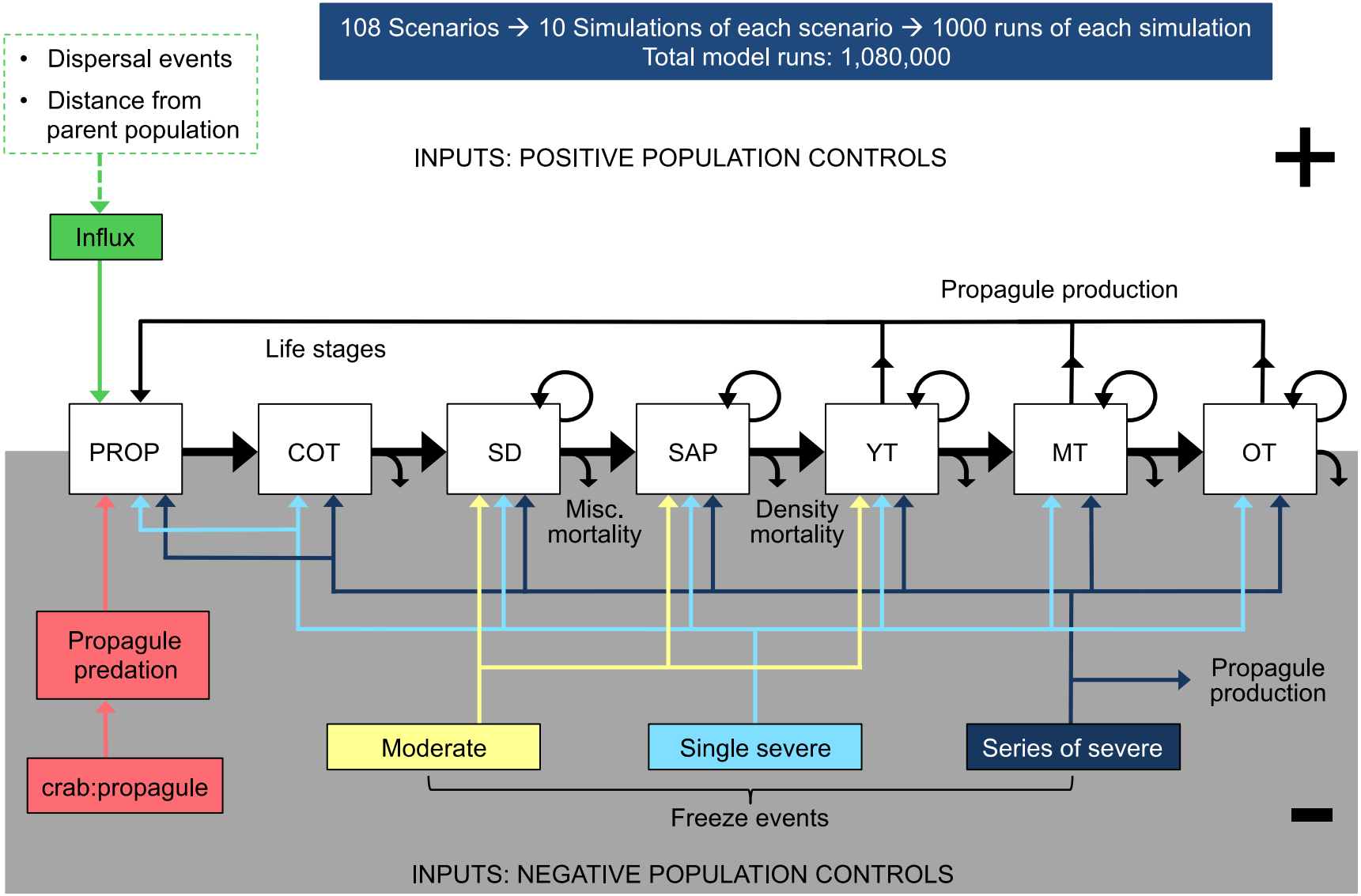

Figure 4-4. Diagrammed structure of the stage-based population growth model. PROP = propagule, COT = seedlings(cotyledons), SD = seedling, SAP = sapling, YT = young tree, MT = mature tree, OT= old tree.

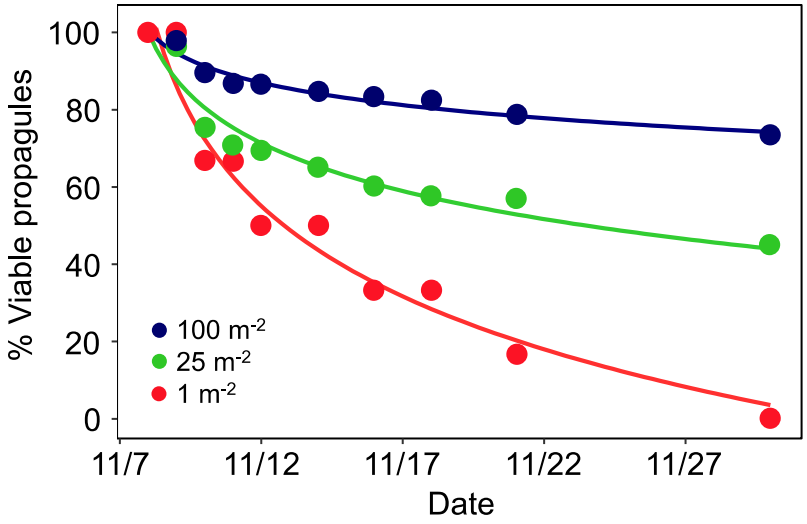

Figure 4-5. Change in percent viable propagules over time by density treatment.

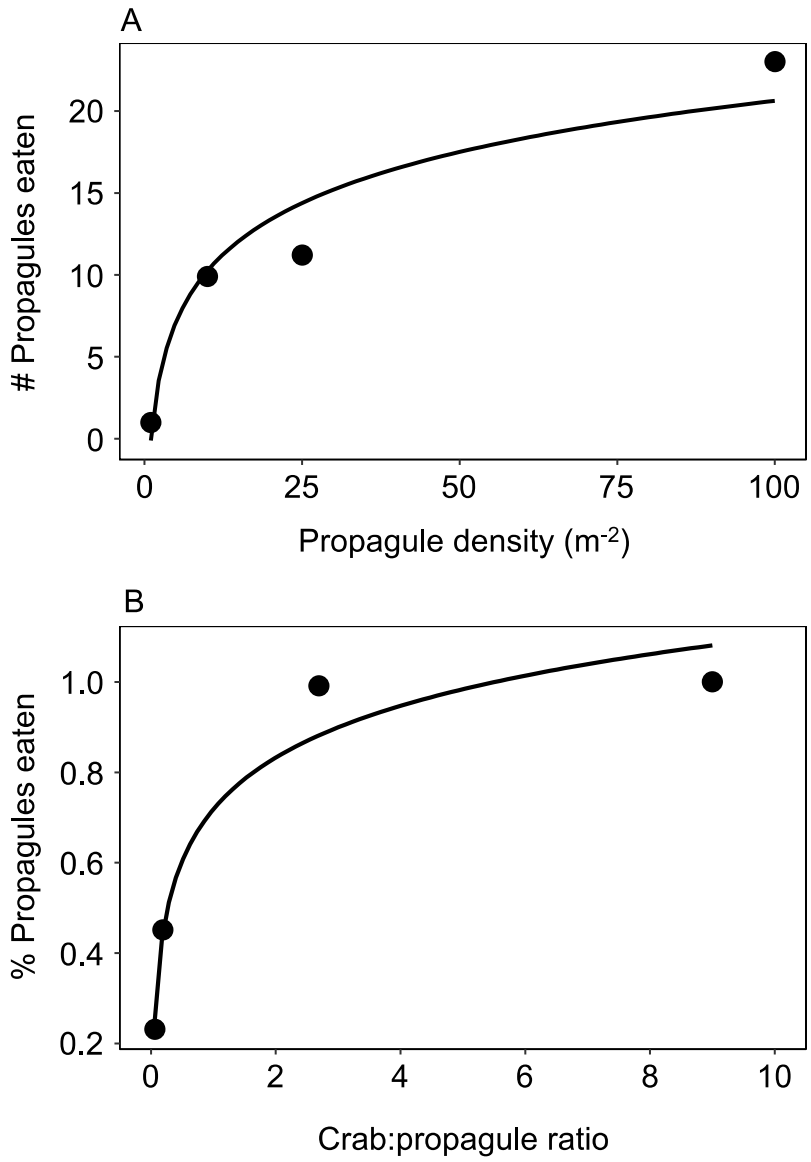

Figure 4-6. Propagule predation based on field data. A) Relationship between number of propagules eaten and propagule density reflects a Holling type II functional response (Holling, 1959b). B) The relationship between % propagules eaten versus crab:propagule ratios was used to calculate relative propagule mortality in the population growth model.

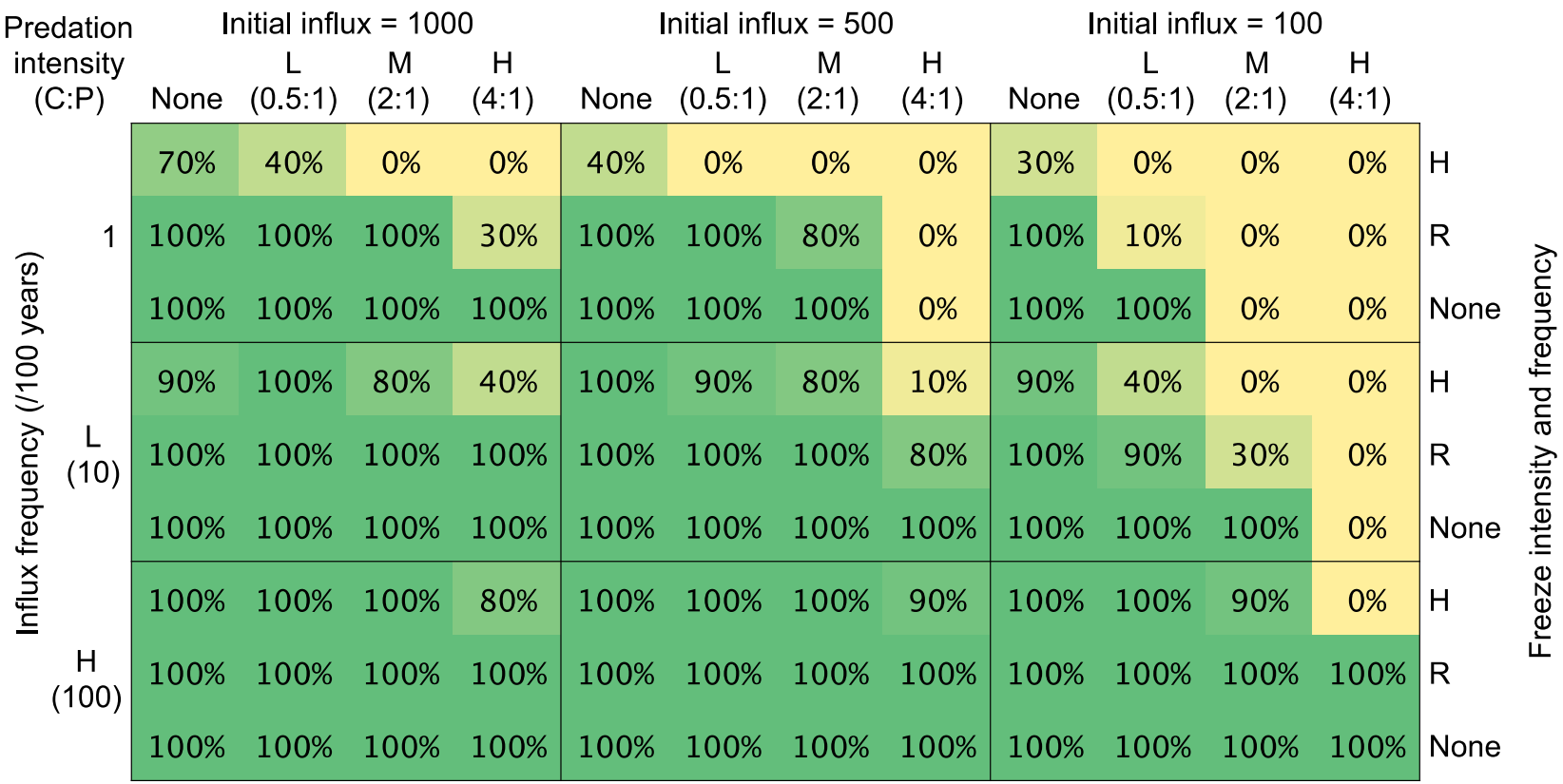

Figure 4-7. Outcomes of model scenarios. Scenarios vary by frequencies and intensities of propagule influxes (1 initial influx only, L=low, H=high), freeze events (None, R=reduced, H=historical), and intensities of propagule predation (None, L=low, M=moderate, H=high) that depend on the ratio of crabs to propagules (C:P).

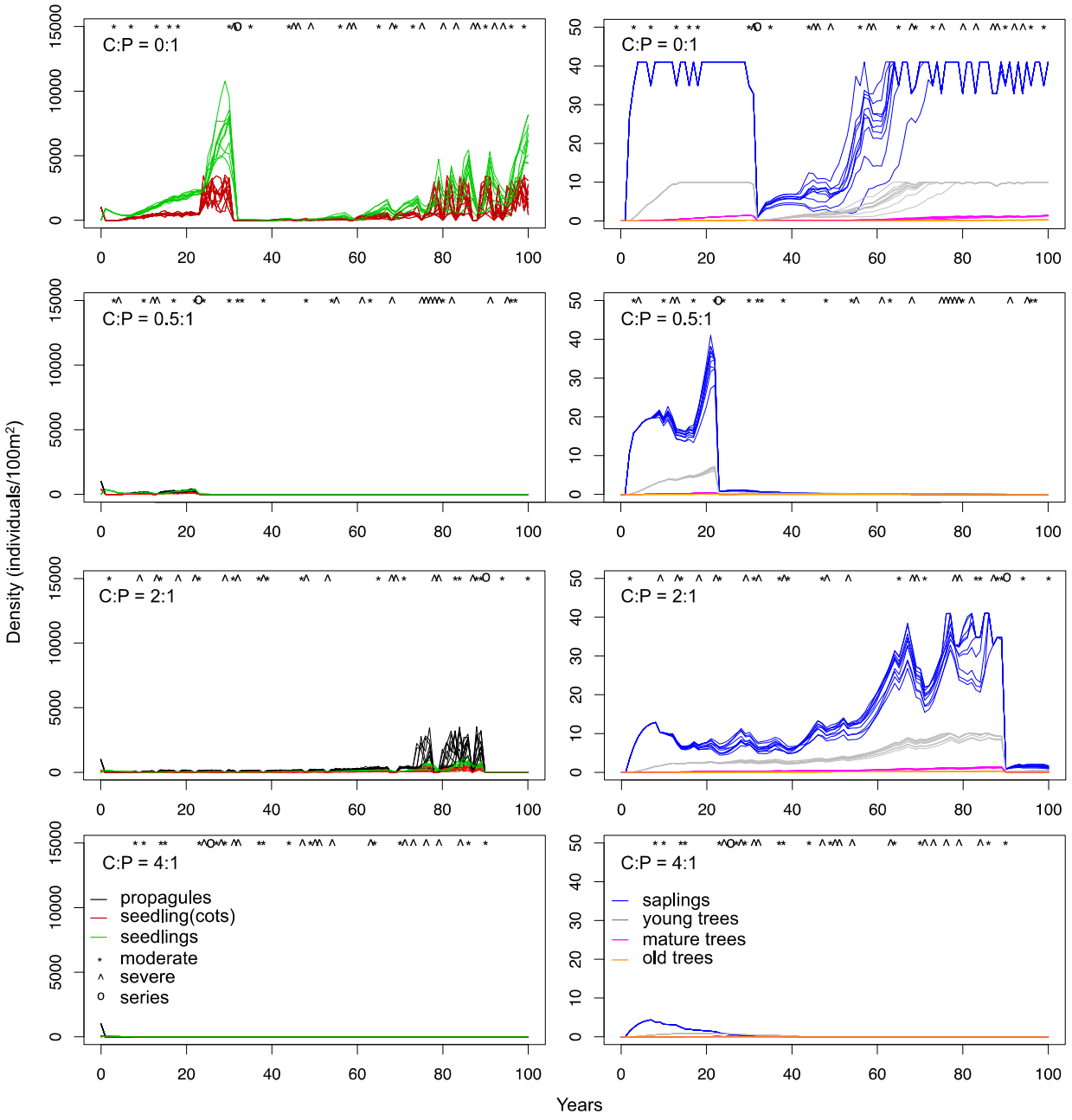

Figure 4-8. Outcomes from scenarios with an initial influx of 1000 propagules, no additional influxes, historical frequencies and intensities of freeze events, and varying intensities of propagule predation. C:P=crab:propagule, occurrences of freeze events are shown at the top of each graph: moderate=moderate freeze event, severe=single severe freeze event, series=series of severe freeze events. Note that life stage densities are split between two graphs for each scenario and have y-axes with different ranges. Densities for propagules, seedlings with cotyledons, and older seedlings are on the left; densities for saplings, young trees, mature trees, and old trees are on the right.

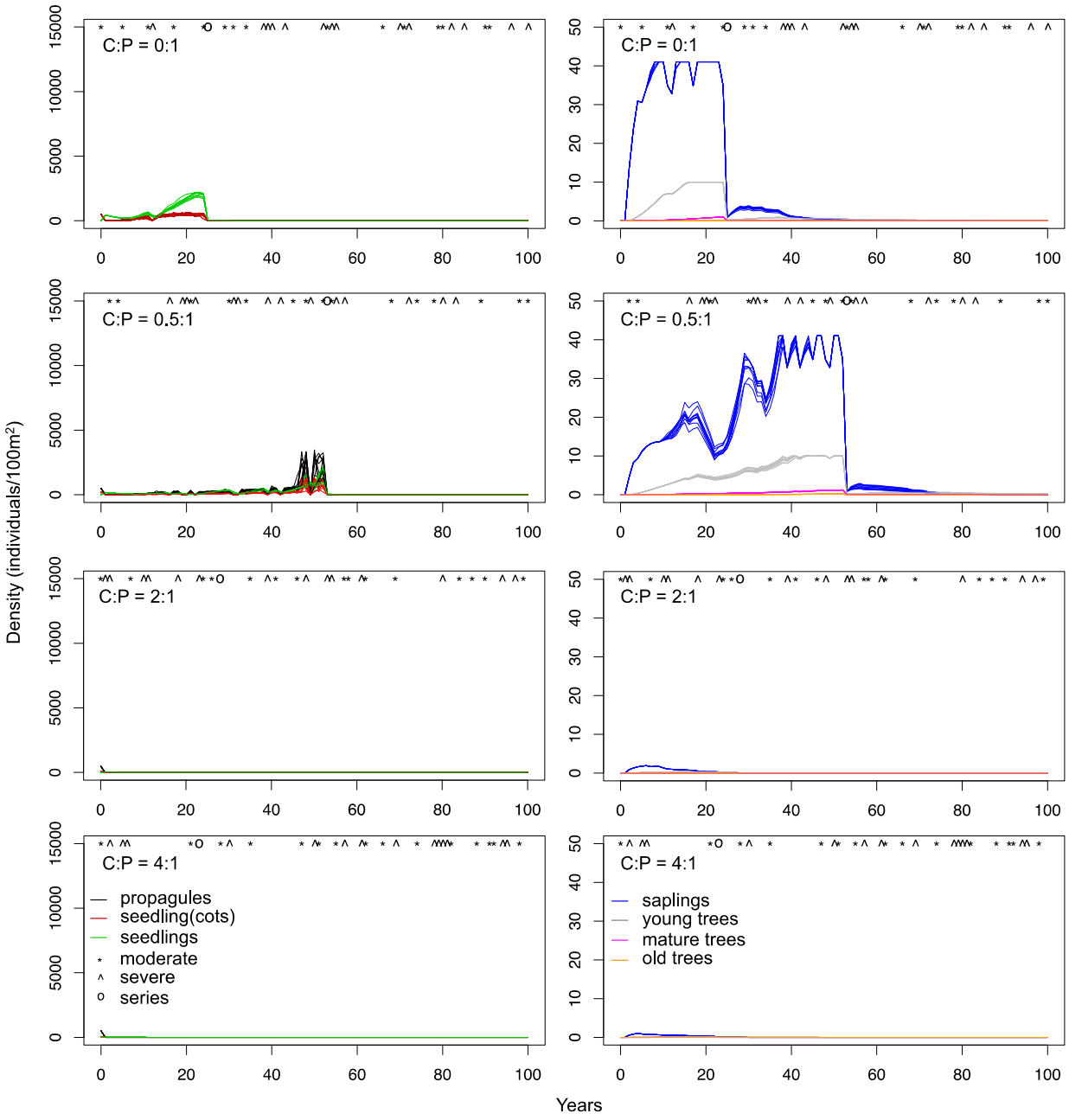

Figure 4-9. Outcomes from scenarios with an initial influx of 500 propagules, no additional influxes, historical frequencies and intensities of freeze events, and varying intensities of propagule predation. C:P=crab:propagule, occurrences of freeze events are shown at the top of each graph: moderate=moderate freeze event, severe=single severe freeze event, series=series of severe freeze events.

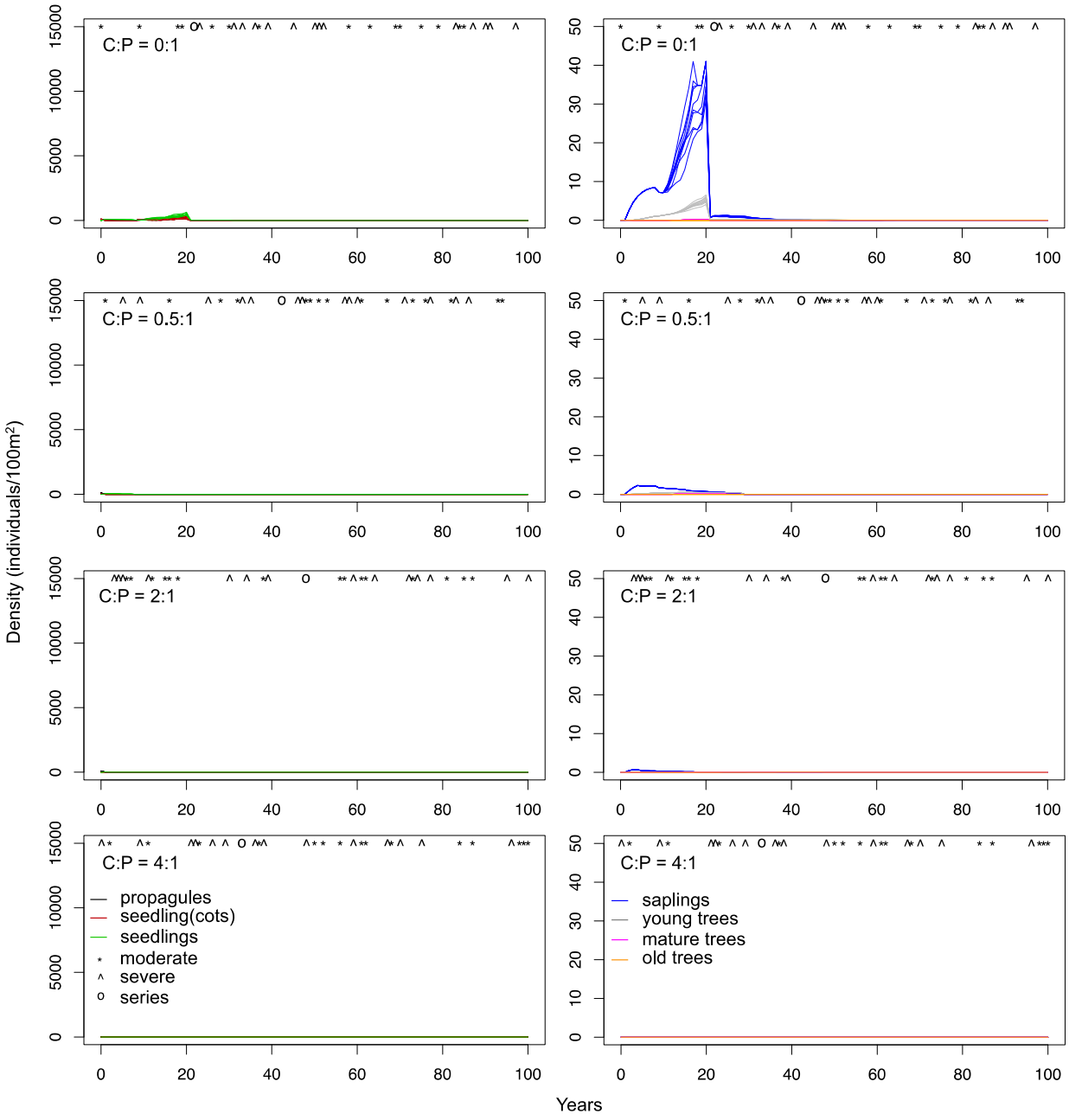

Figure 4-10. Outcomes from scenarios with an initial influx of 100 propagules, no additional influxes, historical frequencies and intensities of freeze events, and varying intensities of propagule predation. C:P=crab:propagule, occurrences of freeze events are shown at the top of each graph: moderate=moderate freeze event, severe=single severe freeze event, series=series of severe freeze events.

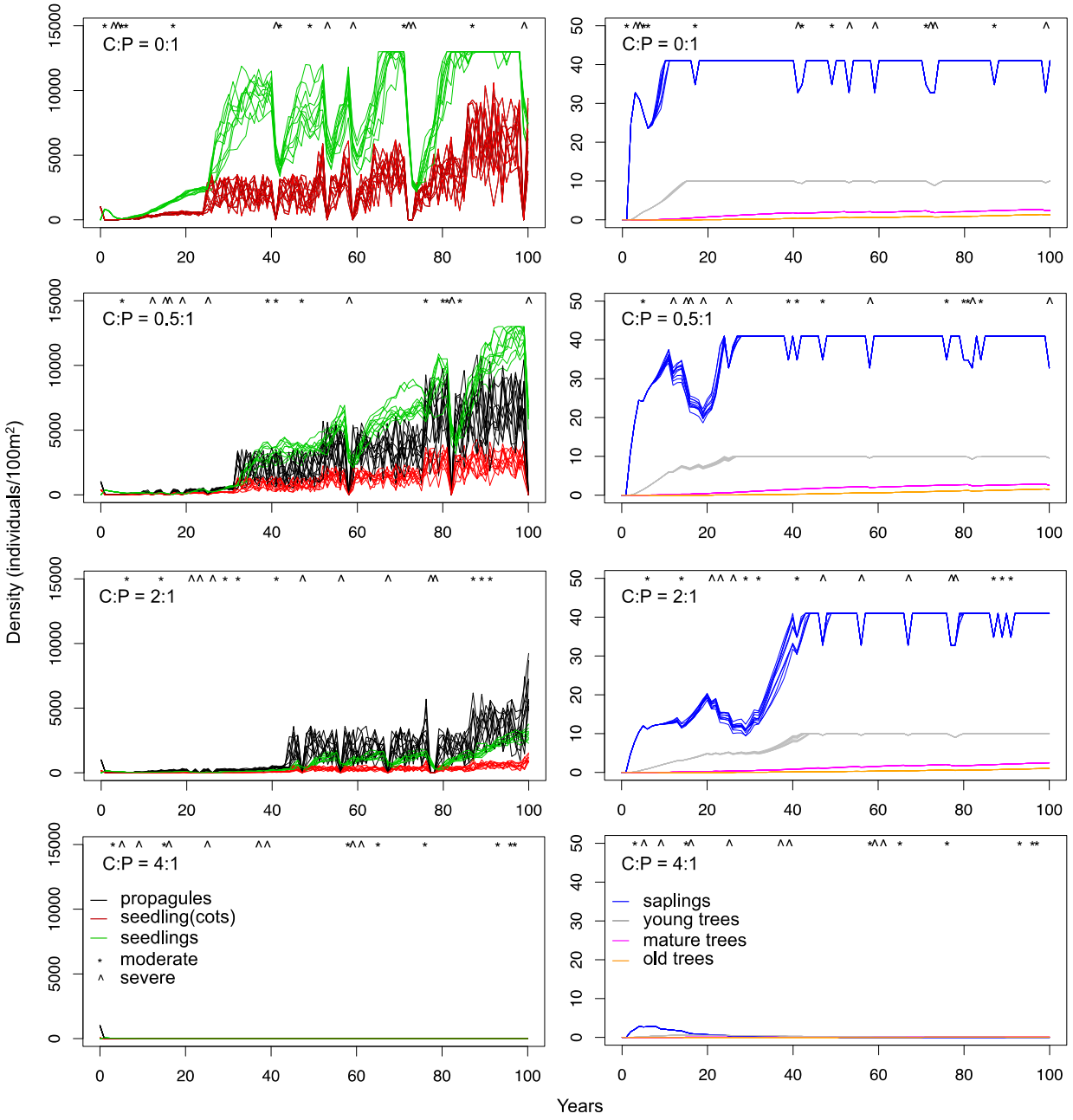

Figure 4-11. Outcomes from scenarios with an initial influx of 1000 propagules, no additional influxes, reduced frequencies and intensities of freeze events, and varying intensities of propagule predation. C:P=crab:propagule, occurrences of freeze events are shown at the top of each graph: moderate=moderate freeze event, severe=single severe freeze event.

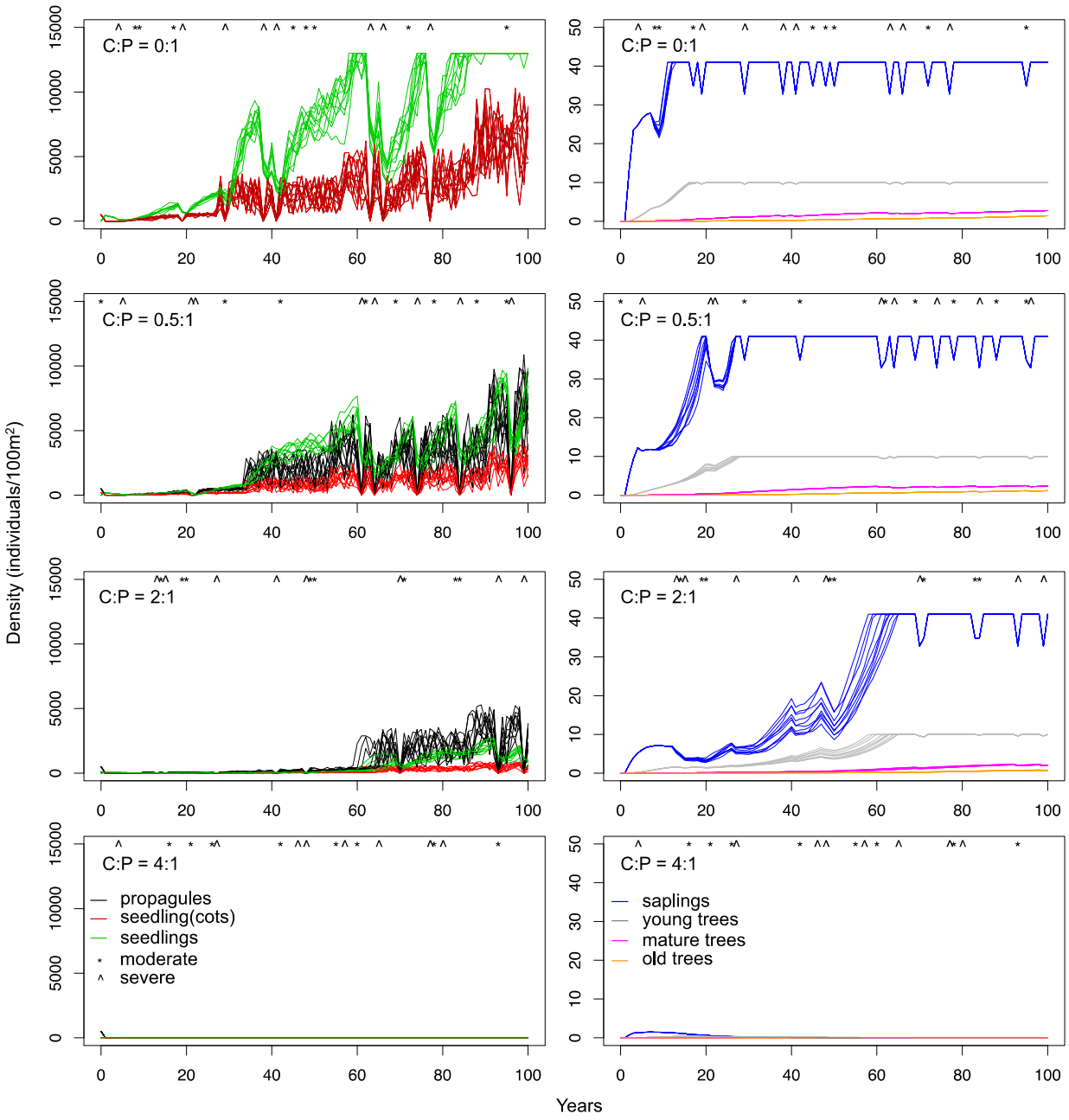

Figure 4-12. Outcomes from scenarios with an initial influx of 500 propagules, no additional influxes, reduced frequencies and intensities of freeze events, and varying intensities of propagule predation. C:P=crab:propagule, occurrences of freeze events are shown at the top of each graph: moderate=moderate freeze event, severe=single severe freeze event.

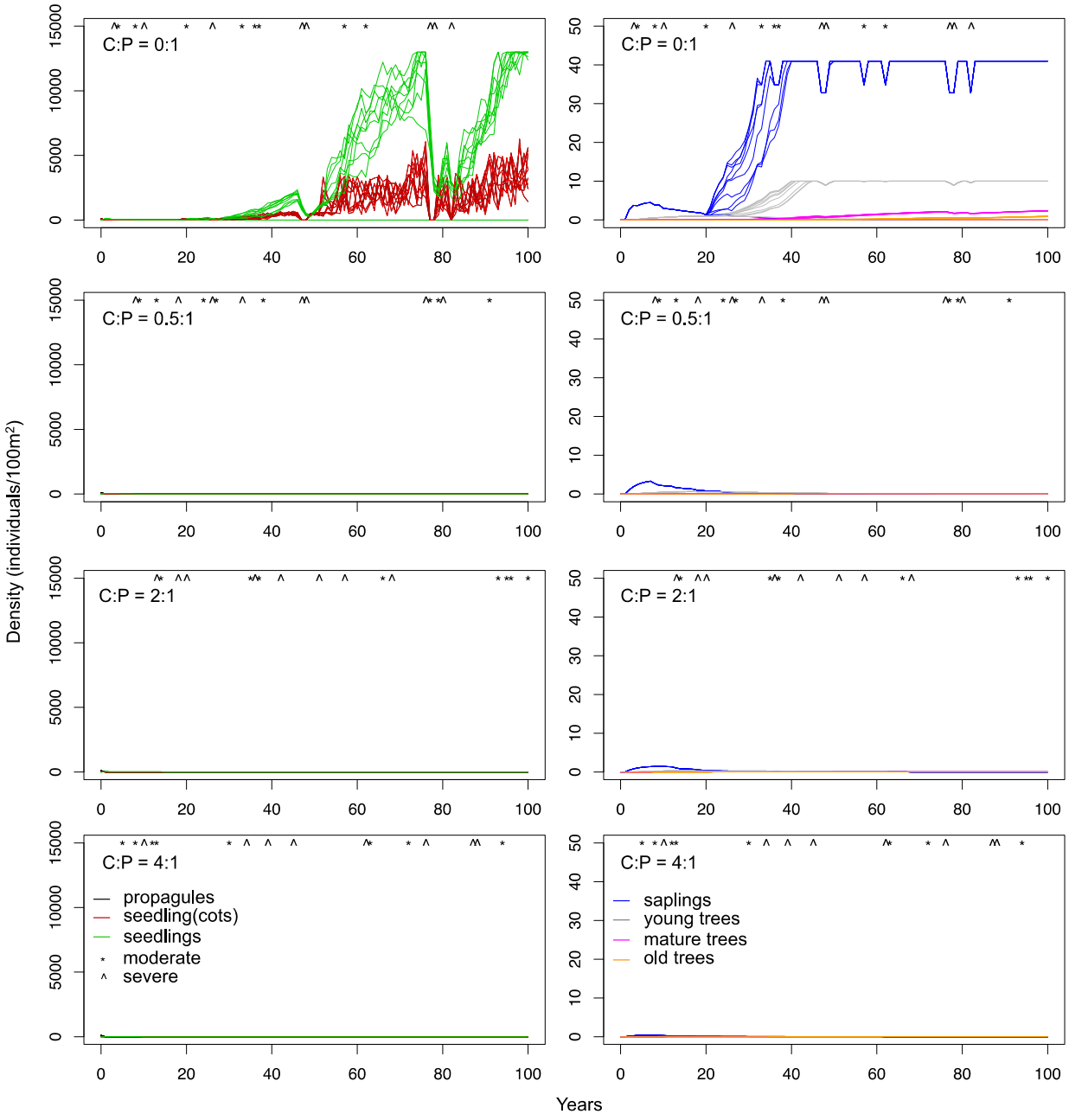

Figure 4-13. Outcomes from scenarios with an initial influx of 100 propagules, no additional influxes, reduced frequencies and intensities of freeze events, and varying intensities of propagule predation. C:P=crab:propagule, occurrences of freeze events are shown at the top of each graph: moderate=moderate freeze event, severe=single severe freeze event.

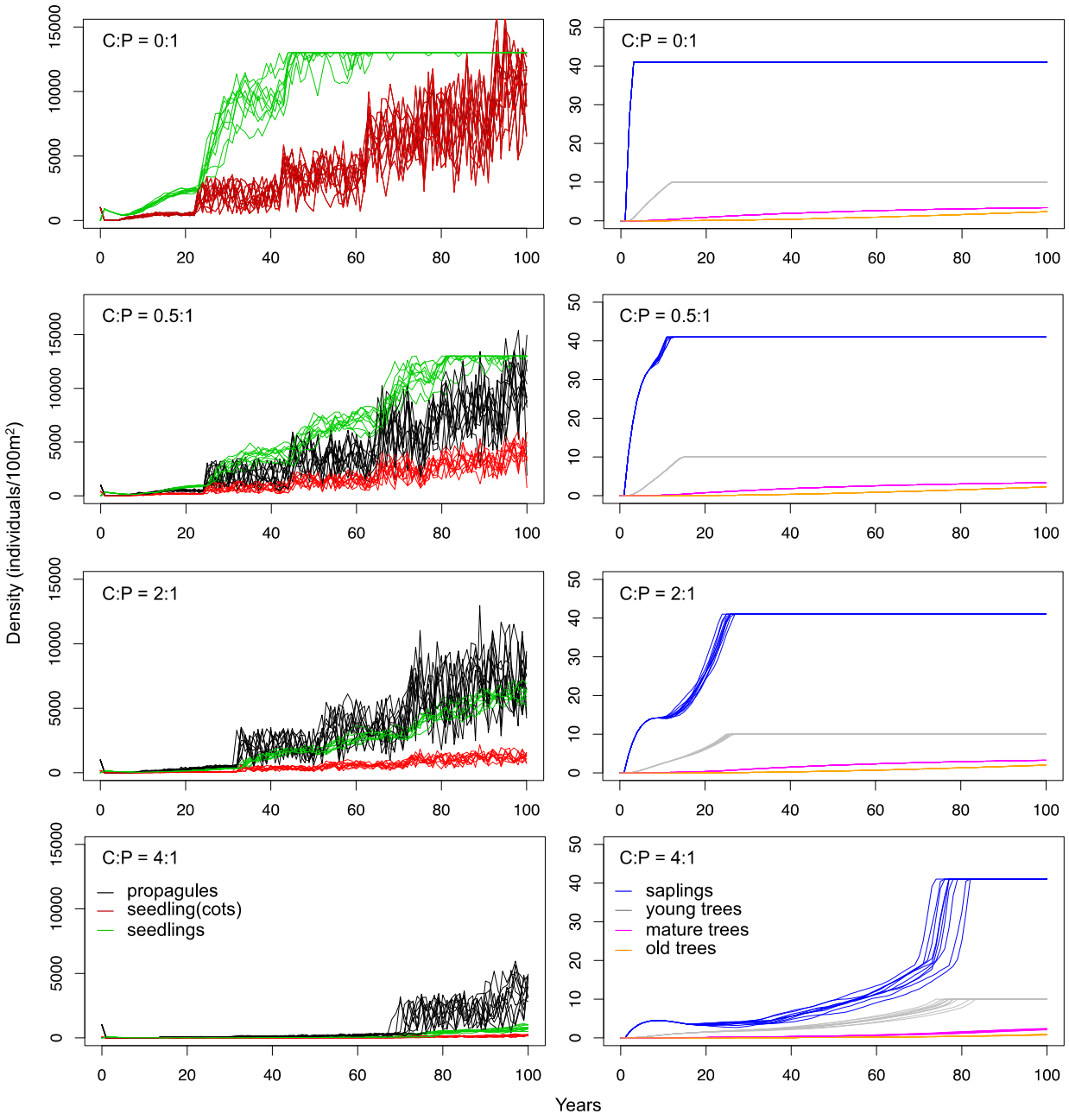

Figure 4-14. Outcomes from scenarios with an initial influx of 1000 propagules, no additional influxes, no freeze events, and varying intensities of propagule predation. C:P=crab:propagule.

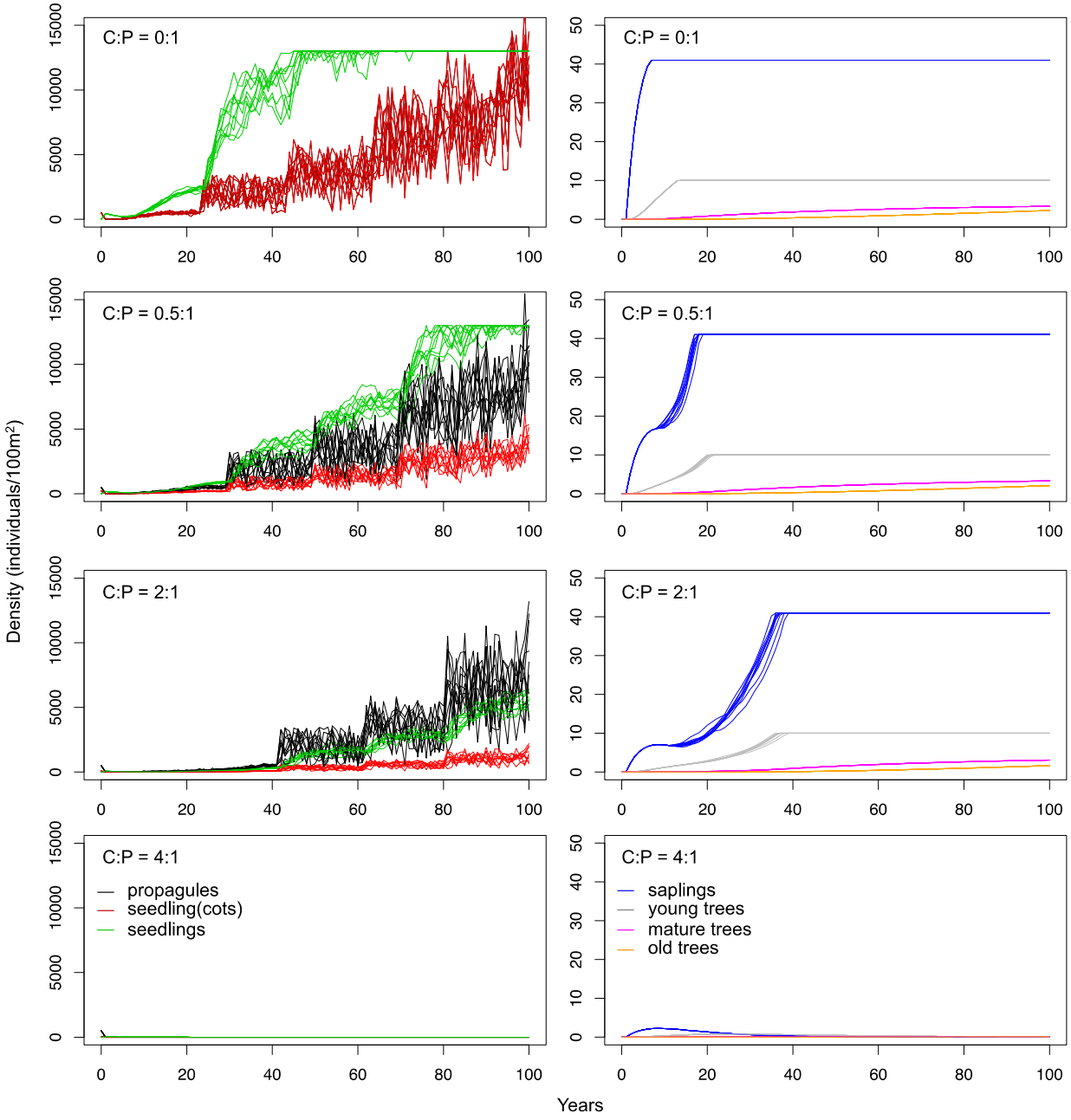

Figure 4-15. Outcomes from scenarios with an initial influx of 500 propagules, no additional influxes, no freeze events, and varying intensities of propagule predation. C:P=crab:propagule.

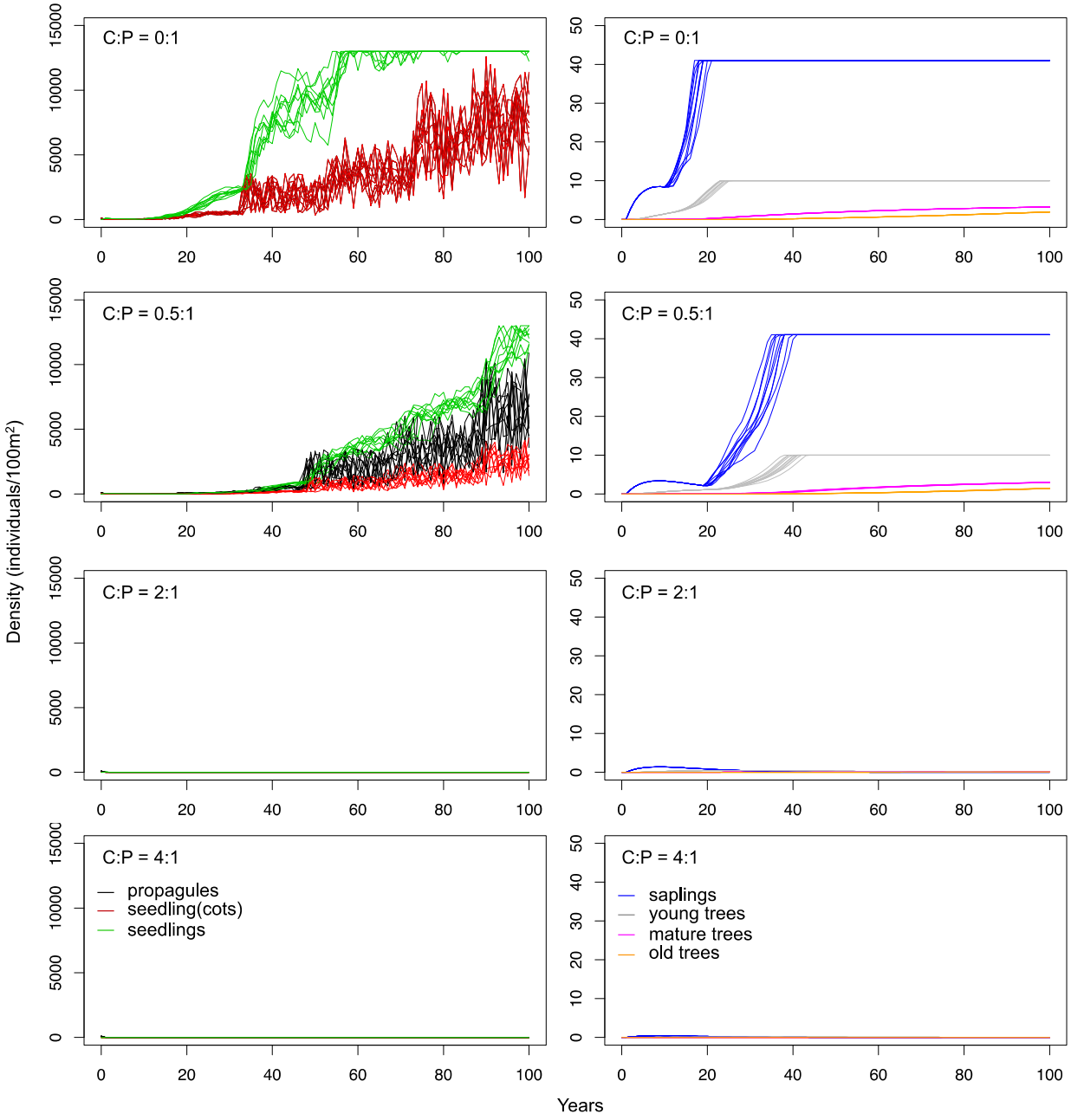

Figure 4-16. Outcomes from scenarios with an initial influx of 100 propagules, no additional influxes, no freeze events, and varying intensities of propagule predation. C:P=crab:propagule.

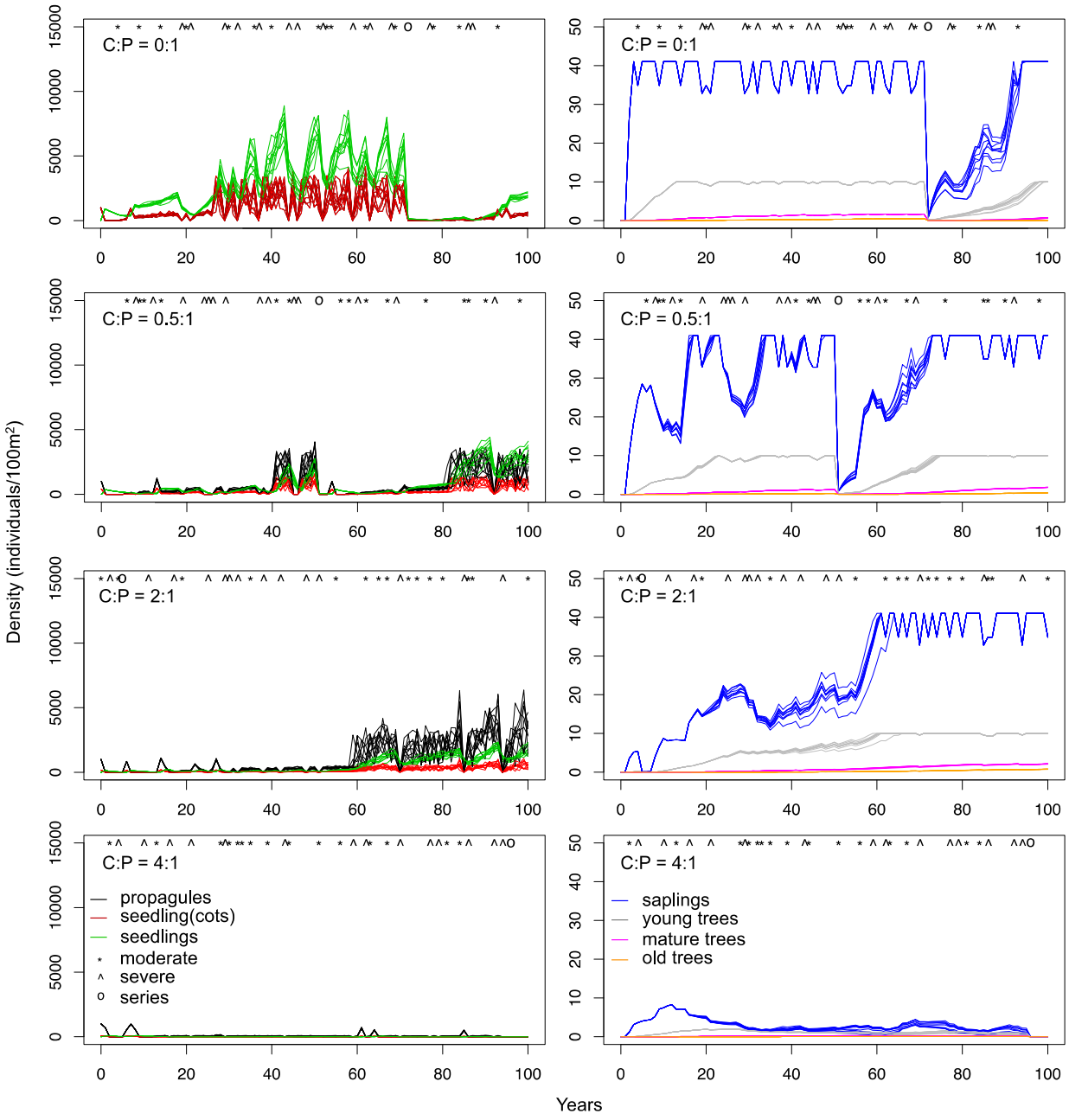

Figure 4-17. Outcomes from scenarios with an initial influx of 1000 propagules, low influx frequency, historical frequencies and intensities of freeze events, and varying intensities of propagule predation. C:P=crab:propagule, occurrences of freeze events are shown at the top of each graph: moderate=moderate freeze event, severe=single severe freeze event, series=series of severe freeze events.

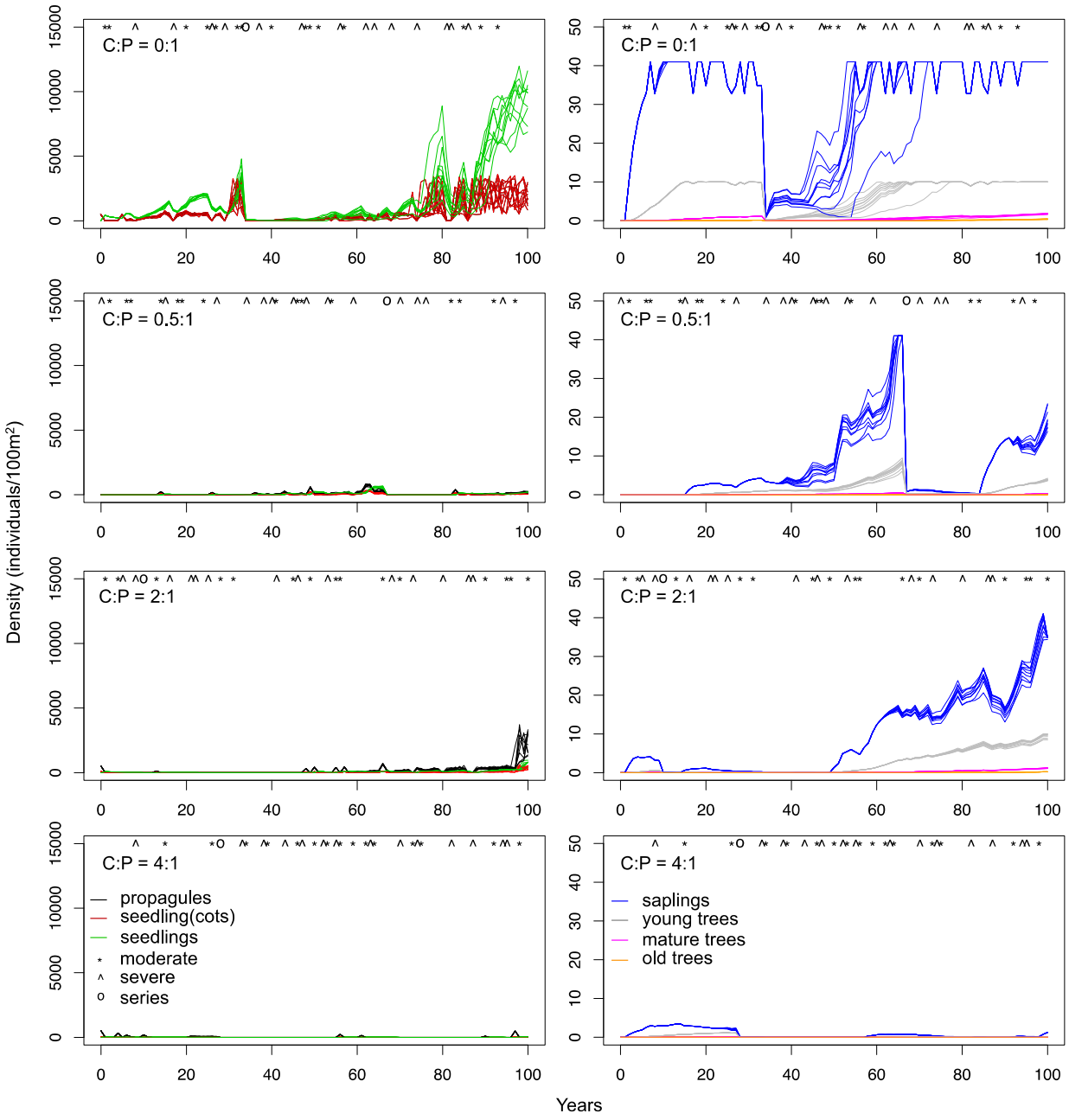

Figure 4-18. Outcomes from scenarios with an initial influx of 500 propagules, low influx frequency, historical frequencies and intensities of freeze events, and varying intensities of propagule predation. C:P=crab:propagule, occurrences of freeze events are shown at the top of each graph: moderate=moderate freeze event, severe=single severe freeze event, series=series of severe freeze events.

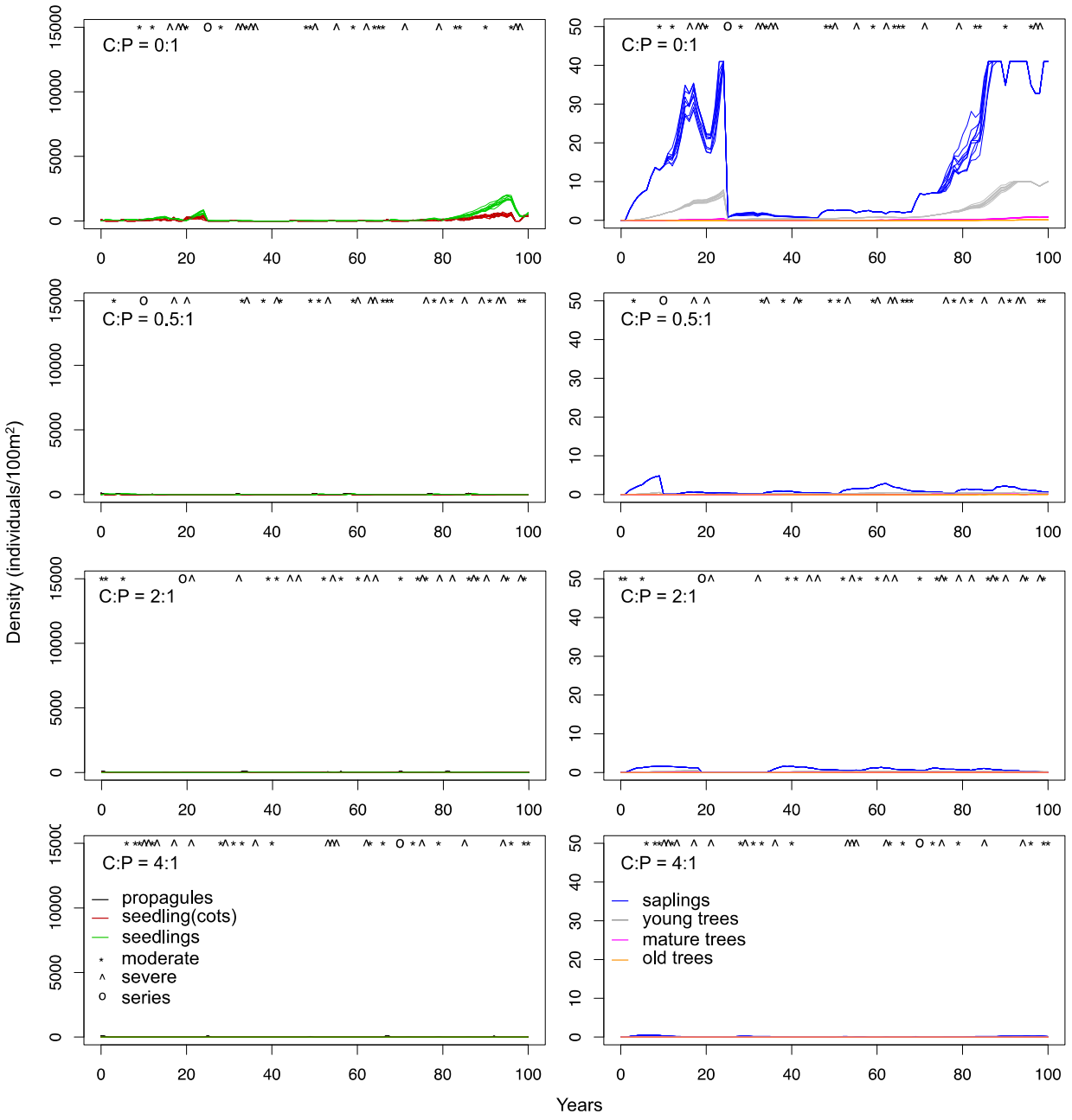

Figure 4-19. Outcomes from scenarios with an initial influx of 100 propagules, low influx frequency, historical frequencies and intensities of freeze events, and varying intensities of propagule predation. C:P=crab:propagule, occurrences of freeze events are shown at the top of each graph: moderate=moderate freeze event, severe=single severe freeze event, series=series of severe freeze events.

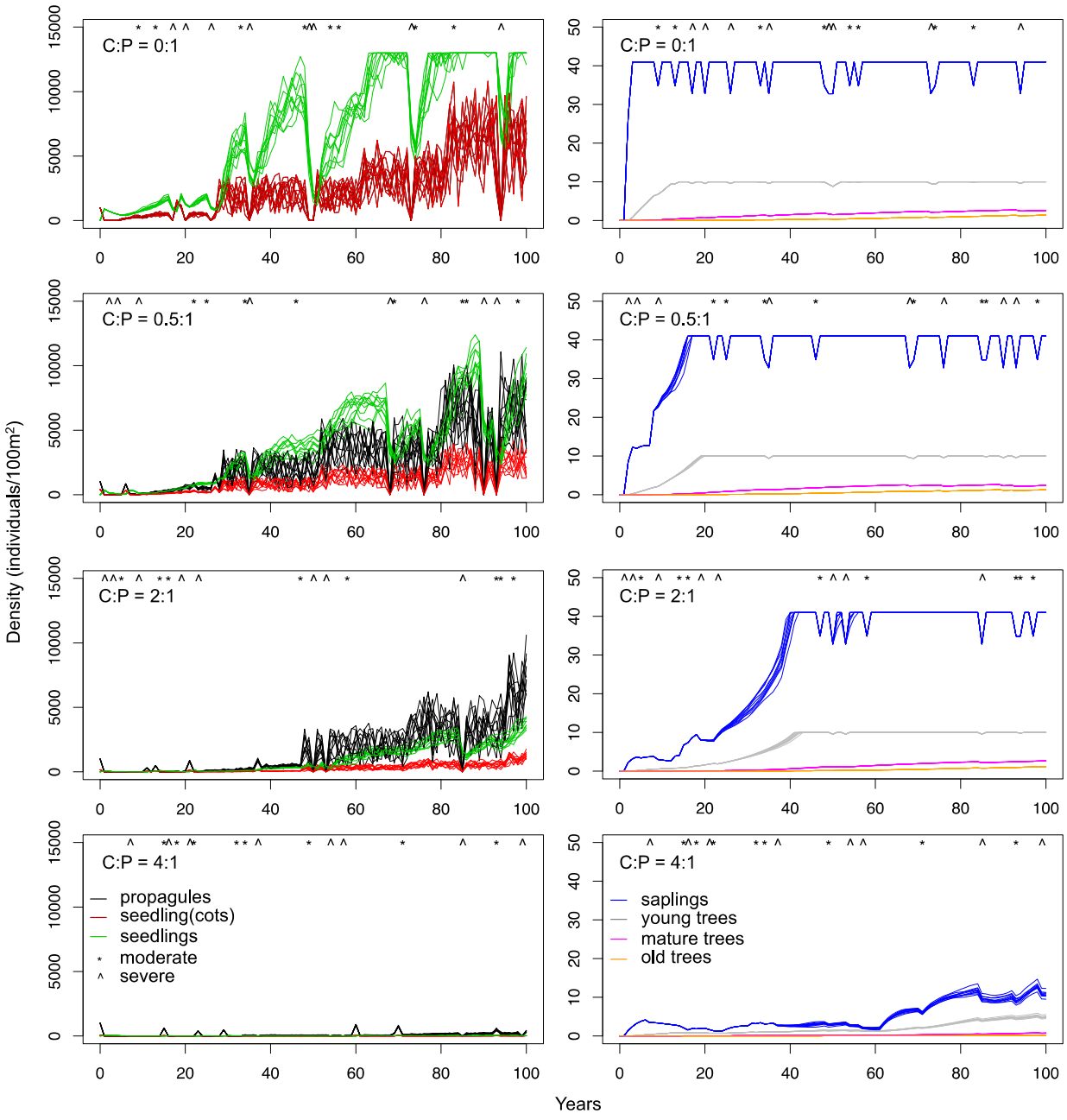

Figure 4-20. Outcomes from scenarios with an initial influx of 1000 propagules, low influx frequency, reduced frequencies and intensities of freeze events, and varying intensities of propagule predation. C:P=crab:propagule, occurrences of freeze events are shown at the top of each graph: moderate=moderate freeze event, severe=single severe freeze event.

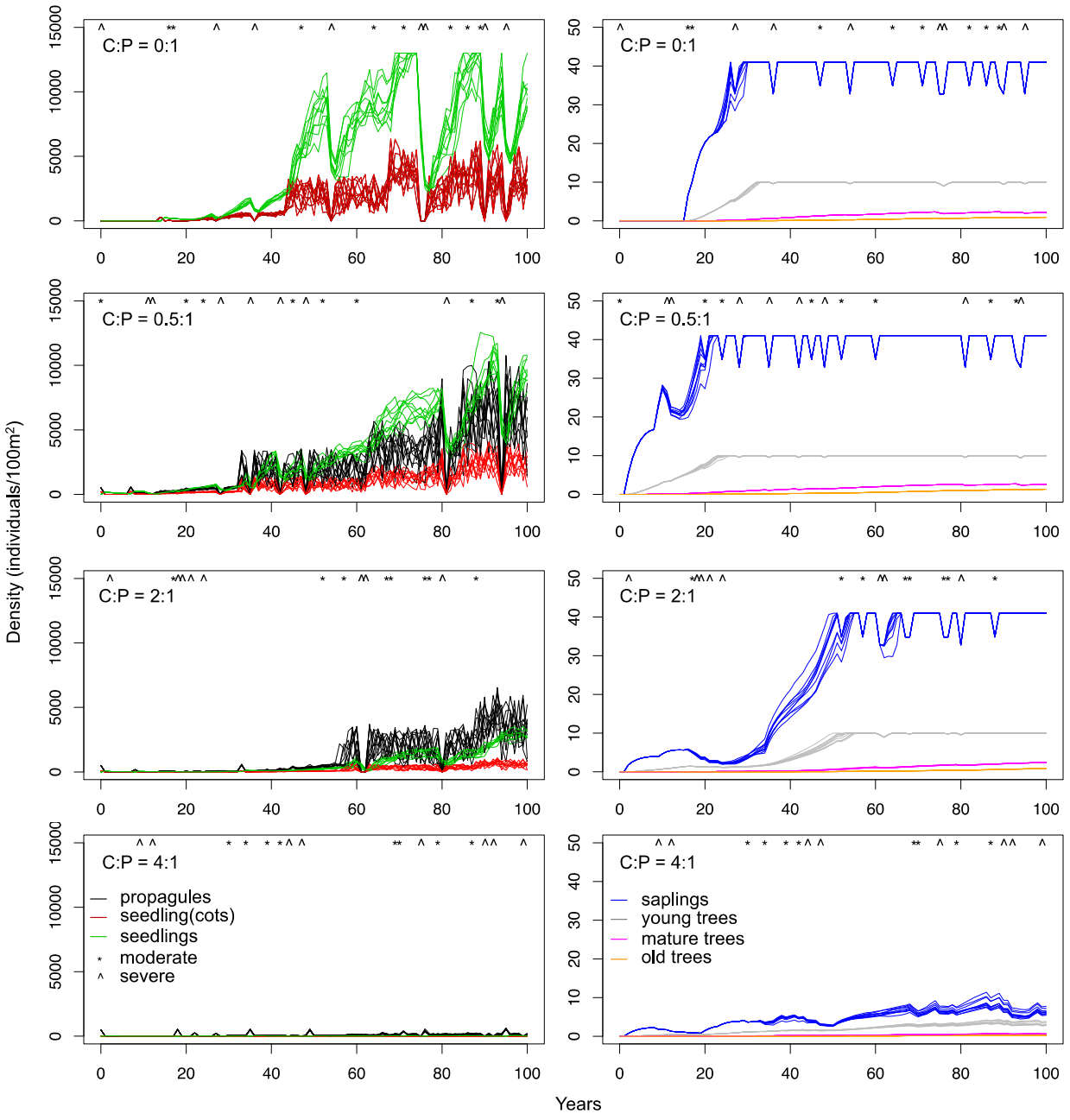

Figure 4-21. Outcomes from scenarios with an initial influx of 500 propagules, low influx frequency, reduced frequencies and intensities of freeze events, and varying intensities of propagule predation. C:P=crab:propagule, occurrences of freeze events are shown at the top of each graph: moderate=moderate freeze event, severe=single severe freeze event.

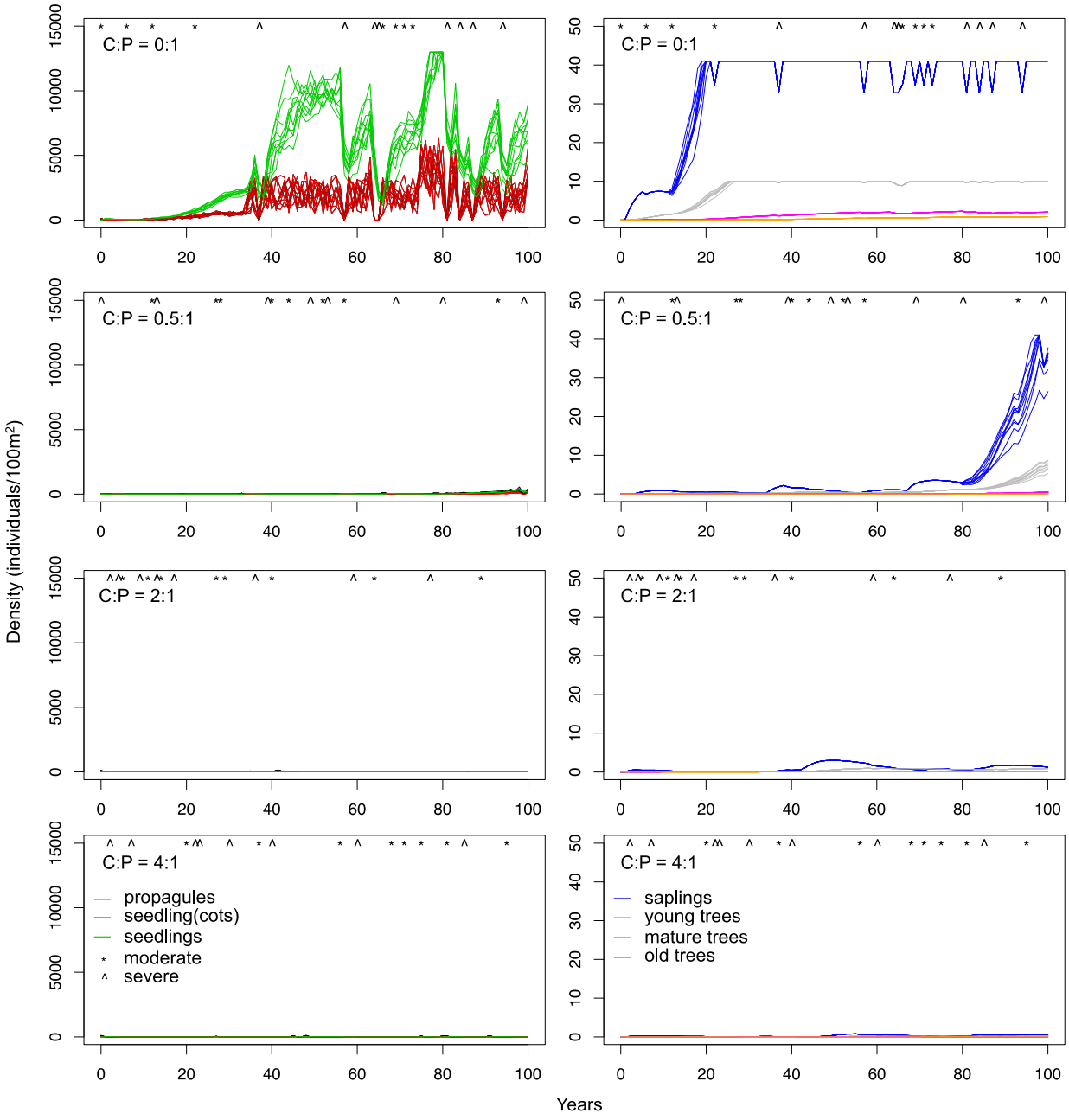

Figure 4-22. Outcomes from scenarios with an initial influx of 100 propagules, low influx frequency, reduced frequencies and intensities of freeze events, and varying intensities of propagule predation. C:P=crab:propagule, occurrences of freeze events are shown at the top of each graph: moderate=moderate freeze event, severe=single severe freeze event.

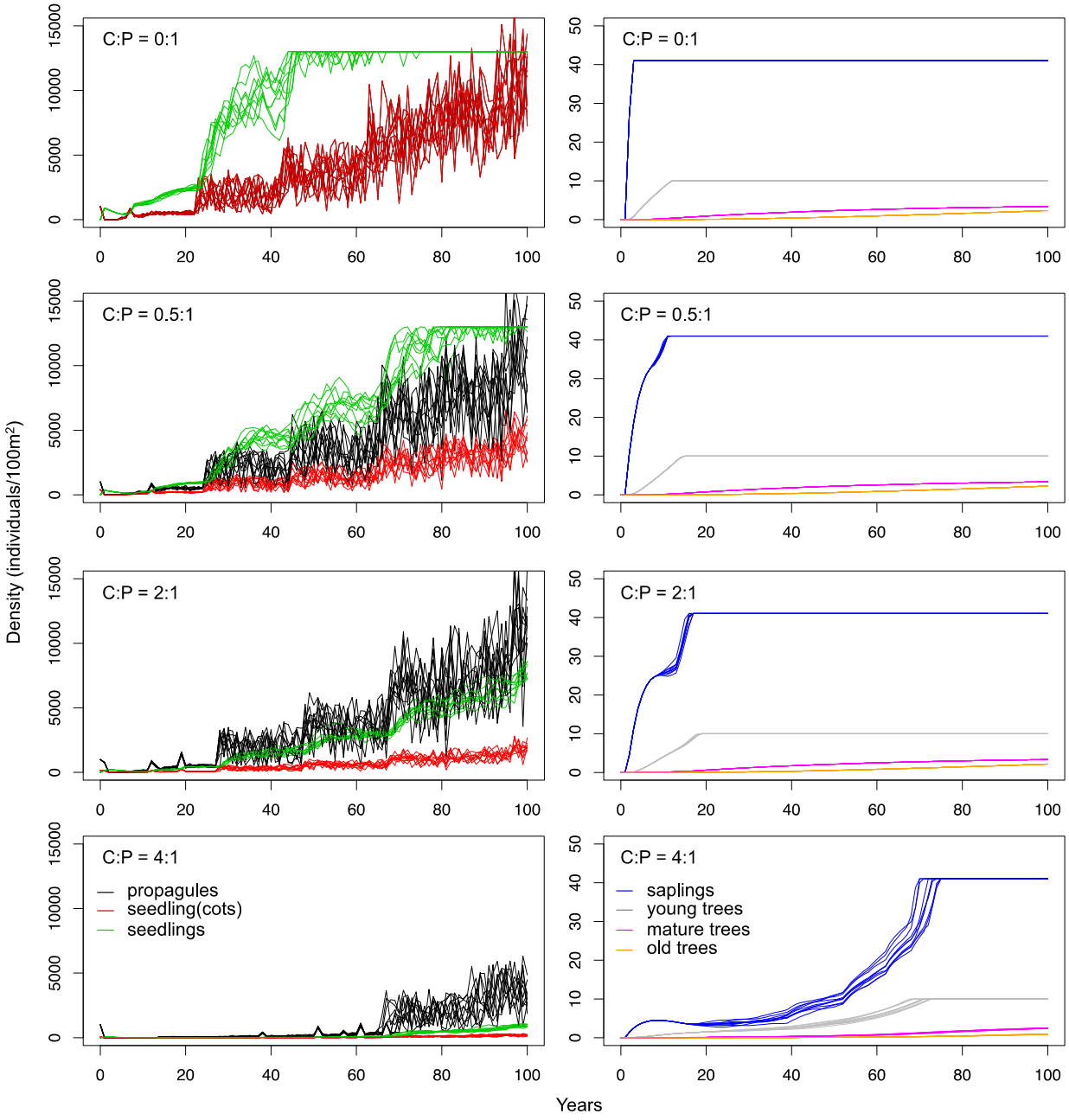

Figure 4-23. Outcomes from scenarios with an initial influx of 1000 propagules, low influx frequency, no freeze events, and varying intensities of propagule predation. C:P=crab:propagule.

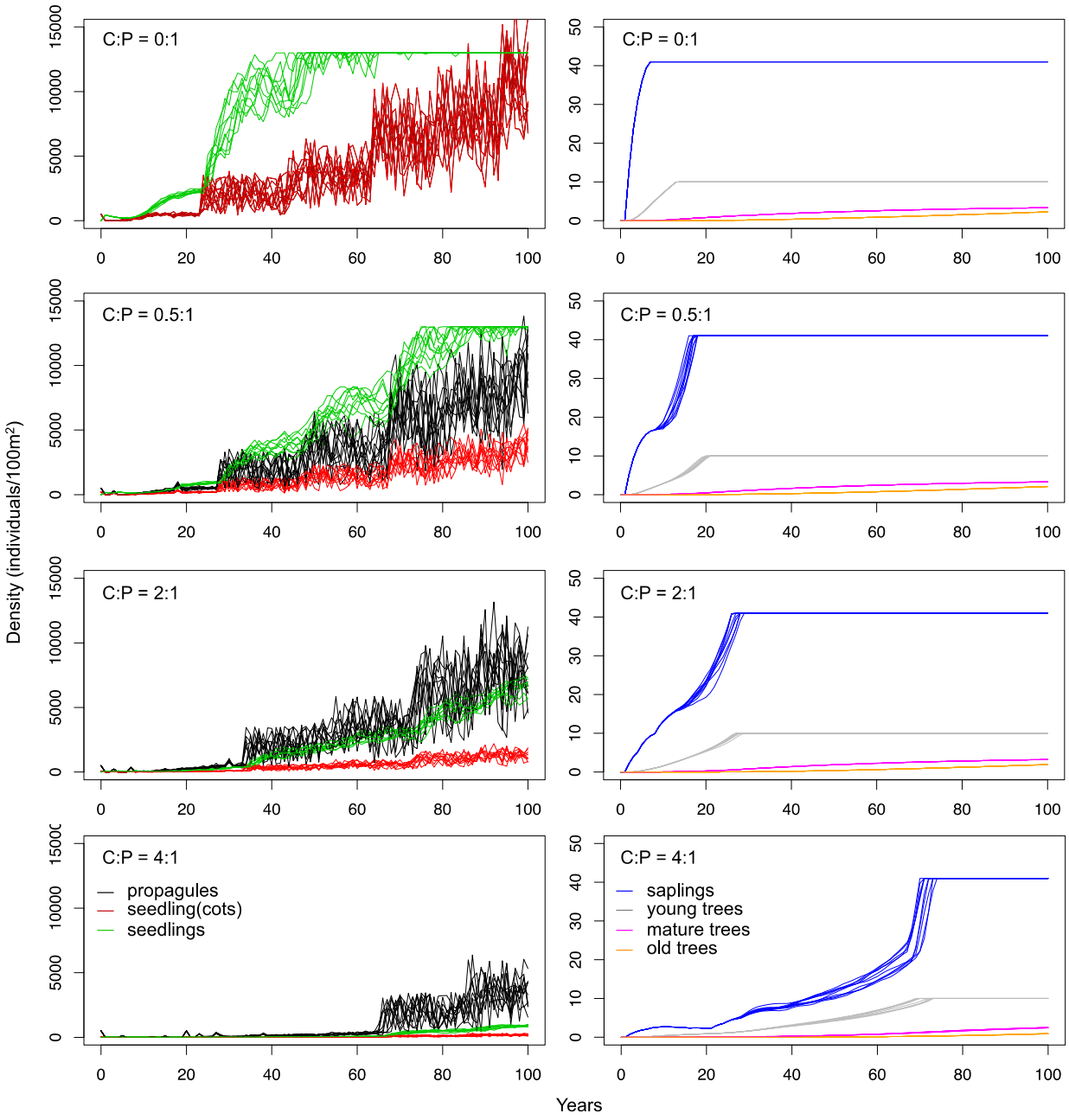

Figure 4-24. Outcomes from scenarios with an initial influx of 500 propagules, low influx frequency, no freeze events, and varying intensities of propagule predation. C:P=crab:propagule.

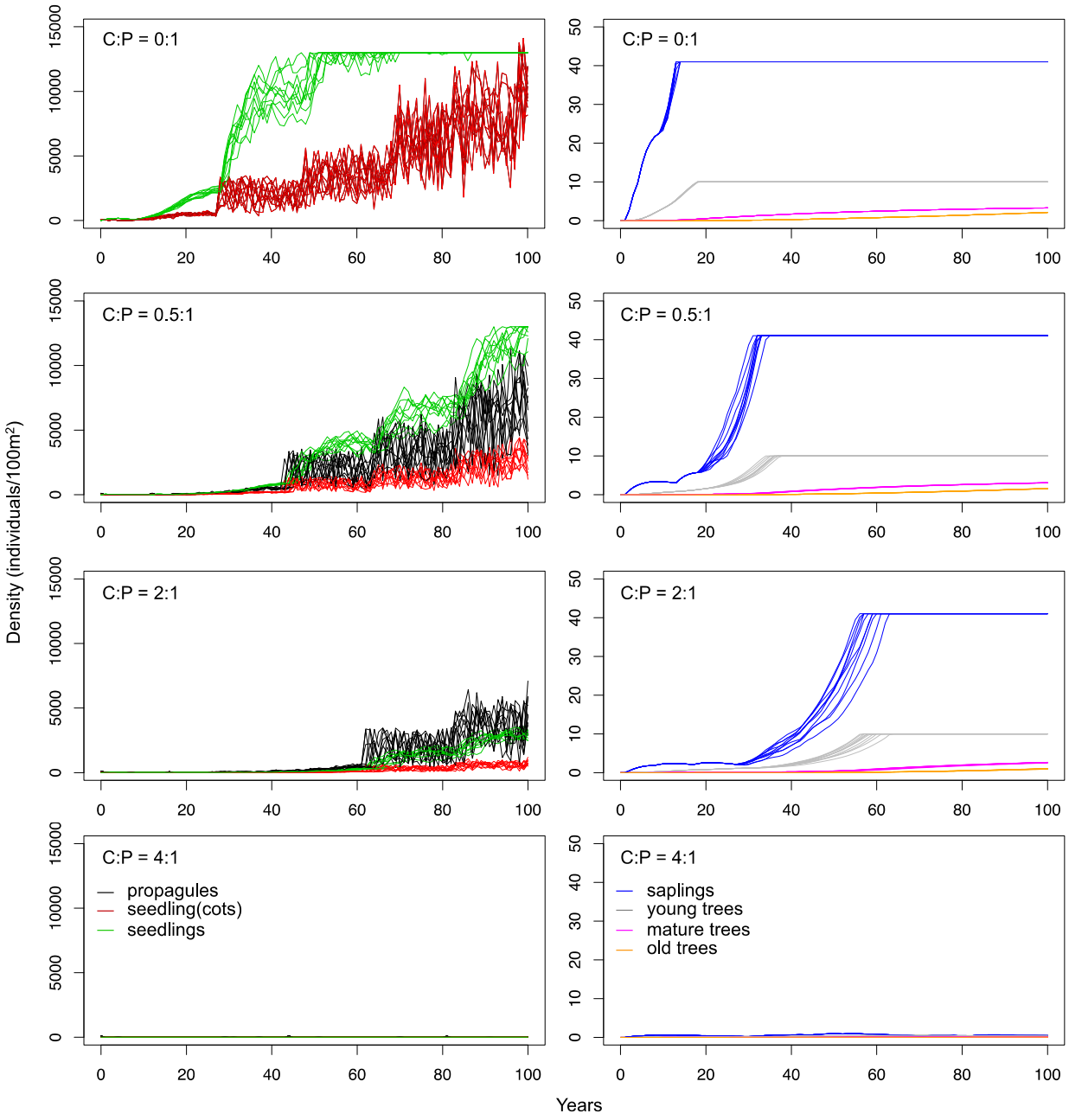

Figure 4-25. Outcomes from scenarios with an initial influx of 100 propagules, low influx frequency, no freeze events, and varying intensities of propagule predation. C:P=crab:propagule.

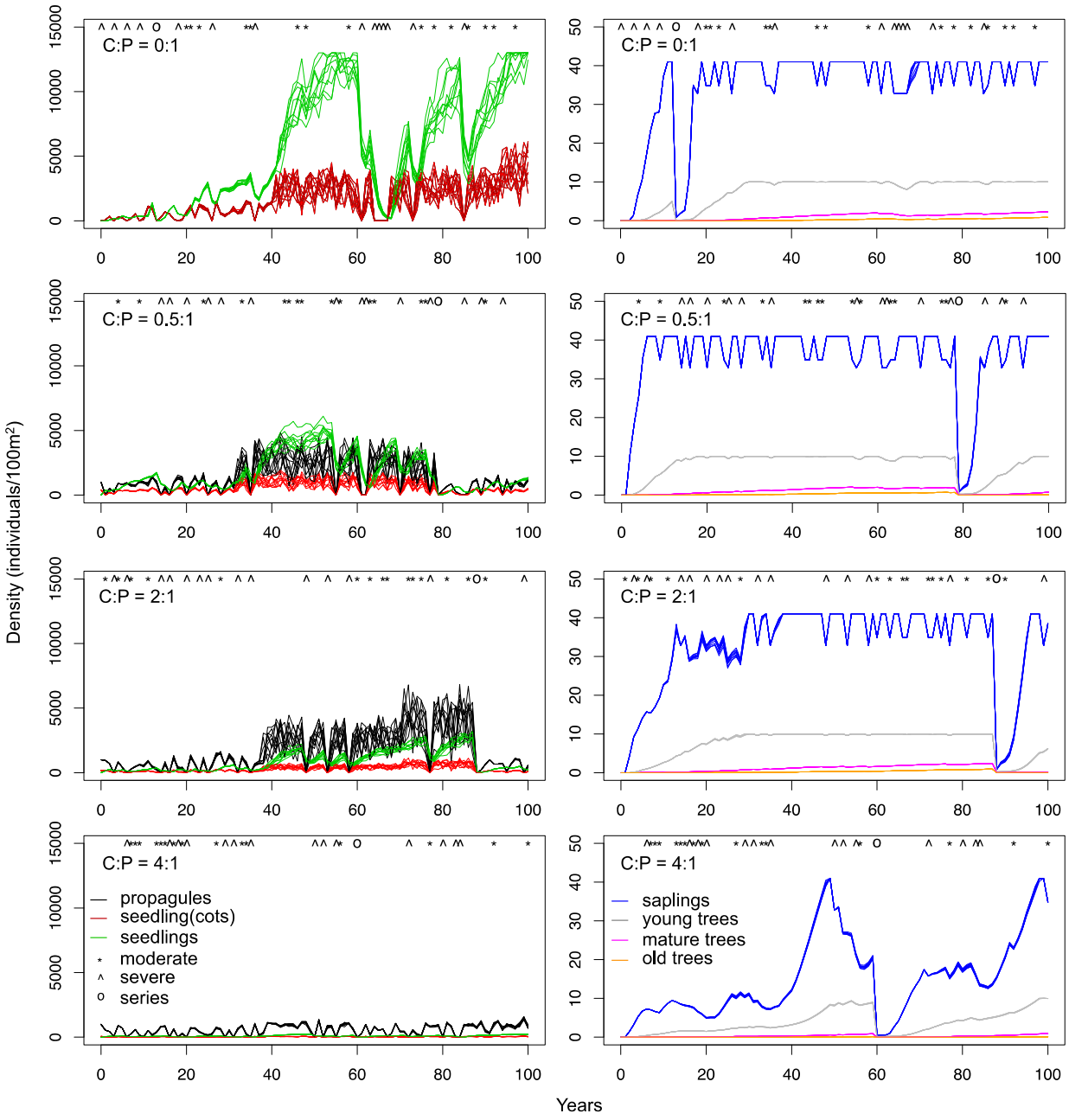

Figure 4-26. Outcomes from scenarios with an initial influx of 1000 propagules, high influx frequency, historical frequencies and intensities of freeze events, and varying intensities of propagule predation. C:P=crab:propagule, occurrences of freeze events are shown at the top of each graph: moderate=moderate freeze event, severe=single severe freeze event, series=series of severe freeze events.

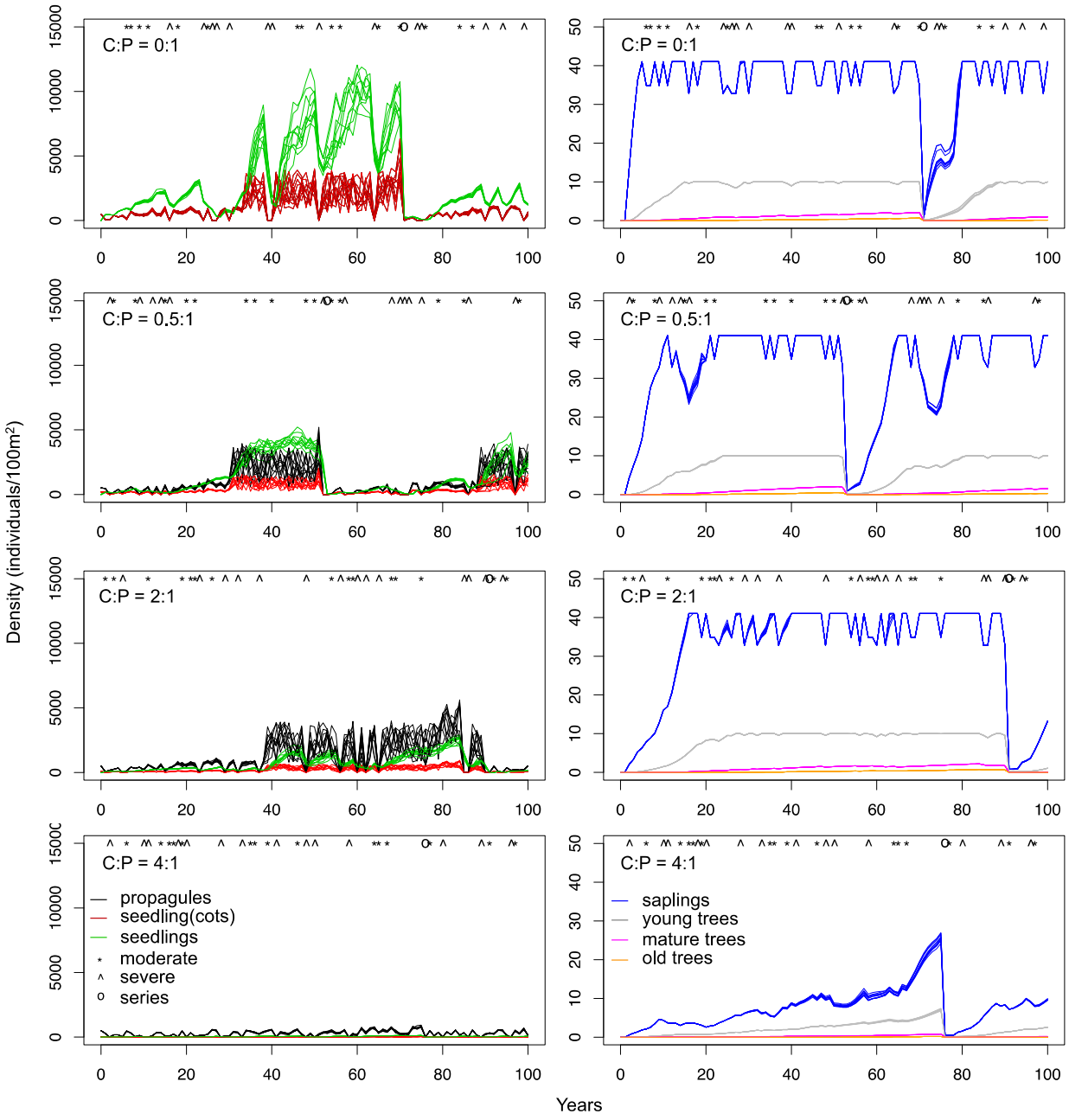

Figure 4-27. Outcomes from scenarios with an initial influx of 500 propagules, high influx frequency, historical frequencies and intensities of freeze events, and varying intensities of propagule predation. C:P=crab:propagule, occurrences of freeze events are shown at the top of each graph: moderate=moderate freeze event, severe=single severe freeze event, series=series of severe freeze events.

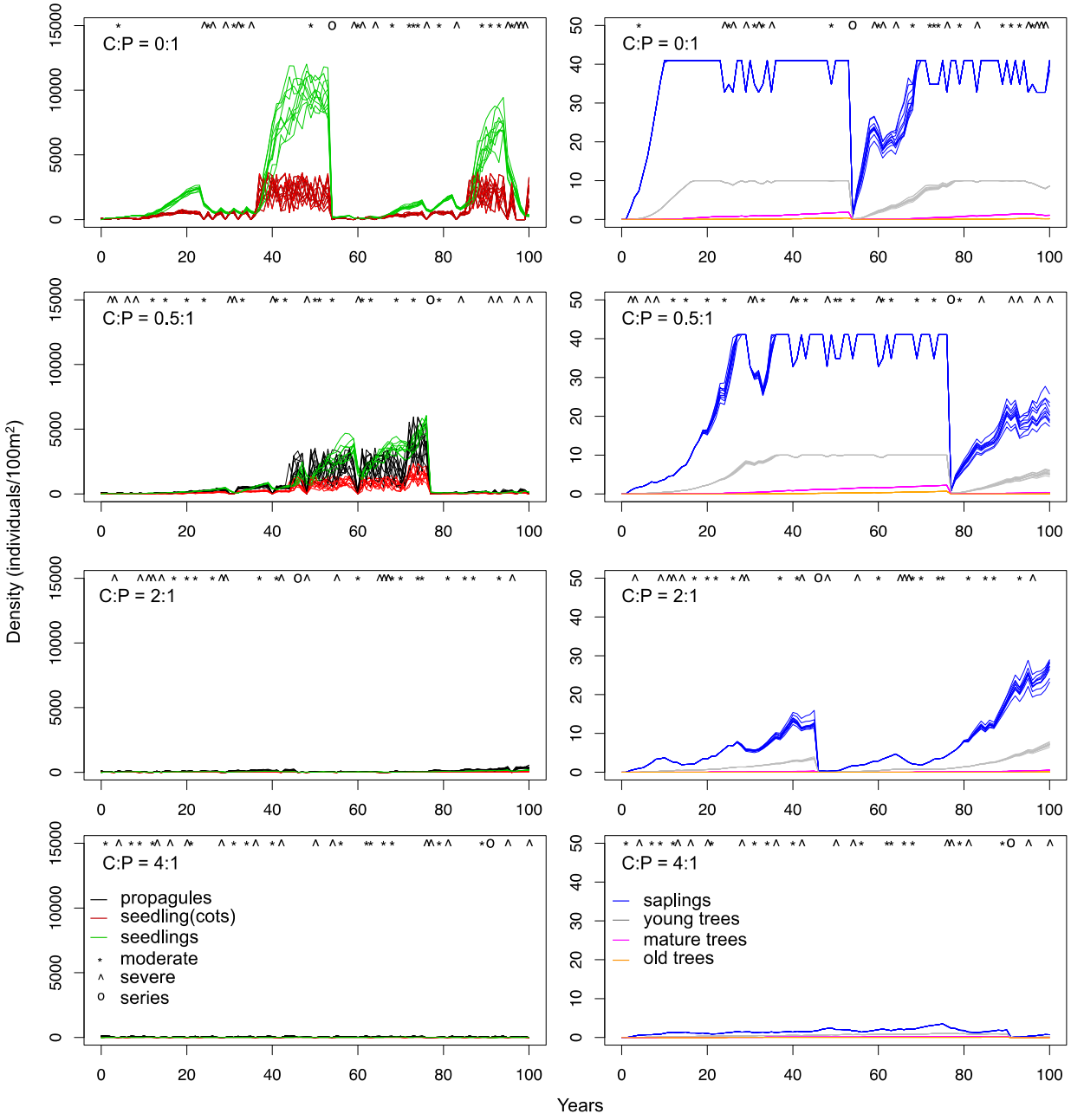

Figure 4-28. Outcomes from scenarios with an initial influx of 100 propagules, high influx frequency, historical frequencies and intensities of freeze events, and varying intensities of propagule predation. C:P=crab:propagule, occurrences of freeze events are shown at the top of each graph: moderate=moderate freeze event, severe=single severe freeze event, series=series of severe freeze events.

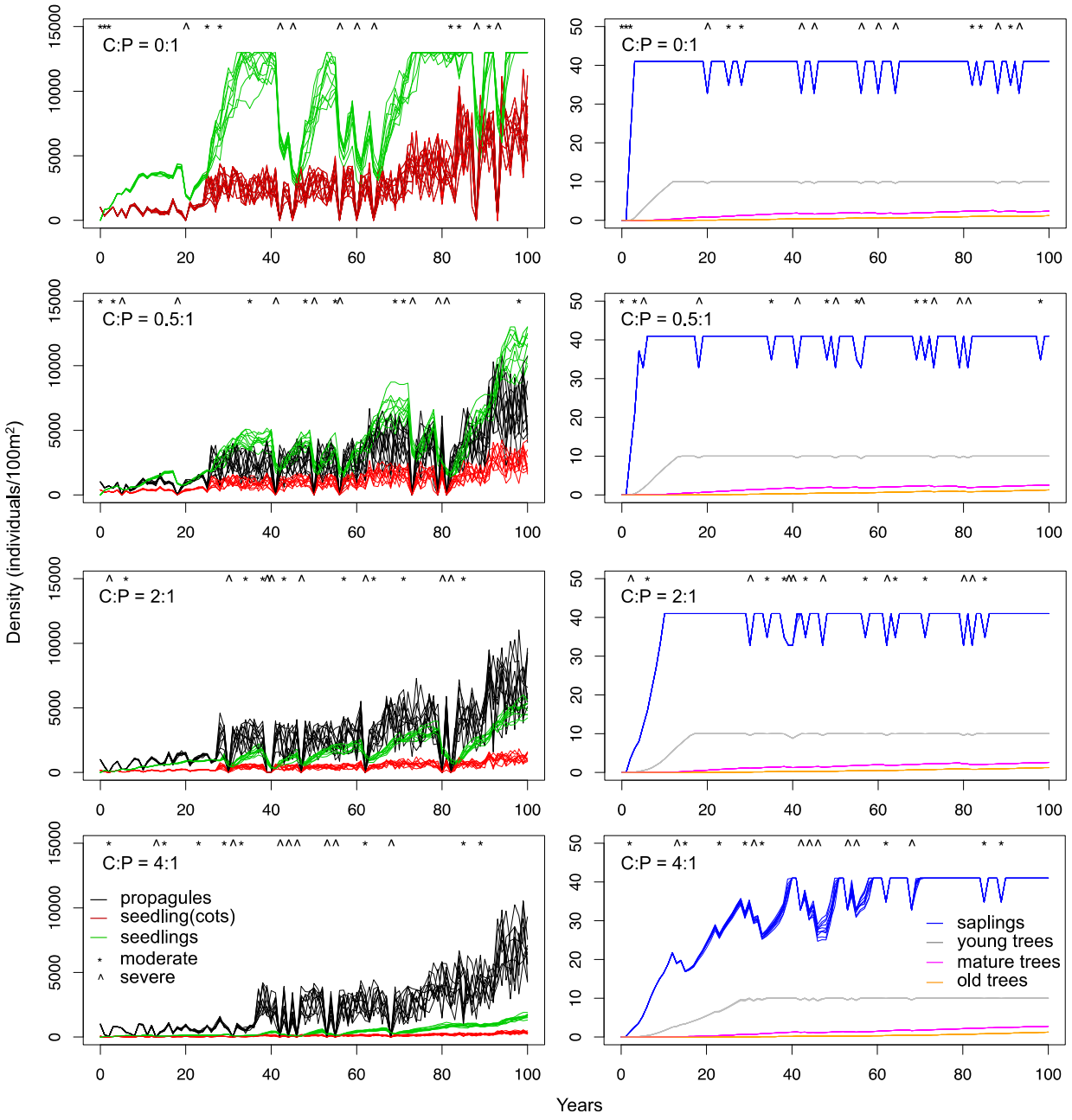

Figure 4-29. Outcomes from scenarios with an initial influx of 1000 propagules, high influx frequency, reduced frequencies and intensities of freeze events, and varying intensities of propagule predation. C:P=crab:propagule, occurrences of freeze events are shown at the top of each graph: moderate=moderate freeze event, severe=single severe freeze event.

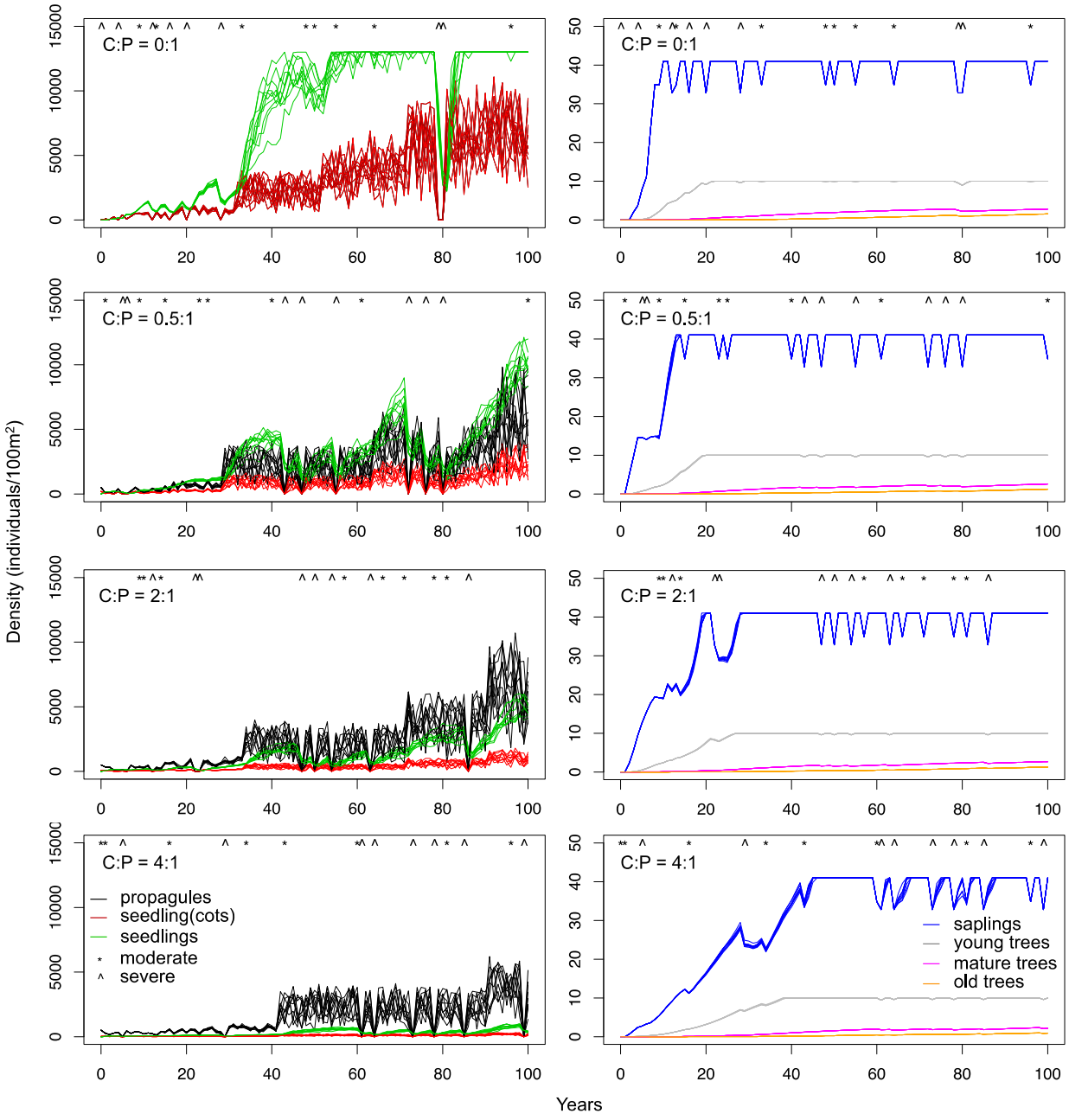

Figure 4-30. Outcomes from scenarios with an initial influx of 500 propagules, high influx frequency, reduced frequencies and intensities of freeze events, and varying intensities of propagule predation. C:P=crab:propagule, occurrences of freeze events are shown at the top of each graph: moderate=moderate freeze event, severe=single severe freeze event.

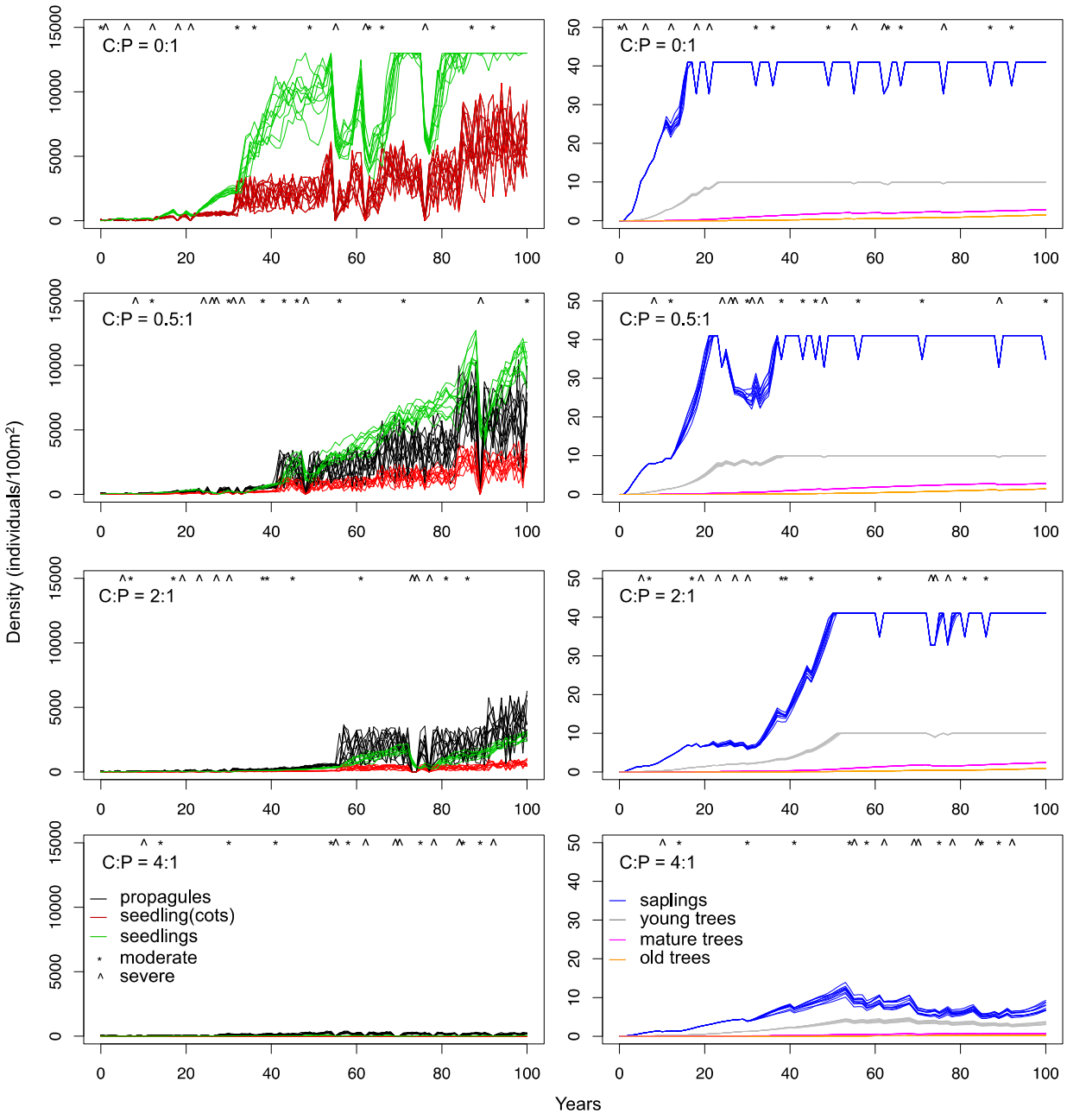

Figure 4-31. Outcomes from scenarios with an initial influx of 100 propagules, high influx frequency, reduced frequencies and intensities of freeze events, and varying intensities of propagule predation. C:P=crab:propagule, occurrences of freeze events are shown at the top of each graph: moderate=moderate freeze event, severe=single severe freeze event.

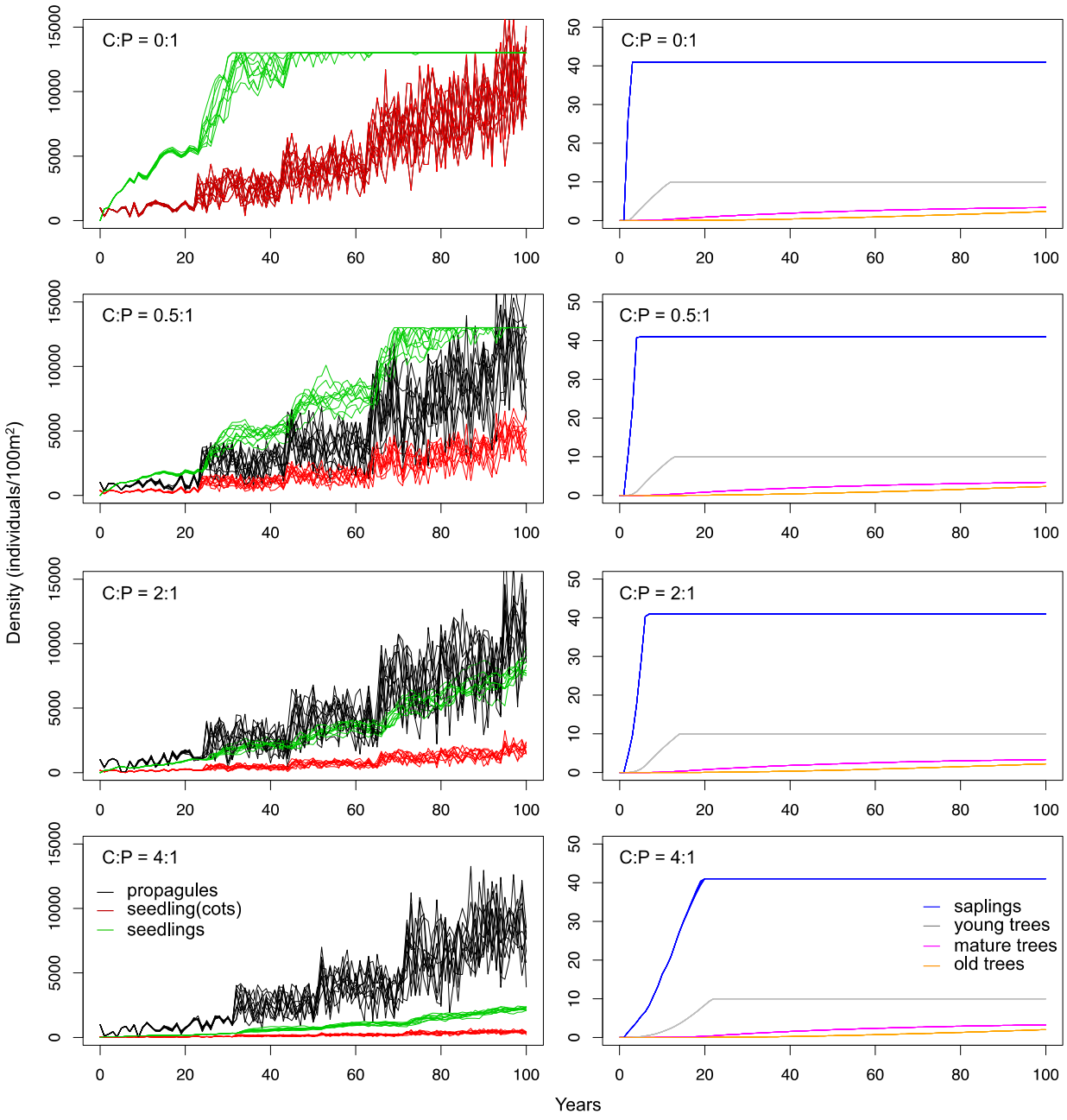

Figure 4-32. Outcomes from scenarios with an initial influx of 1000 propagules, high influx frequency, no freeze events, and varying intensities of propagule predation. C:P=crab:propagule.

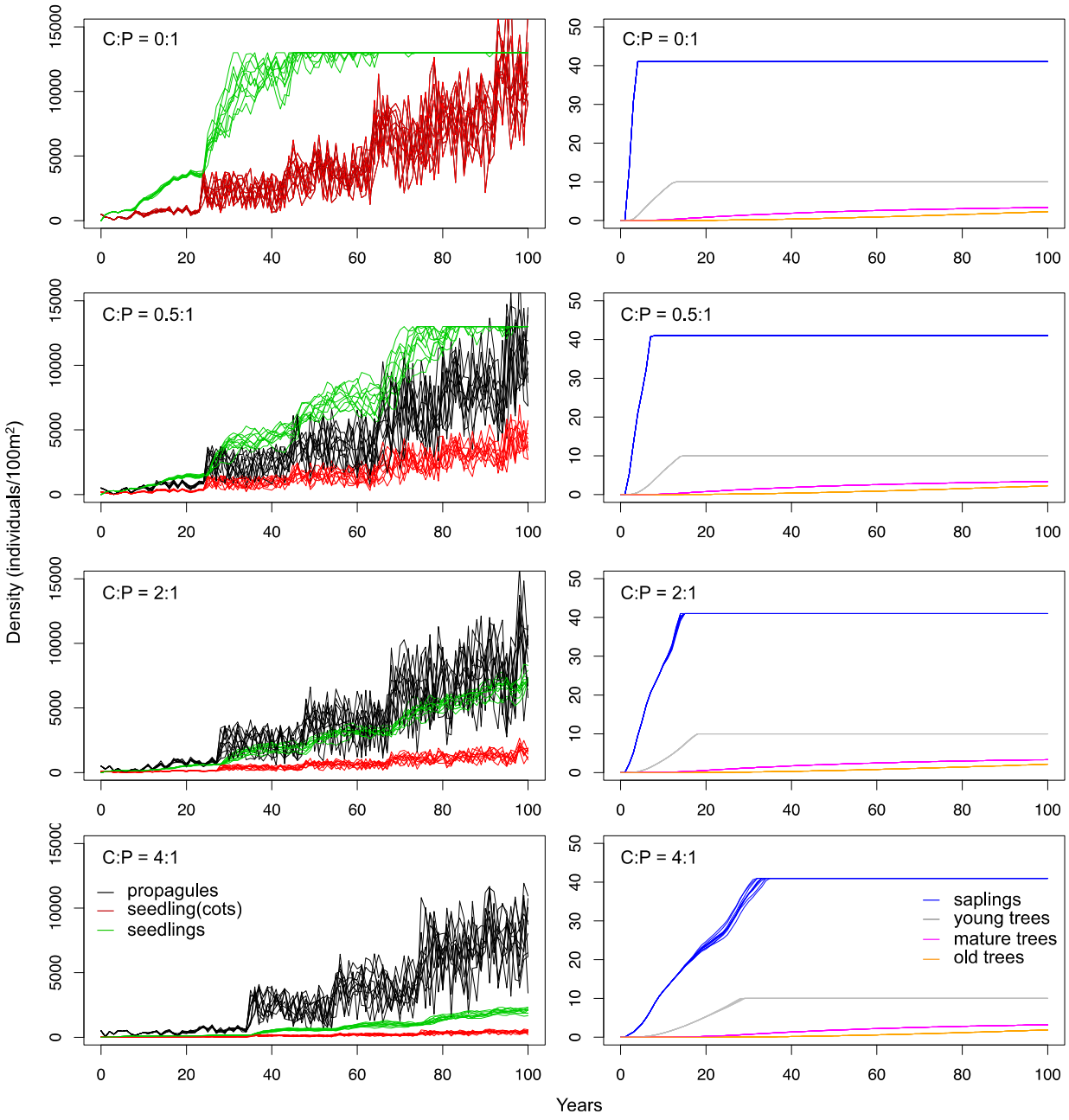

Figure 4-33. Outcomes from scenarios with an initial influx of 500 propagules, high influx frequency, no freeze events, and varying intensities of propagule predation. C:P=crab:propagule.

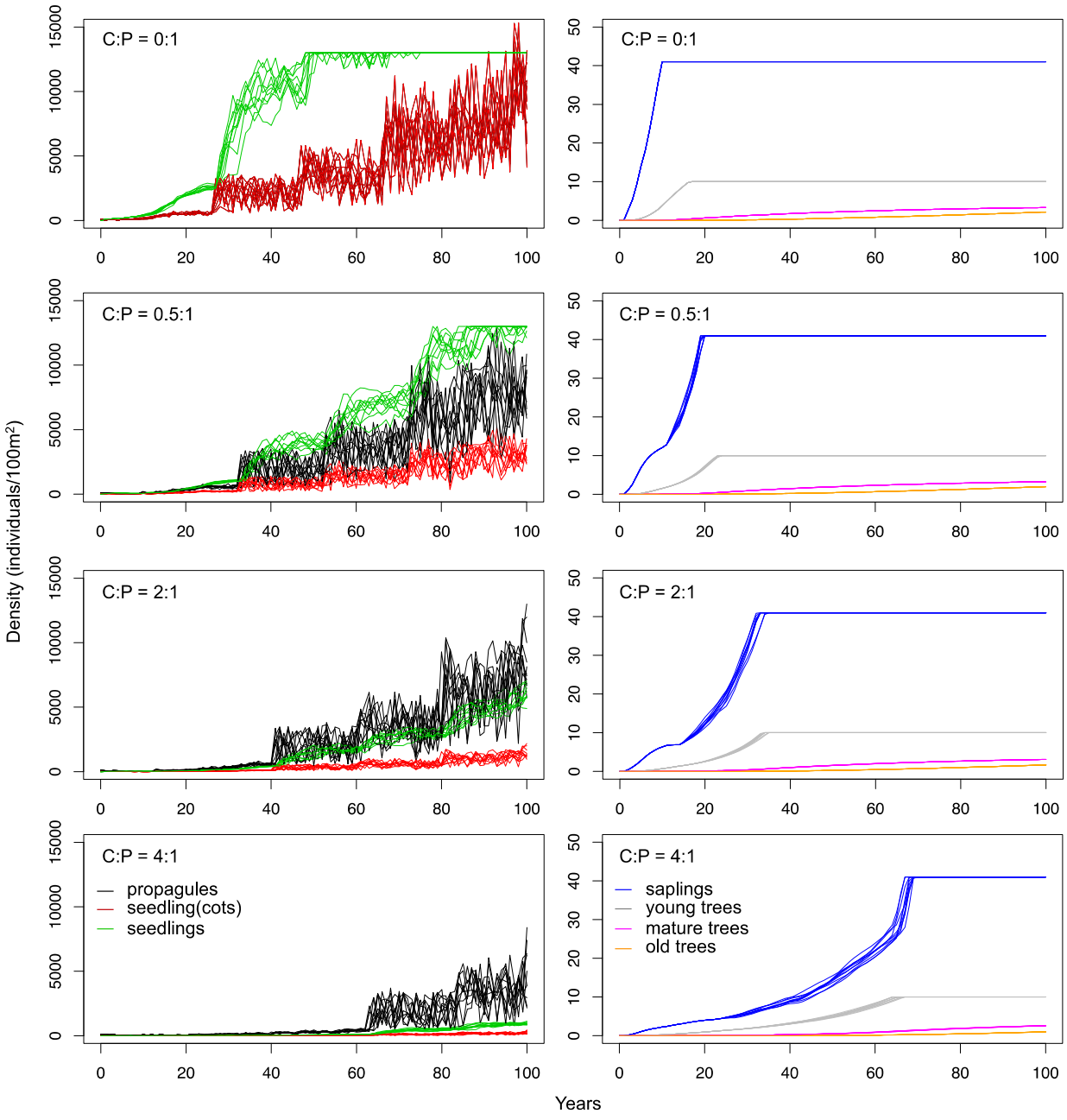

Figure 4-34. Outcomes from scenarios with an initial influx of 100 propagules, high influx frequency, no freeze events, and varying intensities of propagule predation. C:P=crab:propagule.

CHAPTER 5
CONCLUSION

As climate change continues modifying environmental conditions along the Big Bend, coastal ecosystems will continue responding according to their abilities to adapt. Some ecosystems, like islands of freshwater forest, will be replaced by more salt-tolerant communities in response to sea level rise. As discussed in Chapter 2, increased tidal flooding from sea level rise is increasing salinity beyond the tolerance levels of tree seedlings, and as forest regeneration ceases, trees are replaced by halophytic shrubs adapted to withstand higher salinity concentrations. Halophytic shrubs are eventually replaced by herbaceous salt marsh plants along a gradient of increased tidal flooding frequency. Future research on the mechanisms by which halophytic shrubs are replaced by herbaceous marsh (Decreased fruit production? Seedling mortality? Lower tolerances to soil biogeochemical changes driven by increased salinity?) could fill gaps explaining the duration of the shrub phase and mechanisms besides increased salinity that are influencing reassembly.

The reassembly trajectory described in Chapter 2 describes the pattern of species turnover currently happening; other reassembly trajectories are also likely depending on changing environmental conditions and biotic interactions. The work presented in Chapter 2 sets up opportunities for future research to evaluate other potential trajectories. For example, the northward spread of *Schinus terebinthifolia* (Brazilian pepper) follows a pattern similar to northward mangrove expansion and is highly adaptable and highly invasive. Future work could explore the likelihood and potential consequences of climate change creating favorable conditions for *S. terebinthifolia* invasion along the Big Bend.

In Chapter 3, I presented research demonstrating that growing conditions are favorable for encroachment by *Avicennia germinans* (black mangrove) on islands of freshwater forest and in surrounding salt marsh so long as there is sufficient tidal flooding. Consequently, mangrove encroachment could result in a modified reassembly trajectory whereby forests islands are eventually replaced by mangroves. However, propagule predation by *Sesarma reticulatum* exerted strong top-down pressure that restricted seedling establishment. My findings demonstrate that species range shifts resulting from large-scale abiotic drivers (i.e., climate change) can expose shifting species to new biotic interactions that also affect their survival. Additional research motivated by my findings could explore the effects of new interactions encountered by other coastal species undergoing range shifts.

Additional work remains to be done investigating top-down controls on later life stages of *A. germinans*. Though I focused my work on propagule predation, I also found seedling herbivory reduced seedling establishment. I suspected most herbivory was by a grasshopper species common in *Juncus*-dominated salt marsh. Additional work could confirm whether that grasshopper species was the primary herbivore responsible for seedling mortality, potentially revealing yet another new species interaction resulting from mangrove expansion that restricts establishment.

In Chapter 4, I detailed findings from a field experiment that investigated the relationship between propagule predation and propagule density, and the relative influences of propagule dispersal density, predation intensity, and freeze frequency and intensity on mangrove forest establishment based on a stage-based population growth

model I developed. The field experiment supported my hypothesis that propagule predation would depend on propagule density, consistent with a Holling type II functional response. Building upon the field experiment, I recommend conducting feeding trial experiments with *S. reticulatum* to fill knowledge gaps about the feeding behaviors of *Sesarma*, a genus of comprising several species that are pervasive and intensive propagule predators, but for which we know relatively little in terms of their feeding activities.

The population model demonstrates that as long as enough propagules survive for a single fecund tree to develop, a mangrove population can establish and persist under a wide range of freeze and predation intensities supported by variable influx densities and frequencies. Predation pressure was important when crab density was high, and propagule density was low, whether due to low influx densities or to reduced propagule production from freeze events. Predation exacerbated the negative effects of freezes to the point of sometimes causing local extinctions.

Additional work can be conducted to increase the complexity of the model and improve its representativeness of Big Bend salt marshes, such as including spatial variability in propagule and crab densities in the model domain, or making the model spatially explicit to the landscape of the Big Bend. Life stage characteristics for *A. germinans* along the Big Bend are lacking in the literature; field studies that measured population densities of different life stages in a Big Bend mangrove stand, propagule production of individual trees, and propagule influx densities and frequencies along stretches of salt marsh would increase our ability to predict patterns and rates of mangrove establishment through modeling.

This dissertation was motivated by the hypothesis that climate change is shifting the composition of the Big Bend landscape from a mosaic of freshwater forest and salt marsh to a landscape composed exclusively of salt-tolerant communities. The work presented here supports that hypothesis. Over time, with continued environmental change from sea level rise, coastal storms, and changing weather regimes, salt-tolerant communities described in this dissertation may be replaced by other coastal ecosystems. The future of the unique Big Bend landscape will continue to be dynamically reshaped by the effects of climate change.

APPENDIX A
TABLE OF STATE VARIABLES AND PARAMETERS IN POPULATION MODEL

Table A-1. Variables and parameters used in stage-based population model.

Category	Variable/ parameter	Model ID	Value	Units	Description	Source
State variables	Propagule	prop	Varies	/100m^2	Sources of propagules are 1) influx (from outside model population) and 2) reproductively mature trees in the population	Clarke 1995
	Seedlings (cotyledons)	cot	Varies	/100m^2	Young seedlings with cotyledons still attached; develop from propagules that disperse in the same year	Clarke 1995
	Seedling	sd	Varies	/100m^2	Older seedlings that have lost their cotyledons	Clarke 1995
	Sapling	sap	Varies	/100m^2	Reproductively immature, more sensitive to freeze events, crowding, and closed canopy than trees	Clarke 1995, Osland et al. 2015
	Young tree	yt	Varies	/100m^2	Reproductively mature; less fecund than mature and old trees	Clarke 1995
	Mature tree	mt	Varies	/100m^2	Reproductively mature; more fecund than young trees, less than old trees	Clarke 1995
	Old tree	ot	Varies	/100m^2	Reproductively mature; more fecund than young and mature trees	Clarke 1992
Life Table Statistics	Propagules remaining	N/A	0	Proportion	Propagules that remain propagules the following year (none remain)	Clarke 1995, Delgado et al. 1999
	Propagules maturing	p.next	1	Proportion	Propagules that mature to seedlings (cotyledons) in the same year	Assumption
	Seedlings (cotyledons) remaining	c.stay	0	Proportion	Seedlings (cotyledons) that remain seedlings (cotyledons) the following year (none remain)	Assumption

Category	Variable/ parameter	Model ID	Value	Units	Description	Source
Life Table Statistics	Seedlings (cotyledons) maturing	c.next	0.900	Proportion	Seedlings (cotyledons) that mature to seedlings per year	Assumption
	Seedlings (cotyledons) misc. mortality	N/A	0.100	Proportion	Mortality due to rotting, uprooting, desiccation, etc. Not explicitly defined in model; = 1 - c.stay - c.next	Clarke 1995, Langston et al. 2017a
	Seedlings remaining	sd.stay	0.825	Proportion	Seedlings that remain seedlings per year	Clarke 1995
	Seedlings maturing	sd.next	0.030	Proportion	Seedlings that mature to saplings per year	Clarke 1995
	Seedlings misc. mortality	N/A	0.145	Proportion	Mortality due to rotting, uprooting, desiccation, etc. Not explicitly defined in model; = 1 - sd.stay - sd.next	Delgado et al.1999, Langston et al. 2017a
	Saplings remaining	sap.stay	0.920	Proportion	Saplings that remain saplings per year	Clarke 1995, Delgado et al. 1999
	Saplings maturing	sap.next	0.030	Proportion	Saplings that mature to young trees per year	Delgado et al. 1999
	Saplings misc. mortality	N/A	0.050	Proportion	Mortality due to local disturbance (e.g., lightning). Not explicitly defined in model; = 1 - sap.stay - sap.next	Clarke 1995
	Young trees remaining	yt.stay	0.963	Proportion	Young trees that remain young trees per year	Clarke 1995
	Young trees maturing	yt.next	0.008	Proportion	Young trees that become mature trees per year	Clarke 1995
	Young trees misc. mortality	N/A	0.029	Proportion	Mortality due to local disturbance (e.g., lightning). Not explicitly defined in model; = 1 - yt.stay - yt.next	Clarke 1995
	Mature trees remaining	mt.stay	0.980	Proportion	Mature trees that remain mature trees per year	Clarke 1995

Category	Variable/ parameter	Model ID	Value	Units	Description	Source
Life Table Statistics	Mature trees maturing	mt.next	0.012	Proportion	Mature trees that become old trees per year	Clarke 1995
	Mature trees misc. mortality	N/A	0.008	Proportion	Mortality due to local disturbance (e.g., lightning). Not explicitly defined in model; = 1 - mt.stay - mt.next	Clarke 1995
	Old trees remaining	ot.stay	0.999	Proportion	Old trees that remain old trees per year	Clarke 1995
	Old trees misc. mortality	N/A	0.001	Proportion	Mortality due to local disturbance (e.g., lightning). Not explicitly defined in model; = 1 - ot.stay	Clarke 1995
Fecundity	Young tree fecundity	ytfec	0-100	Number/ tree	Annual number of propagules produced by an individual tree that drop; varies/tree	Clarke 1992, Clarke 1995
	Mature tree fecundity	mtfec	0-3000	Number/ tree	Annual number of propagules produced by an individual tree that drop; varies/tree	Clarke 1992
	Old tree fecundity	otfec	0-5300	Number/ tree	Annual number of propagules produced by an individual tree that drop; varies/tree	Clarke 1992
Population density maxima	Seedlings (cotyledons max	c.max	20000	/100m^2	Maximum density model area can support	Jimenez et al. 1985
	Seedlings max	sd.max	13000	/100m^2	Maximum density model area can support	Jimenez et al. 1985
	Saplings max	sap.max	41	/100m^2	Maximum density model area can support; above sapling max, transition proportions = 0 for younger stages (p.next, c.stay, c.next, sd.stay, sd.next	Clarke 1995, Delgado et al. 1999
	Young trees max	yt.max	10	/100m^2	Maximum density model area can support	Clarke 1995, Delgado et al. 1999
	Mature trees max	mt.max	10	/100m^2	Maximum density model area can support	Clarke 1995, Delgado et al. 1999

Category	Variable/ parameter	Model ID	Value	Units	Description	Source
Population density maxima		ot.max	10	/100m^2	Maximum density model area can support	Clarke 1995, Delgado et al. 1999
Propagule predation	Ratio of crabs to propagules	crab	0, 0.5, 2, 4	Ratio	Density of crabs to propagules/m^2, based on field experiment. 0.5=low crab density, 2=moderate density, 4=high density	Field data
	Propagule consumption	fpred	0-1	Proportion	Equation derived from field experiment: y=0.165*ln(x) + 0.7184 (y=proportion of propagules consumed, x=crab:propagule ratio)	Field data
Propagule Influx	Influx frequency	influx	1, 10, 100	/100 years	Frequency of propagules dispersing into the model population from outside	N/A
	Influx density	x_in	0-1100, 0-550, 0-110	/100m^2	Density of propagules that disperse into the model population; based on initial propagule value to test a range of propagule densities. When initial prop=1000, influxes range from 0-1100, when prop=500, influxes range from 0-550, when prop=100, influxes range from 0-110	N/A
Freeze events	Freeze	freeze	Varies	N/A	Distribution of freeze events of varying intensities and frequencies	Stevens et al. 2006, Osland et al. 2017a
	Freeze intensity	1, 2, 3	1, 2, 3	N/A	3 categories of freeze intensities: 1) moderate, 2) severe, and 3) series of severe freezes	Stevens et al. 2006, Pickens and Hester 2011, Osland et al. 2015
	Moderate freeze frequency	mod	Varies	/100 years	Represents freezes when temperature ranges from -6.5˚ C to 0˚ C and lasts < 24 hours; only affects seedlings, saplings, and young trees	Stevens et al. 2006, Osland et al. 2015, Osland et al. 2017a

Category	Variable/ parameter	Model ID	Value	Units	Description	Source
Freeze events	Moderate freeze seedling mortality	sdmodfrz	0.075	Proportion	Based on assumption that approx. half of seedlings correspond to 50-100 cm height category; Osland et al. 2015 reports ~15% mortality to seedlings 50-100 cm tall.	Osland et al. 2015
	Moderate freeze sapling mortality	sapmodfrz	0.150	Proportion	Based on assumption that saplings correspond with 100-150 cm height category; Osland et al. 2015 reports ~15% mortality to individuals 100-150 cm tall.	Osland et al. 2015
	Moderate freeze young tree mortality	ytmodfrz	0.080	Proportion	Based on assumption that young trees correspond with 150-200 cm height category; Osland et al. 2015 reports ~8% mortality to individuals 100-150 cm tall.	Osland et al. 2015
	Severe freeze frequency	sev	Varies	/100 years	Represents single freeze events when temperature is ≤ -6.5˚ C for 12-24 hours	Stevens et al. 2006
	Severe freeze seedling mortality	sdsevfrz	0.500	Proportion	Applies to seedlings (cotyledons) and seedlings	Hester and Pickens 2011
	Severe freeze sapling mortality	sapsevfrz	0.200	Proportion	Assumption that sapling mortality from severe freeze event is higher than from moderate freeze event	Assumption
	Severe freeze tree mortality	tfsevfrz	0.120	Proportion	Based on 12% tree mortality in Cedar Key reported by Stevens et al. 2006	Stevens et al. 20016
	Severe freeze fecundity	pfrz	1	Proportion	No propagules are produced during years when severe freezes occur; applies to fecundity of trees within the model population and influx from trees outside population, also applies to series of severe freezes	Stevens et al. 2006
	Series freeze frequency	series	0, 1	/100 years	Series of severe freeze events represents multiple severe freezes occurring within a few years	Stevens et al. 2006

Category	Variable/ parameter	Model ID	Value	Units	Description	Source
Freeze events	Series freeze mortality	seriesfrz	0.980	Proportion	Based on reports that series of severe freezes in Cedar Key caused 98% population mortality. Applies to all life stages except propagules.	Montague and Odum 1997, Stevens et al. 2006

APPENDIX B
STAGE-BASED POPULATION MODEL

```
#clear memory
rm(list = ls())

#R packages required for running model
library("simecol")
library(deSolve

#------------------------#
#FREEZE EVENTS#
#------------------------#
#to apply a category of freeze events (historic, reduced, none), hash out the code for
#the other options

#for HISTORIC intensities and frequencies of freeze events:
nofrz <- rep(0, 71)
mod <- rep(1, 15)
sev <- rep(2, 14)
series <- rep(3, 1)
frzes <- c(nofrz, mod, sev, series)
freeze <- sample(frzes)

#for REDUCED intensities and frequencies of freeze events:
nofrz <- rep(0, 85)
mod <- rep(1, 8)
sev <- rep(2, 8)
frzes <- c(nofrz, mod, sev)
freeze <- sample(frzes)

#for NO freeze events:
freeze = numeric(101)

#----------------------------------------#
#PROPAGULE INFLUX EVENTS#
#----------------------------------------#
#to apply a category of influx events (every year, 10/100 years, none after year 0), hash
#out the code for the other options

#for influx events every year:
x1 <- 0     #initial influx event at time = 0 is within the body of the simecol model
#for p=1000 use 1:1100, for p=500 use 1:550, for p=100 use 1:110
x_in <- sample(1:1100, 100)
influx <- c(x1, x_in)
```

```
#for 10 influx events per 100 years after time = 0:
x1 <- 0
x_in <- sample(1:1100, 10)
x_0 <- rep(0, 90)
x_in0 <- c(x_in, x_0)
x_in0 <- sample(x_in0)
influx <- c(x1, x_in0)

#for no influxes after time = 0:
influx = numeric(101)

#-----------------------------------------------------------------------------------------------#
#POPULATION MODEL: INITIAL VALUES OF PROP & COT AT TIME =0#
#-----------------------------------------------------------------------------------------------#
main_fun_t0 <- function(time, init, parms, inputs,...){
  #STATE VARIABLES (LIFE STAGES): CALLING INITIAL VALUES
  prop <- init[1]         #propagules
  cot <- init[2]          #seedlings with cotyledons
  Y <- approxTime1(inputs, time, rule = 2)["y.in"]          #freeze event
  d <- approxTime1(inputs, time, rule = 2)["d.in"]          #influx event
  with(as.list(parms), {

#CHANGES IN LIFE STAGES PER TIME STEP
    dprop_t0   <- prop
    dcot_t0     <- fcot_t0(cot, c.stay, prop, p.next, crab, pfrz, sdsevfrz, seriesfrz, Y)
    list(c(dprop_t0, dcot_t0))
  })
}

#FUNCTION FOR PROPAGULE PREDATION; uses specified ratio of crabs:propagules
fpred_t0 = function(crab){
  ifelse(crab==0, 0, 0.165*log(crab) + 0.7184)}

#FUNCTION FOR CHANGE IN SEEDLINGS WITH COTYLEDONS
#occurs on same time step as props
fcot_t0 = function(cot, cotstay, prop, pnext, crab, pfrz, sdsevfrz, seriesfrz, frz)

#propagule mortality from predation and freezes:
pred_t0 = prop*fpred_t0(crab)
  ppop = ifelse(frz == 2,
                (prop - pred_t0) - (prop - pred_t0)*pfrz,
                ifelse(frz == 3,
                       (prop - pred_t0) - (prop - pred_t0)*pfrz,
                       prop- pred_t0))
  psurv = max(0, ppop)
```

```
#remaining propagules become cots:
cpop = ((cot*cotstay) + (psurv*pnext))
  cpop = max(0, cpop)

#mortality of cots from freezes
  csurv = ifelse(frz == 2,
              cpop - cpop*sdsevfrz,
              ifelse(frz == 3,
                    cpop - cpop*seriesfrz,
                    cpop))
  csurv = max(0, csurv)
  csurv = min(csurv, 20000) #density max for cots
  return(csurv)
}
eqn_list_t0 = list(fpred_t0, fcot_t0)

#PARAMETERS
parms_vec_t0 = c(crab=0, #change value to test different crab densities
            p.next=1,          #proportion of propagules that become cots
            c.stay=0,          #propagule of cots that remain cots at next time step
            pfrz=1.0,          #proportion mortality for props by severe/series freeze
            sdsevfrz=0.5,      #proportion mortality for cots by severe freeze
            seriesfrz=0.98)    #proportion mortality for cots by series of severe freezes

times_vec_t0 = c(from=0, to=1, by=1)

#INITIAL VALUES OF STATE VARIABLES
init_vec_t0 = c(prop=1000, cot=0)

#NAME THE MODEL
PropCot_t0 <- new("odeModel", main = main_fun_t0,
                equations = eqn_list_t0, times = times_vec_t0,
                parms = parms_vec_t0,  init = init_vec_t0, solver = "iteration")

#INPUT FREEZE AND INFLUX EVENTS
input_mat_t0 = as.matrix(data.frame(time = c(0:1), y.in = freeze[1], d.in = influx[1]))
inputs(PropCot_t0) <- input_mat_t0

#RUN THE MODEL
#output feeds into population model for time steps after time = 0
PropCot_t0 <- sim(PropCot_t0)
out_PropCot_t0 <- out(PropCot_t0)


#-------------------------------------------------------------------------------------------#
```

```
#POPULATION MODEL: FOR ALL LIFE STAGES DURING TIME=1-100#
#-----------------------------------------------------------------------------------------#
main_fun_t1 = function (time, init, parms, inputs, ...) {
  #STATE VARIABLES (LIFE STAGES): CALLING INITIAL VALUES
  prop <- init[1]        #propagules
  cot <- init[2]         #seedlings with cotyledons
  sd <- init[3]          #seedlings without cotyledons
  sap <- init[4]         #saplings
  yt <- init[5]          #young trees
  mt <- init[6]          #mature trees
  ot <- init[7]          #old trees
  Y <- approxTime1(inputs, time, rule = 2)["y.in"]        #freeze events
  D <- approxTime1(inputs, time, rule = 2)["d.in"]        #influx events

  with(as.list(parms), {
    #changes in state variables per time step
    dprop   <- fprop(prop, yt, mt, ot, pfrz, Y, D, time)
    dcot    <- fcot(cot, c.stay, dprop, p.next, crab, sap, sap.max, c.max, sdsevfrz,
               seriesfrz, Y)
    dsd     <- fsd(sd, sd.stay, cot, c.next, sap, sap.max, sd.max, sdmodfrz, sdsevfrz,
               seriesfrz, Y, time) #change in seedlings
    dsap    <- fsap(sap, sap.stay, sd, sd.next, sap.max, sapmodfrz, sapsevfrz, seriesfrz,
               Y)
    dyt     <- fytree(yt, yt.stay, sap, sap.next, sap.max, yt.max, ytmodfrz, tfsevfrz,
               seriesfrz, Y)
    dmt     <- fmotree(mt, mt.stay, yt, yt.next, mt.max, tfsevfrz, seriesfrz, Y)
    dot     <- fmotree(ot, ot.stay, mt, mt.next, ot.max, tfsevfrz, seriesfrz, Y)
    list(c(dprop, dcot, dsd, dsap, dyt, dmt, dot))
  })
}

#FUNCTIONS FOR CHANGES IN LIFE STAGE DENSITY PER TIME STEP:

#FUNCTION FOR PROPAGULE PRODUCTION by young, mature, & old trees
  frepro = function (ytree, mtree, otree){
#create empty vectors for each tree type (length=value of tree type); fill with repro
     #value/per tree
#young trees: each young tree will produce 0-100 propagules (diff for each tree)
    if(ytree >= 1){
      ytfec <- rep(NA, ytree)
      for(i in 1:ytree){
        ytfec[i] <- sample(0:100, 1)
      }
    } else {ytfec = 0}
 #mature trees: each mature tree will produce 0-3000 propagules (diff for each tree)
    if(mtree >= 1){
```

```
    mtfec <- rep(NA, mtree)
    for(i in 1:mtree){
      mtfec[i] <- sample(0:3000, 1)
    }
  } else {mtfec = 0}

#old trees: each old tree will produce 0-5300 propagules (diff for each tree)
  if(otree >= 1){
    otfec <- rep(NA, otree)
    for(i in 1:otree){
    otfec[i] <- sample(0:5300, 1)
    }
  } else {otfec = 0}


  #total propagules produced per time step
  sum(ytfec) + sum(mtfec) + sum(otfec)
}

 #FUNCTION FOR PROPAGULE PREDATION
 fpred = function(crab){
  ifelse(crab==0, 0, 0.165*log(crab) + 0.7184)}

 #FUNCTION FOR PROPAGULE DENSITY
 #based on fecundity, influx, and freeze events
 fprop = function(prop, ytree, mtree, otree, pfrz, frz, infl, tt){
  allprops = ifelse(tt == 0, prop, prop*0 + infl + frepro(ytree, mtree, otree))
  ppop = ifelse(frz == 2,
                allprops - allprops*pfrz,
                ifelse(frz == 3,
                       allprops - allprops*pfrz,
                       allprops))
  psurv = max(0, ppop)
  return(psurv)
 }

 #FUNCTION FOR CHANGE IN SEEDLINGS WITH COTYLEDONS
  fcot = function(cot, cotstay, prop, pnext, crab, sap, sapmax, cmax, sdsevfrz, seriesfrz,
                  frz) {
  pcot = prop - prop*fpred(crab)
  cpop = ifelse(sap <= sapmax, cot*cotstay + pcot*pnext,     #limited by sapling density
                cot*0+pcot*0)
  cpop = max(0, cpop)
  csurv = ifelse(frz == 2,              #reduced by severe freeze events
                 cpop - cpop*sdsevfrz,
                 ifelse(frz == 3,           #reduced by series of severe freeze events
```

```
                    cpop - cpop*seriesfrz,
                    cpop))
  csurv = max(0, csurv)             #limited by density max for cots
  csurv = min(csurv, cmax)
  return(csurv)
}

 #FUNCTION FOR CHANGE IN SEEDLINGS
fsd = function(seed, sdstay, cot, cnext, sap, sapmax, sdmax, sdmodfrz, sdsevfrz,
               seriesfrz, frz, tt){
  sdpop = ifelse(sap <= sapmax, seed*sdstay + cot*cnext,    #limited by sapling density
                 seed*0+cot*0)

  sdpop = max(0, sdpop)
  sdsurv = ifelse(frz == 1,           #reduced by moderate freeze events
                  sdpop - sdpop*sdmodfrz,
                  ifelse(frz == 2,          #reduced by severe freeze events
                  sdpop - sdpop*sdsevfrz,
                  ifelse(frz == 3,          #reduced by series of severe freeze events
                        sdpop - sdpop*seriesfrz,
                        sdpop)))
  sdsurv = max(0, sdsurv)
  sdsurv = min(sdsurv, sdmax)    #limited by density max for seedlings
  sdsurv = ifelse(tt == 0, 0, sdsurv)
  #return(trunc(sdsurv))
  return(sdsurv)
}

 #FUNCTION FOR CHANGE IN SAPLINGS
 fsap = function(sap, sapstay, seed, sdnext, sapmax, sapmodfrz, sapsevfrz, seriesfrz,
                 frz){         #limited by sapling density
  sappop = ifelse(sap<= sapmax, (sap*sapstay) + (seed*sdnext),
                  sap*sapstay)
  sappop = max(0, sappop)
  sappop = min(sappop, sapmax)
  sapsurv = ifelse(frz == 1,          #reduced by moderate freeze events
                   sappop - sappop*sapmodfrz,
                   ifelse(frz == 2,         #reduced by severe freeze events
                   sappop - sappop*sapsevfrz,
                   ifelse(frz == 3,         #reduced by series of severe freeze events
                         sappop - sappop*seriesfrz,
                         sappop)))
  sapsurv = max(0, sapsurv)
  return(sapsurv)
 }
```

```
 #FUNCTION FOR CHANGE IN YOUNG TREES
 fytree = function(ytree, ytstay, sap, sapnext, sapmax, ytmax, tmodfrz, tsevfrz, seriesfrz,
             frz){
   ytpop = ifelse(sap <=sapmax, ytree*ytstay + sap*sapnext,
                  ytree*ytstay)
   ytpop = max(0, ytpop)
   ytpop = ifelse(frz == 1,            #reduced by moderate freeze events
                  ytpop - ytpop*tmodfrz,
                  ifelse(frz == 2,          #reduced by severe freeze events
                         ytpop - ytpop*tsevfrz,
                         ifelse(frz == 3,    #reduced by series of severe freeze events
                                ytpop - ytpop*seriesfrz,
                                ytpop)))
   ytsurv = max(0, ytpop)
   ytsurv = min(ytsurv, ytmax)       #limited by density max for young trees
   return(ytsurv)
   }

  #FUNCTION CHANGE IN MATURE AND OLD TREES
  fmotree = function(tree, trstay, tprev, tnext, tmax, tsevfrz, seriesfrz, frz){
    tpop = (tree*trstay) + (tprev*tnext)
    tpop = max(0, tpop)
    tpop = ifelse(frz == 2,             #reduced by severe freeze events
                  tpop - tpop*tsevfrz,
                     ifelse(frz == 3,       #reduced by series of severe freeze events
                            tpop - tpop*seriesfrz,
                            tpop))
    tsurv = max(0, tpop)
    tsurv = min(tsurv, tmax)          #limited by density max for mature and old trees
    return(tsurv)
  }

#FUNCTIONS CALLED IN MODEL
eqn_list = list(frepro, fpred, fprop, fcot, fsd, fsap, fytree, fmotree)

#VECTOR OF PARAMETERS (change values to run different scenarios)
parms_vec = c(crab=0,      #ratio of crabs:propagules
              p.next=1,          #proportion of propagules that mature to cots
              c.stay=0,          #propotion of cots that stay cots
              c.next=0.9,        #proportion of cots that mature to seedlings
              c.max=20000,       #max density of cots
              sd.stay=0.825,     #proportion of seedlings that stay seedlings
              sd.next=0.03,      #proportion of seedlings that mature to saplings
              sd.max=13000,      #max density of seedlings
              sap.stay=0.92,     #proportion of saplings that stay saplings
```

```
            sap.next=0.03,     #proportion of saplings that mature to young trees
            sap.max=41,        #max density of saplings
            yt.stay=0.963,     #proportion of young trees that stay young trees
            yt.next=0.008,     #proportion of young trees that become mature trees
            yt.max=10,         #max density of young trees
            mt.stay=0.98,      #proportion of mature trees that stay mature trees
            mt.next=0.012,     #proportion of mature trees that become old trees
            mt.max=10,         #max number of mature trees
            ot.stay=0.999,     #proportion of old trees that stay old trees
            ot.max=10,         #max number of large trees
            sdsevfrz=0.5,      #proportion of mortality from severe freeze (for all seedlings)
            sdmodfrz=0.075,    #proportion of mortality from mod. freeze on seedlings
            sapmodfrz=0.15,    #proportion of mortality from mod. freeze on saplings
            sapsevfrz=0.2,     #proportion of mortality from a severe freeze on saplings
            ytmodfrz=0.08,     #proportion of mortality from mod. freeze on young trees
            tfsevfrz=0.12,     #proportion of mortality from severe freeze on all tree stages
            seriesfrz=0.98,    #proportion of mortality from series of severe freezes on all
                               #life stages, except propagules
            pfrz=1             #proportion of mortality from severe and series of freezes on
                               #propagules
            )

times_vec = c(from=0, to=100, by=1)

#STATE VARIABLES: INITIAL VALUES
init_vec = c(prop=500, cot= cot_t0, sd=0, sap=0, yt=0, mt=0, ot=0)

#NAME THE MODEL
main_fun_t1 <- new("odeModel", main = main_fun_t1,
                equations = eqn_list, times = times_vec,
             parms = parms_vec,  init = init_vec, solver = "iteration")

#INPUT FREEZE AND INFLUX EVENTS
input_mat = as.matrix(data.frame(time = c(0:100), y.in = freeze, d.in = influx))
inputs(main_fun_t1) <- input_mat

#RUN THE MODEL
AVGE_forest <- sim(main_fun_t1)
#generate model output:
out_forest <- out(AVGE_forest)
#View(out_forest)

#MAKE A COPY OF THE MODEL
AVGE <- main_fun_t1
```

```
#RUN MODEL A SPECIFIED NUMBER OF TIMES AND COMPARE OUTPUT:
for(i in 1:1000) {  #run model 1000 times and name output based on run number
  nam <- paste("sim_out", i, sep = "")
  assign(nam, out(sim(AVGE)))
}
#create a list of output:
list_out <- lapply(ls(pattern="sim_out[0-9]+"), function(x) get(x))

#compare average(+/- sd) density of life stages at years 10, 50, 100:
#for year 10:
for(i in 1:1000){
nam <-paste("sub_out", i, sep ="")
assign(nam, subset(list_out[[i]], time == 10))
}
#create list of output:
list_sub10 <- lapply(ls(pattern="sub_out[0-9]+"), function(x) get(x))

#create dataframe of vectors in list:
sub10.df <- as.data.frame(do.call(rbind, list_sub10))

#compute mean, sd for year 10:
apply(sub10.df, 2, mean)
apply(sub10.df, 2, sd)

#for year 50:
for(i in 1:1000){
  nam <-paste("sub_out", i, sep ="")
  assign(nam, subset(list_out[[i]], time == 50))
}
list_sub50 <- lapply(ls(pattern="sub_out[0-9]+"), function(x) get(x))
sub50.df <- as.data.frame(do.call(rbind, list_sub50))
apply(sub50.df, 2, mean)
apply(sub50.df, 2, sd)

#for year 100:
for(i in 1:1000){
  nam <-paste("sub_out", i, sep ="")
  assign(nam, subset(list_out[[i]], time == 100))
}
list_sub100 <- lapply(ls(pattern="sub_out[0-9]+"), function(x) get(x))
sub100.df <- as.data.frame(do.call(rbind, list_sub100))
apply(sub100.df, 2, mean)
apply(sub100.df, 2, sd)
```

APPENDIX C
RESULTS OF MODELED SCENARIOS

Table C-1. Mean density (and standard deviations) of life stages at year 100 for each modeled scenario. Results correspond with output presented in Figures 4-7 through 4-33.

Influx density	Influx frequency (/100 yrs)	Freeze intensity/ frequency	Predation intensity (C:P)	PROP	COT	SD	SAP	YT	MT	OT
1000	1	None	None	10297.2 (2614.9)	10297.2 (2614.9)	13000.0 (0)	41.0 (0)	10.0 (0)	3.4 (0)	2.3 (0)
			L (0.5:1)	10300.9 (2670.5)	4078.8 (1057.4)	12958.0 (174.1)	41.0 (0)	10.0 (0)	3.4 (0)	2.3 (0)
			M (2:1)	7755.7 (2167.7)	1297.0 (362.5)	6467.7 (580.6)	41.0 (0)	10.0 (0)	3.2 (0)	2.0 (0)
			H (4:1)	3468.4 (1251.2)	183.3 (66.1)	806.9 (133.3)	41.0 (0)	10.0 (0)	2.3 (0.1)	0 (0)
1000	1	Reduced	None	6132.9 (1881.0)	6132.9 (1881.0)	6709.8 (735.5)	41.0 (0)	10.0 (0)	2.4 (0)	1.3 (0)
			L (0.5:1)	0 (0)	0 (0)	5999.1 (523.1)	32.8 (0)	9.6 (0)	2.6 (0)	1.4 (0)
			M (2:1)	5790.0 (2112.8)	968.3 (353.3)	2948.7 (397.6)	41.0 (0)	10.0 (0)	2.5 (0)	1.1 (0)
			H (4:1)	0 (0)	0 (0)	0 (0)	0 (0)	0 (0)	0 (0)	0 (0)
1000	1	Historical	None	1837.1 (925.9)	1837.1 (925.9)	6008.5 (1816.7)	39.2 (8.5)	9.6 (2.1)	1.3 (0)	0 (0)
			L (0.5:1)	0 (0)	0 (0)	0 (0)	0 (0)	0 (0)	0 (0)	0 (0)
			M (2:1)	0 (0)	0 (0)	1.83 (0.6)	1.25 (0.4)	0 (0)	0 (0)	0 (0)
			H (4:1)	0 (0)	0 (0)	0 (0)	0 (0)	0 (0)	0 (0)	0 (0)
1000	10	None	None	10249.0 (2686.2)	10249.0 (2686.2)	13000 (0)	41.0 (0)	10.0 (0)	3.4 (0)	2.3 (0)

Influx density	Influx frequency (/100 yrs)	Freeze intensity/ frequency	Predation intensity (C:P)	PROP	COT	SD	SAP	YT	MT	OT
1000	10	None	L (0.5:1)	10187.7 (2495.9)	4034.0 (988.3)	12980.3 (132.5)	41.0 (0)	10.0 (0)	3.4 (0)	2.3 (0)
			M (2:1)	10298.0 (2549.8)	1722.1 (426.4)	7565.3 (674.9)	41.0 (0)	10.0 (0)	3.3 (0)	2.2 (0)
			H (4:1)	3538.9 (1254.0)	187.1 (66.3)	908.1 (102.0)	41.0 (0)	10.0 (0)	2.5 (0)	0 (0)
1000	10	Reduced	None	6172.4 (1978.1)	6172.4 (1978.1)	12985.2 (95.7)	41.0 (0)	10.0 (0)	2.6 (0)	1.4 (0)
			L (0.5:1)	6107.2 (1949.3)	2418.3 (771.9)	9103.2 (1102.6)	41.0 (0)	10.0 (0)	2.4 (0)	1.3 (0)
			M (2:1)	6914.8 (1996.9)	1156.4 (333.9)	3886.6 (477.9)	41.0 (0)	10.0 (0)	2.6 (0)	1.2 (0)
			H (4:1)	341.4 (60.2)	18.0 (3.2)	23.5 (2.7)	10.7 (0.9)	4.9 (0.3)	0 (0)	0 (0)
1000	10	Historical	None	465.3 (101.4)	465.3 (101.4)	1848.4 (367.9)	41.0 (0)	9.8 (0.6)	0 (0.1)	0 (0)
			L (0.5:1)	1998.7 (882.8)	791.4 (349.5)	3324.3 (532.5)	41.0 (0)	10.0 (0)	1.8 (0)	0 (0)
			M (2:1)	3453.4 (1228.5)	577.7 (205.4)	1701.0 (279.0)	34.9 (0)	9.99 (0)	2.1 (0)	0 (0)
			H (4:1)	0 (0)	0 (0)	0 (0)	0 (0)	0 (0)	0 (0)	0 (0)
1000	100	None	None	10207.7 (2641.3)	10207.7 (2641.3)	13000 (0)	41.0 (0)	10.0 (0)	3.4 (0)	2.3 (0)
			L (0.5:1)	11093.6 (2671.6)	4392.7 (1057.9)	12976.2 (116.2)	41.0 (0)	10.0 (0)	3.4 (0)	2.3 (0)
			M (2:1)	11372.7 (2646.1)	1901.9 (442.5)	8463.8 (676.7)	41.0 (0)	10.0 (0)	3.4 (0)	2.3 (0)

Influx density	Influx frequency (/100 yrs)	Freeze intensity/ frequency	Predation intensity (C:P)	PROP	COT	SD	SAP	YT	MT	OT
1000	100	None	H (4:1)	7685.0 (2134.8)	406.2 (112.8)	2199.5 (171.9)	41.0 (0)	10.0 (0)	3.3 (0)	2.0 (0)
1000	100	Reduced	None	6875.0 (1987.8)	6875.0 (1987.8)	12988.1 (92.4)	41.0 (0)	10.0 (0)	2.4 (0)	1.2 (0)
			L (0.5:1)	6310.7 (1983.1)	2498.8 (785.3)	11761.3 (992.5)	41.0 (0)	10.0 (0)	2.6 (0)	1.3 (0)
			M (2:1)	7069.7 (1982.8)	1182.3 (331.6)	5376.6 (528.6)	41.0 (0)	10.0 (0)	2.6 (0)	1.3 (0)
			H (4:1)	6869.5 (1936.7)	363.1 (102.3)	1606.1 (158.7)	41.0 (0)	10.0 (0)	2.8 (0)	1.3 (0)
1000	100	Historical	None	3742.6 (1263.1)	3742.6 (1263.1)	12874.4 (312.8)	41.0 (0)	10.0 (0)	2.3 (0)	0 (0)
			L (0.5:1)	1163.8 (91.5)	460.8 (36.2)	1267.6 (53.0)	41.0 (0)	10.0 (0)	0 (0)	0 (0)
			M (2:1)	525.4 (66.9)	87.9 (11.2)	226.1 (4.8)	38.4 (0.2)	6.2 (0)	0 (0)	0 (0)
			H (4:1)	821.4 (94.0)	43.4 (5.0)	229.0 (6.9)	34.9 (0)	10.0 (0)	1.0 (0)	0 (0)
500	1	None	None	10274.0 (2675.2)	10274.0 (2675.2)	13000.0 (0)	41.0 (0)	10.0 (0)	3.4 (0)	2.3 (0)
			L (0.5:1)	10393.7 (2640.9)	4115.6 (1045.7)	12940.2 (215.6)	41.0 (0)	10.0 (0)	3.3 (0)	2.1 (0)
			M (2:1)	7691.3 (2154.0)	1286.2 (360.2)	5887.6 (540.4)	41.0 (0)	10.0 (0)	3.1 (0)	1.7 (0)
			H (4:1)	0 (0)	0 (0)	0 (0)	0 (0)	0 (0)	0 (0)	0 (0)
500	1	Reduced	None	6141.3 (1940.1)	6141.3 (1940.1)	12982.7 (105.9)	41.0 (0)	10.0 (0)	2.7 (0)	1.4 (0)

Influx density	Influx frequency (/100 yrs)	Freeze intensity/ frequency	Predation intensity (C:P)	PROP	COT	SD	SAP	YT	MT	OT
500	1	Reduced	L (0.5:1)	6069.0 (1955.9)	2403.1 (774.5)	7634.8 (1058.5)	41.0 (0)	10.0 (0)	2.3 (0)	1.1 (0)
			M (2:1)	2146.4 (1040.7)	358.9 (174.0)	868.8 (147.9)	41.0 (0)	10.0 (0)	2.0 (0)	0 (0)
			H (4:1)	0 (0)	0 (0)	0 (0)	0 (0)	0 (0)	0 (0)	0 (0)
500	1	Historical	None	0 (0)	0 (0)	0 (0)	0 (0)	0 (0)	0 (0)	0 (0)
			L (0.5:1)	0 (0)	0 (0)	0 (0)	0 (0)	0 (0)	0 (0)	0 (0)
			M (2:1)	0 (0)	0 (0)	0 (0)	0 (0)	0 (0)	0 (0)	0 (0)
			H (4:1)	0 (0)	0 (0)	0 (0)	0 (0)	0 (0)	0 (0)	0 (0)
500	10	None	None	10258.1 (2610.7)	10258.1 (2610.7)	13000.0 (0)	41.0 (0)	10.0 (0)	3.4 (0)	2.3 (0)
			L (0.5:1)	10192.4 (2588.1)	4035.9 (1024.8)	12946.4 (197.2)	41.0 (0)	10.0 (0)	3.3 (0)	2.1 (0)
			M (2:1)	7560.4 (2207.3)	1264.3 (369.1)	6388.8 (586.2)	41.0 (0)	10.0 (0)	3.2 (0)	1.9 (0)
			H (4:1)	3515.3 (1220.8)	185.8 (64.5)	916.7 (103.1)	41.0 (0)	10.0 (0)	2.5 (0)	0 (0)
500	10	Reduced	None	3476.6 (1267.1)	4376.6 (1267.1)	11259.5 (1466.7)	41.0 (0)	10.0 (0)	2.2 (0)	0 (0)
			L (0.5:1)	6220.4 (1947.4)	2463.1 (771.1)	9547.8 (1168.4)	41.0 (0)	10.0 (0)	2.6 (0)	1.3 (0)
			M (2:1)	3446.2 (1248.1)	576.3 (208.7)	2836.6 (340.8)	41.0 (0)	10.0 (0)	2.5 (0)	0 (0)
			H (4:1)	120.7 (51.0)	6.4 (2.7)	15.9 (2.3)	5.9 (0.7)	3.0 (0.3)	0 (0)	0 (0)
500	10	Historical	None	1956.8 (881.4)	1956.8 (881.4)	9357.0 (1364.6)	41.0 (0)	10.0 (0)	1.8 (0)	0 (0)

Influx density	Influx frequency (/100 yrs)	Freeze intensity/ frequency	Predation intensity (C:P)	PROP	COT	SD	SAP	YT	MT	OT
500	10	Historical	L (0.5:1)	147.9 (50.3)	58.6 (19.9)	160.0 (29.1)	18.2 (2.2)	3.8 (0.2)	0 (0)	0 (0)
			M (2:1)	2257.4 (881.7)	377.5 (147.4)	718.3 (238.1)	34.7 (0.6)	9.4 (0.5)	1.2 (0)	0 (0)
			H (4:1)	0 (0)	0 (0)	15.0 (0)	1.3 (0)	0 (0)	0 (0)	0 (0)
500	100	None	None	10721.3 (2651.1)	10721.3 (2651.1)	13000.0 (0)	41.0 (0)	10.0 (0)	3.4 (0)	2.3 (0)
			L (0.5:1)	10438.2 (2602.3)	4133.2 (1030.4)	12980.2 (106.0)	41.0 (0)	10.0 (0)	3.4 (0)	2.3 (0)
			M (2:1)	10471.4 (2704.2)	1751.1 (452.2)	7421.6 (648.8)	41.0 (0)	10.0 (0)	3.3 (0)	2.1 (0)
			H (4:1)	8181.9 (2119.3)	432.5 (112.0)	2076.4 (180.2)	41.0 (0)	10.0 (0)	3.2 (0)	1.9 (0)
500	100	Reduced	None	6291.5 (1958.0)	6291.5 (1958.0)	12986.5 (100.4)	41.0 (0)	10.0 (0)	2.8 (0)	1.6 (0)
			L (0.5:1)	6160.0 (2005.1)	2439.2 (794.0)	10407.6 (1103.4)	34.9 (0)	10.0 (0)	2.6 (0)	1.2 (0)
			M (2:1)	6255.6 (1931.1)	1046.1 (322.9)	4987.4 (322.9)	41.0 (0)	10.0 (0)	2.7 (0)	1.3 (0)
			H (4:1)	3512.1 (1205.4)	185.7 (63.7)	360.3 (40.4)	41.0 (0.2)	10.0 (0)	2.1 (0)	0 (0)
500	100	Historical	None	586.3 (84.7)	586.3 (84.7)	1239.6 (53.1)	41.0 (0)	10.0 (0)	0 (0)	0 (0)
			L (0.5:1)	2314.8 (880.5)	916.6 (348.6)	2404.2 (433.1)	41.0 (0)	10.0 (0)	1.5 (0)	0 (0)
			M (2:1)	502.0 (0)	83.9 (0)	127.2 (0.1)	13.3 (0.1)	1.1 (0)	0 (0)	0 (0)

Influx density	Influx frequency (/100 yrs)	Freeze intensity/ frequency	Predation intensity (C:P)	PROP	COT	SD	SAP	YT	MT	OT
500	100	Historical	H (4:1)	126.2 (42.1)	6.7 (2.2)	72.6 (2.8)	9.8 (0.2)	2.6 (0)	0 (0)	0 (0)
100	1	None	None	7695.5 (2177.2)	7695.5 (2177.2)	12996.2 (53.5)	41.0 (0)	10.0 (0)	3.2 (0)	2.0 (0)
			L (0.5:1)	6182.4 (2013.3)	2248.0 (797.2)	11809.1 (980.8)	41.0 (0)	10.0 (0)	3.0 (0)	1.4 (0)
			M (2:1)	0 (0)	0 (0)	0 (0)	0 (0)	0 (0)	0 (0)	0 (0)
			H (4:1)	0 (0)	0 (0)	0 (0)	0 (0)	0 (0)	0 (0)	0 (0)
100	1	Reduced	None	3498.1 (1283.8)	3498.1 (1283.8)	12666.4 (1346.4)	40.6 (4.1)	9.9 (1.0)	2.4 (0.2)	0 (0)
			L (0.5:1)	0 (0)	0 (0)	0 (0)	0 (0)	0 (0)	0 (0)	0 (0)
			M (2:1)	0 (0)	0 (0)	0 (0)	0 (0)	0 (0)	0 (0)	0 (0)
			H (4:1)	0 (0)	0 (0)	0 (0)	0 (0)	0 (0)	0 (0)	0 (0)
100	1	Historical	None	0 (0)	0 (0)	0 (0)	0 (0)	0 (0)	0 (0)	0 (0)
			L (0.5:1)	0 (0)	0 (0)	0 (0)	0 (0)	0 (0)	0 (0)	0 (0)
			M (2:1)	0 (0)	0 (0)	0 (0)	0 (0)	0 (0)	0 (0)	0 (0)
			H (4:1)	0 (0)	0 (0)	0 (0)	0 (0)	0 (0)	0 (0)	0 (0)
100	10	None	None	10423.1 (2655.1)	10423.1 (2655.1)	13000.0 (0)	41.0 (0)	10.0 (0)	3.3 (0)	2.1 (0)
			L (0.5:1)	7731.9 (2175.5)	3061.6 (861.4)	12281.0 (832.2)	41.0 (0)	10.0 (0)	3.1 (0)	1.6 (0)
			M (2:1)	4089.2 (1757.9)	683.8 (294.0)	2988.7 (341.4)	41.0 (0)	10.0 (0)	2.6 (0)	1.0 (0)
			H (4:1)	0 (0)	0 (0)	0 (0)	0 (0)	0 (0)	0 (0)	0 (0)
100	10	Reduced	None	3493.2 (1278.4)	3493.2 (1278.4)	7570.1 (1312.1)	41.0 (0)	10.0 (0)	2.0 (0)	0 (0)

Influx density	Influx frequency (/100 yrs)	Freeze intensity/ frequency	Predation intensity (C:P)	PROP	COT	SD	SAP	YT	MT	OT
100	10	Reduced	L (0.5:1)	292.8 (83.4)	115.9 (33.0)	135.1 (26.1)	33.6 (3.2)	7.1 (0.9)	0 (0)	0 (0)
			M (2:1)	0 (0)	0 (0)	0 (0)	0 (0)	0 (0)	0 (0)	0 (0)
			H (4:1)	0 (0)	0 (0)	0 (0)	0 (0)	0 (0)	0 (0)	0 (0)
100	10	Historical	None	449.1 (87.1)	449.1 (87.1)	646.1 (77.0)	41.0 (0)	10.0 (0)	0 (0)	0 (0)
			L (0.5:1)	0 (0)	0 (0)	0 (0)	0 (0)	0 (0)	0 (0)	0 (0)
			M (2:1)	0 (0)	0 (0)	0 (0)	0 (0)	0 (0)	0 (0)	0 (0)
			H (4:1)	0 (0)	0 (0)	0 (0)	0 (0)	0 (0)	0 (0)	0 (0)
100	100	None	None	10203.4 (2687.8)	10203.4 (2687.8)	13000 (0)	41.0 (0)	10.0 (0)	3.3 (0)	2.2 (0)
			L (0.5:1)	7814.9 (2142.9)	3094.4 (848.5)	12793.6 (382.3)	41.0 (0)	10.0 (0)	3.3 (0)	2.0 (0)
			M (2:1)	7747.0 (2102.4)	1295.5 (351.6)	6003.1 (577.8)	41.0 (0)	10.0 (0)	3.1 (0)	1.7 (0)
			H (4:1)	4505.4 (2013.9)	238.2 (106.5)	946.6 (102.9)	41.0 (0)	10.0 (0)	2.6 (0)	1.0 (0)
100	100	Reduced	None	6248.1 (1949.3)	6248.1 (1949.3)	12985.4 (104.8)	41.0 (0)	10.0 (0)	2.8 (0)	1.5 (0)
			L (0.5:1)	6291.1 (1874.1)	2491.1 (742.1)	10496.9 (1079.8)	34.9 (0)	10.0 (0)	2.8 (0)	1.4 (0)
			M (2:1)	3665.3 (1252.5)	612.9 (209.5)	2812.7 (323.8)	41.0 (0)	10.0 (0)	2.4 (0)	0 (0)
			H (4:1)	201.4 (54.3)	10.6 (2.9)	37.5 (5.4)	7.6 (0.8)	3.3 (0.2)	0 (0)	0 (0)
100	100	Historical	None	1962.6 (875.5)	1962.6 (875.5)	305.0 (64.4)	40.1 (1.2)	8.7 (0)	1.1 (0)	0 (0)

Influx density	Influx frequency (/100 yrs)	Freeze intensity/ frequency	Predation intensity (C:P)	PROP	COT	SD	SAP	YT	MT	OT
100	100	Historical	L (0.5:1)	0 (0)	0 (0)	117.6 (18.5)	20.1 (2.4)	5.4 (0.5)	0 (0)	0 (0)
			M (2:1)	333.1 (72.5)	55.7 (12.1)	159.6 (17.6)	26.0 (1.8)	7.0 (0.4)	0 (0)	0 (0)
			H (4:1)	0 (0)	0 (0)	0 (0)	0 (0)	0 (0)	0 (0)	0 (0)

LIST OF REFERENCES

Abbott, J. R. & W. S. Judd, 2000. Floristic inventory of the Waccasassa Bay State Preserve, Levy County, Florida. Rhodora 102: 439-513.

Alongi, D. M., 2015. The impact of climate change on mangrove forests. Current Climate Change Reports 1: 30-39.

Angelini, C. & B. R. Silliman, 2012. Patch size dependent community recovery after massive disturbance. Ecology 93: 101-110.

Arditi, R. & L. R. Ginzburg, 1989. Coupling in predator-prey dynamics: ratio-dependence. Journal of Theoretical Biology 139: 311-326.

Beaugrand, G., M. Edwards, K. Brander, C. Luczak & F. Ibanez, 2008. Causes and projections of abrupt climate-driven ecosystem shifts in the North Atlantic. Ecology Letters 11: 1157-1168.

Berryman, A. A., 1992. The orgins and evolution of predator-prey theory. Ecology 73: 1530-1535.

Bertness, M. D., C. Holdredge & A. H. Altieri, 2009. Substrate mediates consumer control of salt marsh cordgrass on Cape Cod, New England. Ecology 90: 2108-2117.

Bonsall, M. B. & A. Hastings, 2004. Demographic and environmental stochasticity in predator-prey metapopulation dynamics. Journal of Animal Ecology 73: 1043-1055.

Bosire, J. O., J. G. Kairo, J. Kazungu, N. Koedam & F. Dahdouh-Guebas, 2005. Predation on propagules regulates regeneration in a high-density reforested mangrove plantation. Marine Ecology Progress Series 299: 149-155.

Brown, J. H., T. J. Valone & C. G. Curtin, 1997. Reorganization of an arid ecosystem in response to recent climate change. Proceedings of the National Academy of Sciences of USA 94: 9729-9733.

Burns, B. & J. Ogden, 1985. The demography of the temperate mangrove [*Avicennia marina* (Forsk.) Vierh.] at its southern limit in New Zealand. Australian Journal of Ecology 10: 125-133.

Cannicci, S., D. Burrows, S. Fratini, T. J. Smith Iii, J. Offenberg & F. Dahdouh-Guebas, 2008. Faunal impact on vegetation structure and ecosystem function in mangrove forests: a review. Aquatic Botany 89: 186-200.

Castaneda, H. & F. Putz, 2007. Predicting sea-level rise effects on a nature preserve on the Gulf Coast of Florida: a landscape perspective. Florida Scientist 70: 166-175.

Cavanaugh, K. C., J. R. Kellner, A. J. Forde, D. S. Gruner, J. D. Parker, W. Rodriguez & I. C. Feller, 2014. Poleward expansion of mangroves is a threshold response to decreased frequency of extreme cold events. Proceedings of the National Academy of Sciences of USA 111: 723-727.

Clarke, P., 1995. The population dynamics of the mangrove *Avicennia marina*; demographic synthesis and predictive modelling. Hydrobiologia 295: 83-88.

Clarke, P. J., 1992. Predispersal mortality and fecundity in the grey mangrove (*Avicennia marina*) in southeastern Australia. Australian Journal of Ecology 17: 161-168.

Comeaux, R. S., M. A. Allison & T. S. Bianchi, 2012. Mangrove expansion in the Gulf of Mexico with climate change: implications for wetland health and resistance to rising sea levels. Estuarine, Coastal and Shelf Science 96: 81-95.

Cormier, N., K. W. Krauss & W. H. Conner, 2013. Periodicity in stem growth and litterfall in tidal freshwater forested wetlands: influence of salinity and drought on nitrogen recycling. Estuaries and Coasts 36: 533-546.

Cox, P. M., R. A. Betts, C. D. Jones, S. A. Spall & I. J. Totterdell, 2000. Acceleration of global warming due to carbon-cycle feedbacks in a coupled climate model. Nature 408: 184-187.

Craft, C., J. Clough, J. Ehman, S. Joye, R. Park, S. Pennings, H. Y. Guo & M. Machmuller, 2009. Forecasting the effects of accelerated sea-level rise on tidal marsh ecosystem services. Frontiers in Ecology and the Environment 7: 73-78.

Dahdouh-Guebas, F., M. Verneirt, J. Tack, D. Van Speybroeck & N. Koedam, 1998. Propagule predators in Kenyan mangroves and their possible effect on regeneration. Marine and Freshwater Research 49: 345-350.

Delgado, P., J. A. Jiménez & D. Justic, 1999. Population dynamics of mangrove *Avicennia bicolor* on the Pacific coast of Costa Rica. Wetlands Ecology and Management 7: 113-120.

DeSantis, L. R., S. Bhotika, K. Williams & F. E. Putz, 2007. Sea-level rise and drought interactions accelerate forest decline on the Gulf Coast of Florida, USA. Global Change Biology 13: 2349-2360.

Doyle, T. W., K. W. Krauss, W. H. Conner & A. S. From, 2010. Predicting the retreat and migration of tidal forests along the northern Gulf of Mexico under sea-level rise. Forest Ecology and Management 259: 770-777.

Dunne, J. A., J. Harte & K. J. Taylor, 2003. Subalpine meadow flowering phenology responses to climate change: integrating experimental and gradient methods. Ecological Monographs 73: 69-86.

Enwright, N. M., K. T. Griffith & M. J. Osland, 2016. Barriers to and opportunities for landward migration of coastal wetlands with sea-level rise. Frontiers in Ecology and the Environment 14: 307-316.

Fagherazzi, S., M. L. Kirwan, S. M. Mudd, G. R. Guntenspergen, S. Temmerman, A. D'Alpaos, J. van de Koppel, J. M. Rybczyk, E. Reyes, C. Craft & J. Clough, 2012. Numerical models of salt marsh evolution: ecological, geomorphic, and climatic factors. Reviews of Geophysics 50: RG1002.

Farnsworth, E. J. & A. M. Ellison, 1997. Global patterns of pre-dispersal propagule predation in mangrove forests. Biotropica 29: 318-330.

FCC: Florida Climate Center, 2014. Average Annual Precipitation. In: Center for Ocean-Atmospheric Prediction Studies. Florida State University. http://climatecenter.fsu.edu/products-services/data/weather-planner-maps/average-annual-precipitation Accessed February 2015.

Fitter, A. H., R. S. R. Fitter, I. T. B. Harris & M. H. Williamson, 1995. Relationship between first flowering date and temperature in the flora of a locality in central England. Functional Ecology 9: 55-60.

Fletcher, Q. E., S. Boutin, J. E. Lane, J. M. LaMontagne, A. G. McAdam, C. J. Krebs & M. M. Humphries, 2010. The functional response of a hoarding seed predator to mast seeding. Ecology 91: 2673-2683.

FNAI, 2015. Florida Land Cover Classification System Definitions for the Cooperative Land Cover Map v3.1. Florida Natural Areas Inventory, Tallahassee, FL.

FNAI, 2017. Florida Land Cover Classification System Definitions for the Cooperative Land Cover Map v3.2. Florida Natural Areas Inventory, Tallahassee, FL.

Gabler, C. A., M. J. Osland, J. B. Grace, C. L. Stagg, R. H. Day, S. B. Hartley, N. M. Enwright, A. S. From, M. L. McCoy & J. L. McLeod, 2017. Macroclimatic change expected to transform coastal wetland ecosystems this century. Nature Climate Change 7: 142-147.

Geselbracht, L., K. Freeman, E. Kelly, D. R. Gordon & F. E. Putz, 2011. Retrospective and prospective model simulations of sea level rise impacts on Gulf of Mexico coastal marshes and forests in Waccasassa Bay, Florida. Climatic Change 107: 35-57.

Geselbracht, L. L., K. Freeman, A. P. Birch, J. Brenner & D. R. Gordon, 2015. Modeled sea level rise impacts on coastal ecosystems at six major estuaries on Florida's Gulf Coast: implications for adaptation planning. PLoS One 10: e0132079.

Giri, C. & J. Long, 2016. Is the geographic range of mangrove forests in the conterminous United States really expanding? Sensors 16: 2010.

Goodbred, S. L. & A. C. Hine, 1995. Coastal storm deposition: salt-marsh response to a severe extratropical storm, March 1993, west-central Florida. Geology 23: 679-682.

Grabherr, G., M. Gottfried & H. Pauli, 1994. Climate effects on mountain plants. Nature 369: 448-448.

Guo, H., C. Weaver, S. P. Charles, A. Whitt, S. Dastidar, P. D'Odorico, J. D. Fuentes, J. S. Kominoski, A. R. Armitage & S. C. Pennings, 2017. Coastal regime shifts: rapid responses of coastal wetlands to changes in mangrove cover. 98: 762-772.

Guo, H., Y. Zhang, Z. Lan & S. C. Pennings, 2013. Biotic interactions mediate the expansion of black mangrove (*Avicennia germinans*) into salt marshes under climate change. Global Change Biology 19: 2765-2774.

Hamann, A. & T. Wang, 2006. Potential effects of climate change on ecosystem and tree species distribution in British Columbia. Ecology 87: 2773-2786.

Hamby, D., 1994. A review of techniques for parameter sensitivity analysis of environmental models. Environmental Monitoring and Assessment 32: 135-154.

He, Q. & B. R. Silliman, 2016. Consumer control as a common driver of coastal vegetation worldwide. Ecological Monographs 86: 278-294.

Holdredge, C., M. D. Bertness & A. H. Altieri, 2009. Role of crab herbivory in die-off of New England salt marshes. Conservation Biology 23: 672-679.

Holling, C. S., 1959a. The components of predation as revealed by a study of small-mammal predation of the European pine sawfly. The Canadian Entomologist 91: 293-320.

Holling, C. S., 1959b. Some characteristics of simple types of predation and parasitism. The Canadian Entomologist 91: 385-398.

Hook, D. D., M. A. Buford & T. M. Williams, 1991. Impact of Hurricane Hugo on the South Carolina coastal plain forest. Journal of Coastal Research 8: 291-300.

Hubbell, S. P., 1980. Seed predation and the coexistence of tree species in tropical forests. Oikos: 214-229.

Inouye, D. W., 2008. Effects of climate change on phenology, frost damage, and floral abundance of montane wildflowers. Ecology 89: 353-362.

IPCC, 2013. Climate Change 2013: The Physical Science Basis. Contribution of Working Group I to the Fifth Assessment Report of the Intergovernmental Panel on Climate Change [Stocker, T. F., et al. (eds)]. Cambridge University Press, Cambridge, United Kingdom and New York, NY, USA, 1535 pp.

Jackson, L. J., A. S. Trebitz & K. L. Cottingham, 2000. An introduction to the practice of ecological modeling. Bioscience 50: 694-706.

Janzen, D. H., 1970. Herbivores and the number of tree species in tropical forests. The American Naturalist 104: 501-528.

Jimenez, J. A., A. E. Lugo & G. Cintron, 1985. Tree mortality in mangrove forests. Biotropica: 177-185.

Jørgensen, S. E., 1999. State-of-the-art of ecological modelling with emphasis on development of structural dynamic models. Ecological Modelling 120: 75-96.

Kaplan, D., R. Muñoz-Carpena & A. Ritter, 2010a. Untangling complex shallow groundwater dynamics in the floodplain wetlands of a southeastern US coastal river. Water Resources Research 46: doi: 10.1029/2009WR009038.

Kaplan, D., R. Munoz-Carpena, Y. Wan, M. Hedgepeth, F. Zheng, R. Roberts & R. Rossmanith, 2010b. Linking river, floodplain, and vadose zone hydrology to improve restoration of a coastal river affected by saltwater intrusion. Journal of Environmental Quality 39: 1570-1584.

Keeling, C. D., R. B. Bacastow, A. Carter, S. C. Piper, T. P. Whorf, M. Heimann, W. G. Mook & H. Roeloffzen, 1989. A three-dimensional model of atmospheric CO_2 transport based on observed winds: 1. Analysis of observational data. In Peterson, D. H. (ed), Aspects of climate variability in the Pacific and the Western Americas. American Geophysical Union, Washington, DC, 165-236.

Kelly, A. E. & M. L. Goulden, 2008. Rapid shifts in plant distribution with recent climate change. Proceedings of the National Academy of Sciences of USA 105: 11823-11826.

Kilkenny, F. F. & L. F. Galloway, 2016. Evolution of marginal populations of an invasive vine increases the likelihood of future spread. New Phytologist 209: 1773-1780.

Kimberlain, T. B., 2012. Tropical Cyclone Report: Tropical Storm Debby (AL042012) 23-27 June 2012. 1-51 pp.

Kirwan, M. L., G. R. Guntenspergen & J. T. Morris, 2009. Latitudinal trends in *Spartina alterniflora* productivity and the response of coastal marshes to global change. Global Change Biology 15: 1982-1989.

Kirwan, M. L. & J. P. Megonigal, 2013. Tidal wetland stability in the face of human impacts and sea-level rise. Nature 504: 53-60.

Krauss, K. W., A. S. From, T. W. Doyle, T. J. Doyle & M. J. Barry, 2011. Sea-level rise and landscape change influence mangrove encroachment onto marsh in the Ten Thousand Islands region of Florida, USA. Journal of Coastal Conservation 15: 629-638.

Kurz, H. & K. A. Wagner, 1957. Tidal marshes of the Gulf and Atlantic coasts of northern Florida and Charleston, South Carolina. Florida State University, Studies No 24: 168.

Lancaster, L. T., G. Morrison & R. N. Fitt, 2016. Life history trade-offs, the intensity of competition, and coexistence in novel and evolving communities under climate change. Philosophical Transactions of the Royal Society B: Biological Sciences 372: 20160046.

Lande, R., S. Engen & B.-E. Saether, 2003. Stochastic Population Dynamics in Ecology and Conservation. Oxford University Press, Oxford, UK, 212 pp.

Langston, A. K., D. A. Kaplan & C. Angelini, 2017a. Predation restricts black mangrove (*Avicennia germinans*) colonization at its northern range limit along Florida's Gulf Coast. Hydrobiologia 803: 317-331.

Langston, A. K., D. A. Kaplan & F. E. Putz, 2017b. A casualty of climate change? Loss of freshwater forest islands on Florida's Gulf Coast. Global Change Biology 23: 5383-5397.

Leffler, A. J., E. S. Klein, S. F. Oberbauer & J. M. Welker, 2016. Coupled long-term summer warming and deeper snow alters species composition and stimulates gross primary productivity in tussock tundra. Oecologia 181: 287-297.

Leonardi, N., N. K. Ganju & S. Fagherazzi, 2016. A linear relationship between wave power and erosion determines salt-marsh resilience to violent storms and hurricanes. Proceedings of the National Academy of Sciences of USA 113: 64-68.

Lewis, R. & F. Dunstan, 1975. The possible role of *Spartina alterniflora* Loisel in establishment of mangroves in Florida. Proceedings for Second Annual Conference on the Restoration of Coastal Vegetation in Florida May 17, 1975 Hillsborough Community College, Tampa: 82-100.

Lin, N., K. Emanuel, M. Oppenheimer & E. Vanmarcke, 2012. Physically based assessment of hurricane surge threat under climate change. Nature Climate Change 2: 462-467.

Liu, X., W. H. Conner, B. Song & A. D. Jayakaran, 2017. Forest composition and growth in a freshwater forested wetland community across a salinity gradient in South Carolina, USA. Forest Ecology and Management 389: 211-219.

Lugo, A. E. & C. Patterson-Zucca, 1977. The impact of low temperature stress on mangrove structure and growth. Tropical Ecology 18: 149-161.

Lugo, A. E. & S. C. Snedaker, 1974. The ecology of mangroves. Annual Review of Ecology and Systematics: 39-64.

Marella, R. L., 2014. Water withdrawals, use, and trends in Florida, 2010. Scientific Investigations Report, U. S. Geological Survey, Reston, VA, 72 pp.

Mattson, R. A., T. K. Frazer, J. Hale, S. Blitch & L. Ahijevych, 2007. Florida Big Bend. U.S. Geological Survey Scientific Investigations Report 2006-5287 and U.S. Environmental Protection Agency 855-R-04-003, 171-188 pp.

McGuinness, K. A., 1997. Seed predation in a tropical mangrove forest: a test of the dominance-predation model in northern Australia. Journal of Tropical Ecology 13: 293-302.

McKee, K. L., 1995. Mangrove species distribution and propagule predation in Belize: an exception to the dominance-predation hypothesis. Biotropica 27: 334-345.

McKee, K. L., K. Rogers & N. Saintilan, 2012. Response of salt marsh and mangrove wetlands to changes in atmospheric CO_2, climate, and sea level. In Middleton, B. A. (ed), Global Change and the Function and Distribution of Wetlands. vol 1. Springer, Dordrecht, 63-96.

McKee, K. L. & J. E. Rooth, 2008. Where temperate meets tropical: multi-factorial effects of elevated CO_2, nitrogen enrichment, and competition on a mangrove-salt marsh community. Global Change Biology 14: 971-984.

McKee, K. L., J. E. Rooth & I. C. Feller, 2007. Mangrove recruitment after forest disturbance is facilitated by herbaceous species in the Caribbean. Ecological Applications 17: 1678-1693.

Mendelsohn, R., K. Emanuel, S. Chonabayashi & L. Bakkensen, 2012. The impact of climate change on global tropical cyclone damage. Nature Climate Change 2: 205-209.

Michener, W. K., E. R. Blood, K. L. Bildstein, M. M. Brinson & L. R. Gardner, 1997. Climate change, hurricanes and tropical storms, and rising sea level in coastal wetlands. Ecological Applications 7: 770-801.

Minchinton, T. E., 2006. Consequences of pre-dispersal damage by insects for the dispersal and recruitment of mangroves. Oecologia 148: 70-80.

Møller, A. P., D. Rubolini & E. Lehikoinen, 2008. Populations of migratory bird species that did not show a phenological response to climate change are declining. Proceedings of the National Academy of Sciences of USA 105: 16195-16200.

Montague, C. & H. Odum, 1997. The Setting and Function of Intertidal Marsh on Florida's Gulf Coast. In Coultas, C. & Y.-P. Hsieh (eds), Ecology and Management of Tidal Marshes: A Model from the Gulf of Mexico. St. Lucie Press, Delray Beach, FL, 1-33.

Moreira, X., I. M. Pérez-Ramos, L. Abdala-Roberts & K. A. Mooney, 2017. Functional responses of contrasting seed predator guilds to masting in two Mediterranean oak species. Oikos 126: 1042-1050.

Nitto, D. D., G. Neukermans, N. Koedam, H. Defever, F. Pattyn, J. Kairo & F. Dahdouh-Guebas, 2014. Mangroves facing climate change: landward migration potential in response to projected scenarios of sea level rise. Biogeosciences 11: 857-871.

NOAA: Center for Operational Oceanographic Products and Services, 2013. Mean sea level trend 8727520 Cedar Key, Florida. In: Tides & Currents. National Oceanic and Atmospheric Administration. https://tidesandcurrents.noaa.gov/sltrends/sltrends_station.shtml?stnid=8727520 Accessed October 2013.

NOAA: Climate Prediction Center, 2015. Cold and warm episodes by season 1950-2015. In: Historical El Nino/La Nina episodes (1950-Present). National Weather Service. https://cpc.ncep.noaa.gov/products/analysis_monitoring/ensostuff/ensoyears.shtml Accessed April 2016.

NOAA: National Centers for Environmental Information, 2016. Global Climate Report: Annual 2015. In: State of the Climate. National Oceanic and Atmospheric Administration. https://ncdc.noaa.gov/sotc/global/201513 Accessed April 2016.

Novak, M., J. W. Moore & R. A. Leidy, 2011. Nestedness patterns and the dual nature of community reassembly in California streams: a multivariate permutation-based approach. Global Change Biology 17: 3714-3723.

Osborne, K. & T. Smith, 1990. Differential predation on mangrove propagules in open and closed canopy forest habitats. Vegetatio 89: 1-6.

Osland, M. J., R. H. Day, A. S. From, M. L. McCoy, J. L. McLeod & J. J. Kelleway, 2015. Life stage influences the resistance and resilience of black mangrove forests to winter climate extremes. Ecosphere 6: 1-15.

Osland, M. J., R. H. Day, C. T. Hall, M. D. Brumfield, J. L. Dugas & W. R. Jones, 2017a. Mangrove expansion and contraction at a poleward range limit: climate extremes and land-ocean temperature gradients. Ecology 98: 125-127.

Osland, M. J., N. Enwright, R. H. Day & T. W. Doyle, 2013. Winter climate change and coastal wetland foundation species: salt marshes vs. mangrove forests in the southeastern United States. Global Change Biology 19: 1482-1494.

Osland, M. J., N. M. Enwright, R. H. Day, C. A. Gabler, C. L. Stagg & J. B. Grace, 2016. Beyond just sea-level rise: considering macroclimatic drivers within coastal wetland vulnerability assessments to climate change. Global Change Biology 22: 1-11.

Osland, M. J., L. C. Feher, K. T. Griffith, K. C. Cavanaugh, N. M. Enwright, R. H. Day, C. L. Stagg, K. W. Krauss, R. J. Howard, J. B. Grace & K. Rogers, 2017b. Climatic controls on the global distribution, abundance, and species richness of mangrove forests. Ecological Monographs doi: 10.1002/ecm.1248.

Parmesan, C., 2006. Ecological and evolutionary responses to recent climate change. Annual Review of Ecology, Evolution, and Systematics 37: 637-669.

Parmesan, C. & G. Yohe, 2003. A globally coherent fingerprint of climate change impacts across natural systems. Nature 421: 37-42.

Parson, K. A. & A. A. De La Cruz, 1980. Energy flow and grazing behavior of conocephaline grasshoppers in a *Juncus roemerianus* marsh. Ecology 61: 1045-1050.

Patterson, C. S., I. A. Mendelssohn & E. M. Swenson, 1993. Growth and survival of *Avicennia germinans* seedlings in a mangal/salt marsh community in Louisiana, USA. Journal of Coastal Research: 801-810.

Patterson, S., K. L. McKee & I. A. Mendelssohn, 1997. Effects of tidal inundation and predation on *Avicennia germinans* seedling establishment and survival in a sub-tropical mangal/salt marsh community. Mangroves and Salt Marshes 1: 103-111.

Peck, J. E., 2010. Multivariate Analysis for Community Ecologists: Step-by-Step using PC-ORD (eds)]. MjM Software Design, Gleneden Beach, OR, 162 pp.

Perry, A. L., P. J. Low, J. R. Ellis & J. D. Reynolds, 2005. Climate change and distribution shifts in marine fishes. Science 308: 1912-1915.

Perry, L. & K. Williams, 1996. Effects of salinity and flooding on seedlings of cabbage palm (*Sabal palmetto*). Oecologia 105: 428-434.

Petzoldt, T. & K. Rinke, 2007. simecol: an object-oriented framework for ecological modeling in R. Journal of Statistical Software 22: 1-31.

Pickens, C. N. & M. W. Hester, 2011. Temperature tolerance of early life history stages of black mangrove *Avicennia germinans*: implications for range expansion. Estuaries and Coasts 34: 824-830.

Pounds, J. A., M. R. Bustamante, L. A. Coloma, J. A. Consuegra, M. P. L. Fogden, P. N. Foster, E. La Marca, K. L. Masters, A. Merino-Viteri, R. Puschendorf, S. R. Ron, G. A. Sanchez-Azofeifa, C. J. Still & B. E. Young, 2006. Widespread amphibian extinctions from epidemic disease driven by global warming. Nature 439: 161-167.

R Core Team, 2017. R: A Language and Environment for Statistical Computing. R Foundation for Statistical Computing, Vienna. www.R-project.org.

Raabe, E. A., A. E. Streck & R. P. Stumpf, 2004. Historic topographic sheets to satellite imagery: a methodology for evaluating coastal change in Florida's Big Bend tidal marsh. US Geological Survey, Center for Coastal and Regional Marine Studies, Open-file Report 2002-211.

Raabe, E. A. & R. P. Stumpf, 2016. Expansion of tidal marsh in response to sea-level rise: Gulf Coast of Florida, USA. Estuaries and Coasts 39: 145-157.

Record, S., N. D. Charney, R. M. Zakaria & A. M. Ellison, 2013. Projecting global mangrove species and community distributions under climate change. Ecosphere 4: 1-23.

Reddy, K. R., M. W. Clark, R. D. DeLaune & M. Kongchum, 2013. Physicochemical characterization of wetland soils. In DeLaune, R. D., K. R. Reddy, C. J. Richardson & J. P. Megonigal (eds), Methods in Biogeochemistry of Wetlands. Soil Science Society of America, Madison, WI, 41-53.

Reed, D. J., 1995. The response of coastal marshes to sea-level rise: survival or submergence? Earth Surface Processes and Landforms 20: 39-48.

Rhoades, J., 1996. Salinity: Electrical Conductivity and Total Dissolved Solids. In Swift, R. & D. Sparks (eds), Methods of Soil Analysis, Part 3: Chemical Methods. Soil Science Society of America and American Society of Agronomy, Madison, WI, 417-435.

Robertson, A., R. Giddins & T. Smith, 1990. Seed predation by insects in tropical mangrove forests: extent and effects on seed viability and the growth of seedlings. Oecologia 83: 213-219.

Ross, M. S., J. P. Sah, J. F. Meeder, P. L. Ruiz & G. Telesnicki, 2014. Compositional effects of sea-level rise in a patchy landscape: the dynamics of tree islands in the southeastern coastal Everglades. Wetlands 34: 91-100.

Saintilan, N., N. C. Wilson, K. Rogers, A. Rajkaran & K. W. Krauss, 2014. Mangrove expansion and salt marsh decline at mangrove poleward limits. Global Change Biology 20: 147-157.

Scavia, D., J. C. Field, D. F. Boesch, R. W. Buddemeier, V. Burkett, D. R. Cayan, M. Fogarty, M. A. Harwell, R. W. Howarth & C. Mason, 2002. Climate change impacts on US coastal and marine ecosystems. Estuaries 25: 149-164.

Schaefer, H.-C., W. Jetz & K. Boehning-Gaese, 2008. Impact of climate change on migratory birds: community reassembly versus adaptation. Global Ecology and Biogeography 17: 38-49.

Scott, A. J. & J. W. Morgan, 2012. Early life-history stages drive community reassembly in Australian old-fields. Journal of Vegetation Science 23: 721-731.

Seiple, W., 1979. Distribution, habitat preferences and breeding periods in the crustaceans *Sesarma cinereum* and *S. reticulatum* (Brachyura: Decapoda: Grapsidae). Marine Biology 52: 77-86.

Seiple, W. & M. Salmon, 1982. Comparative social behavior of two grapsid crabs, *Sesarma reticulatum* (Say) and *S. cinereum* (Bosc). Journal of Experimental Marine Biology and Ecology 62: 1-24.

Sheil, D., D. F. Burslem & D. Alder, 1995. The interpretation and misinterpretation of mortality rate measures. Journal of Ecology 83: 331-333.

Smith, T. J., 1987. Seed predation in relation to tree dominance and distribution in mangrove forests. Ecology 68: 266-273.

Smith, T. J., H. T. Chan, C. C. McIvor & M. B. Robblee, 1989. Comparisons of seed predation in tropical, tidal forests from three continents. Ecology 70: 146-151.

Soetaert, K., T. Petzoldt & R. W. Setzer, 2010. Solving differential equations in R: package deSolve. Journal of Statistical Software 33: 1-25.

Sousa, W. P., P. G. Kennedy & B. J. Mitchell, 2003. Propagule size and predispersal damage by insects affect establishment and early growth of mangrove seedlings. Oecologia 135: 564-575.

Sousa, W. P. & B. J. Mitchell, 1999. The effect of seed predators on plant distributions: is there a general pattern in mangroves? Oikos 86: 55-66.

Souza, M. M. A. & E. V. S. B. Sampaio, 2011. Predation on propagules and seedlings in mature and regenerating mangroves in the coast of Ceará, Brazil. Hydrobiologia 661: 179-186.

Sparks, E. L. & J. Cebrian, 2015. Does bird removal affect grasshopper grazing on *Juncus roemerianus* (black needlerush) marshes? Wetlands Ecology and Management 23: 1083-1089.

Sparks, T. H. & T. J. Yates, 1997. The effect of spring temperature on the appearance dates of British butterflies 1883-1993. Ecography 20: 368-374.

Spector, T. & F. E. Putz, 2006. Biomechanical plasticity facilitates invasion of maritime forests in the southern USA by Brazilian pepper (*Schinus terebinthifolius*). Biological Invasions 8: 255-260.

Steele, O. C., K. C. Ewel & G. Goldstein, 1999. The importance of propagule predation in a forest of nonindigenous mangrove trees. Wetlands 19: 705-708.

Stevens, P., S. Fox & C. Montague, 2006. The interplay between mangroves and saltmarshes at the transition between temperate and subtropical climate in Florida. Wetlands Ecology and Management 14: 435-444.

Subrahmanyam, C., W. L. Kruczynski & S. H. Drake, 1976. Studies on the animal communities in two North Florida salt marshes: Part II. Macroinvertebrate communities. Bulletin of Marine Science 26: 172-195.

Svenning, J.-C. & B. Sandel, 2013. Disequilibrium vegetation dynamics under future climate change. American Journal of Botany 100: 1266-1286.

Tomlinson, P. B., 2016. The Botany of Mangroves, Second Edition. Cambridge University Press, Cambridge, UK, 454 pp.

Travers, S. E., B. Marquardt, N. J. Zerr, J. B. Finch, M. J. Boche, R. Wilk & S. C. Burdick, 2015. Climate change and shifting arrival date of migratory birds over a century in the northern Great Plains. The Wilson Journal of Ornithology 127: 43-51.

USGS: National Water Information System, 2012. 02313700 Waccasassa River NR Gulf Hammock, FLA. In: National Water Information System: Web Interface. U.S. Geological Survey. https://waterdata.usgs.gov/nwis/inventory/?site_no=02313700&agency_cd=USGS Accessed August 2016.

Van Nedervelde, F., S. Cannicci, N. Koedam, J. Bosire & F. Dahdouh-Guebas, 2015. What regulates crab predation on mangrove propagules? Acta Oecologica 63: 63-70.

Verdi, R. J., S. A. Tomlinson & R. L. Marella, 2006. The Drought of 1998-2002: Impacts on Florida's Hydrology and Landscape. U.S. Geological Survey, Circular 1295, Reston, VA, 34 pp.

Vince, S. W., S. R. Humphrey & R. W. Simons, 1989. The Ecology of Hydric Hammocks: A Community Profile. U.S. Department of the Interior, Fish and Wildlife Service, Research and Development.

Vitousek, P. M., 1994. Beyond global warming: ecology and global change. Ecology 75: 1862-1876.

Walther, G.-R., E. Post, P. Convey, A. Menzel, C. Parmesan, T. J. C. Beebee, J.-M. Fromentin, O. Hoegh-Guldberg & F. Bairlein, 2002. Ecological responses to recent climate change. Nature 416: 389-395.

Ward, R. D., D. A. Friess, R. H. Day & R. A. MacKenzie, 2016. Impacts of climate change on mangrove ecosystems: a region by region overview. Ecosystem Health and Sustainability 2: e01211.

Wells, B. W. & I. V. Shunk, 1938. Salt spray: an important factor in coastal ecology. Bulletin of the Torrey Botanical Club 65: 485-492.

White, E. & D. Kaplan, 2017. Restore or retreat? Saltwater intrusion and water management in coastal wetlands. Ecosystem Health and Sustainability 3: doi: 10.1002/ehs2.1258.

Williams, D., E. Muchugu, W. Overholt & J. Cuda, 2007a. Colonization patterns of the invasive Brazilian peppertree, *Schinus terebinthifolius*, in Florida. Heredity 98: 284-293.

Williams, K., K. C. Ewel, R. P. Stumpf, F. E. Putz & T. W. Workman, 1999a. Sea-level rise and coastal forest retreat on the west coast of Florida, USA. Ecology 80: 2045-2063.

Williams, K., M. MacDonald, K. McPherson & T. H. Mirti, 2007b. Chapter 10: Ecology of the Coastal Edge of Hydric Hammocks on the Gulf Coast of Florida. In Conner, W., T. Doyle & K. Krauss (eds), Ecology of Tidal Freshwater Forested Wetlands of the Southeastern United States. Springer, Netherlands, 255-289.

Williams, K., M. MacDonald & L. d. S. L. Sternberg, 2003. Interactions of storm, drought, and sea-level rise on coastal forest: a case study. Journal of Coastal Research 19: 1116-1121.

Williams, K., M. V. Meads & D. A. Sauerbrey, 1998. The roles of seedling salt tolerance and resprouting in forest zonation on the west coast of Florida, USA. American Journal of Botany 85: 1745-1752.

Williams, K., Z. S. Pinzon, R. P. Stumpf & E. A. Raabe, 1999b. Sea-level rise and coastal forests on the Gulf of Mexico. US Geological Survey, Center for Coastal Geology, Open-file Report 99-441.

Wolfe, S. H., R. D. Drew & L. Handley, 1990. Ecological characterization of the Tampa Bay watershed. 20 pp.

Zhai, L., J. Jiang, D. DeAngelis & L. S. L. Sternberg, 2016. Prediction of plant vulnerability to salinity increase in a coastal ecosystem by stable isotope composition (δ18O) of plant stem water: a model study. Ecosystems 19: 32-49.

Zimmerman, T. & D. Felder, 1991. Reproductive ecology of an intertidal brachyuran crab, *Sesarma* sp. (nr. *reticulatum*), from the Gulf of Mexico. The Biological Bulletin 181: 387-401.

BIOGRAPHICAL SKETCH

Amy Langston earned a bachelor's degree in ecology and systematic biology from California Polytechnic State University, San Luis Obispo, and a master's degree in biology from San Francisco State University prior to entering the doctoral program in environmental engineering sciences at University of Florida in 2013. She is pursuing a career in academia and plans to continue her research on the effects on climate change on plant communities.